



**Politecnico
di Torino**

POLITECNICO DI TORINO

Master of Science in Architecture Construction City

Master of Science Thesis

**Seismic Performance of Unitized Glazed Façades:
A Parametric Study**

Supervisors:

Professor Mauro CORRADO (DISEG)

Professor Anna REGGIO (DISEG)

Candidate:

Ezgi OZALP

JULY 2025

Academic Year 2024/2025

Acknowledgment

I would like to express my deepest gratitude to my supervisors, Professor Mauro Corrado and Professor Anna Reggio, for their close guidance in the various stages of this thesis. Their technical knowledge, support and generous guidance with regard to my work helped me overcome a number of challenges. I feel extraordinarily fortunate to have had them as mentors. They made this difficult yet rewarding journey very enriching both on intellectual and personal levels.

I would also like to extend my gratitude to the research group that worked on the Permasteelisa experimental campaign, their works provided relevant contributions that shaped the foundation of this thesis.

To my wonderful family, my mother Seval and father Sezgin, I extend my deepest gratitude for supporting me unconditionally. It was all possible with their love along with an incredible source of strength whenever I needed. Additionally, I thank my aunt, Professor Hayat Yalin, for her professional guidance as well as for being a role model whose passion has inspired people throughout her life.

I especially would like to thank my brother Oguz Ozalp, who provided motivation through his consistent presence during all my path at Politecnico di Torino. I am very lucky because he has always been by my side and he will be.

I would like to extend my gratitude to all of my friends who were there for me during my time in Torino, thank you for being my Torinese family. Your enduring support together with your friendship made it remarkable.

Architecture has been my way of translating ideas into space. This thesis has deepened my understanding of how design and construction create enduring environments.

Lastly, I dedicate this work to those who work to improve the level of safety, intelligence and innovation in our constructed environment.

Abstract

Glass-aluminum façade systems, especially unitized curtain walls, are commonly used in high-rise buildings for their flexibility and aesthetic openness. However, the glazed surfaces of buildings suffer from severe brittle fracturing and posing a glass failure risk, particularly with regard to façade partitions; these pose significant issues when subjected to seismic forces.

This thesis seeks to explore the numerical approach for evaluating the seismic performance of these systems. This study is based on the *“Influence of Design Variables on Seismic Performance of Unitized Curtain Walls: A Parametric Experimental Study”* by Bianchi et al. (2024) in collaboration with Permasteelisa Group and TU Delft, which analyzed inter-story drift imposed onto full scale glazing units.

In this work, the in-plane seismic response of façade panels due to inter-story drift was modelled using SAP2000 with a Finite Element Method (FEM) approach. Frame elements represented the aluminum structures, shell elements for the triple-glazed units and silicone connectors were modeled as nonlinear spring elements. A study on structural performance included changes to geometry parameters of the connectors, dimensions of the panel and boundary restraint conditions. The numerical analyses for these parameters cover multiple indicators: integrated frame displacement, rotational strain of the glazing panel, distribution of bending moments in aluminum members and stress distribution both in glass and frame components.

Moreover, international regulations from Eurocode 8, ASCE 7-16, NZS 1170.5, JASS 14 and AAMA guidelines were also reviewed to understand the contextual design practices and performance criteria within a specific region. These codes capture several paradigms of designing a system which may span from force-based approaches to displacement-driven methods with varying degrees of deformation compatibility emphasis.

The results indicate that façade seismic performance is not only reliant on material strength but also influenced by connector configuration, panel geometry and boundary conditions which will aid in guiding the glazing systems towards future performance-based design objectives.

Keywords: *Seismic performance, Glass façades, Unitized curtain walls, International regulations, Inter-story drift, SAP2000 modeling, Parametric analysis.*

Table of Contents

Acknowledgment	i
Abstract	ii
Acronyms and Abbreviations.....	vii
List of Figures	x
List of Tables	xv
Chapter 1	1
Introduction.....	1
1.1. Seismic Behavior of Glazing Systems	4
1.2. Research Foundation and Aim	6
1.3. Relevance and Thesis Structure	7
Chapter 2	9
Structural Glass in Architecture	9
2.1. Evolution and Architectural Role of Glass	9
2.2. Mechanical Properties of Glass.....	15
2.3. Glass Types for Façade Systems	18
2.3.1. Annealed Glass	18
2.3.2. Heat-Strengthened Glass	19
2.3.3. Fully Tempered Glass	20
2.3.4. Laminated Glass	21
2.3.5. Chemically Tempered Glass	24
2.4. Safety and Design Considerations	25
2.5. Glass Façade Components	28
2.6. Unitized Curtain Wall Systems	33
2.6.1 Component Roles.....	33
2.6.2. Unitized and Stick-Built Curtain Wall Systems	36
2.6.3. Seismic Behavior	39
2.7. Architectural Applications of Glass Façades	41

2.7.1. Planar Curtain-Wall Façades	42
2.7.2. Curved-Form Glass Façades	44
2.7.3. Cable-Net Glass Façades.....	45
2.7.4. Climate-Adaptive (Double-Skin) Glass Façades	47
2.7.5. Point-Supported Glass Façades.....	48
Chapter 3	50
Seismic Design and Regulations	50
3.1. Global Seismic Context	51
3.2. Code Requirements for Façade Systems	54
3.2.1. European: Eurocode 8 (EN 1998)	55
3.2.2. American: ASCE 7-16 and FEMA 460/461	57
3.2.3. New Zealand: NZS 1170.5	59
3.2.4. Japan: JASS 14	62
3.2.5. American Testing Standards: AAMA 501.4 and AAMA 501.6	63
3.3. Seismic Code Comparison	66
3.4. Future Directions and Research Gaps	67
Chapter 4	69
Reference Experimental Study	69
Chapter 5	72
Numerical Modeling Strategy and Tools	72
5.1. Software and Modeling Environment	72
5.2. Element Types and Modeling Approach	73
5.3. Geometric and Mechanical Properties of the Model	74
5.3.1. Overall Panel Geometry	74
5.3.2. Aluminum Frame Properties	75
5.3.3. Glass Panel Properties	76
5.3.4. Silicone Connector Properties	77
5.4. Boundary Conditions and Loading.....	81

Chapter 6	83
Structural Response of the Glazing Unit	83
6.1. Displacement Response of the Frame	83
6.1.1. Frame Elongation (ϵ)	84
6.1.2. Frame Rotation (α)	85
6.1.3. Frame Distortion (θ)	85
6.2. Bending Moment Distribution in the Aluminum Frame	86
6.3. Von Mises Stress Distribution in the Aluminum Frame	88
6.4. Displacement Response of the Glass	91
6.5. Principal Stress in the Glass Panel.....	96
6.6. Principal Stress in the Silicone Connectors	98
Chapter 7	101
Parametric Numerical Study	101
7.1. Influence of Silicone Geometry	102
7.1.1. Bending Moment Distribution in the Aluminum Frame	103
7.1.2. Von Mises Stress Distribution in the Aluminum Frame	105
7.1.3. Displacement Response of the Glass.....	106
7.1.4. Principal Stress in the Glass Panel	108
7.1.5. Principal Stress in the Silicone Connectors.....	109
7.1.6. Parametric Evaluation of Silicone Geometry	112
7.2. Influence of Panel Dimension	113
7.2.1. Displacement Response of the Frame	115
7.2.2. Bending Moment Distribution in the Aluminum Frame	116
7.2.3. Von Mises Stress Distribution in the Aluminum Frame	117
7.2.4. Displacement Response of the Glass.....	119
7.2.5. Principal Stress in the Glass Panel	123
7.2.6. Parametric Evaluation of Panel Dimension	125
7.3. Influence of Restraint Condition.....	127
7.3.1. Displacement Response of the Frame	128

7.3.2. Bending Moment Distribution in the Aluminum Frame	130
7.3.3. Von Mises Stress Distribution in the Aluminum Frame	132
7.3.4. Glass Panel Displacement and Rotation	134
7.3.5. Principal Stress in the Glass Panel	139
7.3.6. Parametric Evaluation of Restraint Condition	141
Chapter 8	144
Conclusion	144
REFERENCES	146

Acronyms and Abbreviations

IGUs	Insulated Glazing Units
PBEE	Performance-Based Earthquake Engineering
PEER	Pacific Earthquake Engineering Research Center
PBD	Performance-Based Design
SAP2000	Structural Analysis Program
FEA	Finite Element Analysis
PBPD	Performance-Based Design
UCW	Unitized Curtain Wall
BIM	Building Information Modeling
NEHRP	National Earthquake Hazards Reduction Program
FEMA	Federal Emergency Management Agency
NIST	National Institute of Standards and Technology
NSF	National Science Foundation
USGS	United States Geological Survey
ASCE	American Society of Civil Engineers
SEI	Structural Engineering Institute
ULS	Ultimate Limit States
SLS	Serviceability Limit State
AII	Architectural Institute of Japan
AAMA	American Architectural Manufacturers Association
F_y	Yielding Strength
M_w	Moment Magnitude
F_a	Seismic design force (<i>Eurocode 8</i>)
W_a	Weight of the non-structural element (<i>Eurocode 8</i>)
γ_a	Importance factor (<i>Eurocode 8</i>)
q_a	Behavior factor (<i>Eurocode 8</i>)
S_a	Seismic coefficient (<i>Eurocode 8</i>)
α	Design ground acceleration ratio a _g /g (<i>Eurocode 8</i>)

S	Soil amplification factor (<i>Eurocode 8</i>)
T_a	Period of the non-structural component (<i>Eurocode 8</i>)
T₁	Period of the building (<i>Eurocode 8</i>)
Z	Height of the component above the seismic base (<i>Eurocode 8</i>)
H	Total height of the building (<i>Eurocode 8</i>)
F_p	Seismic design force (<i>ASCE 7</i>)
W_p	Weight of the component (<i>ASCE 7</i>)
I_p	Importance factor (<i>ASCE 7</i>)
a_p	Component amplification factor (<i>ASCE 7</i>)
R_p	Component response modification factor (<i>ASCE 7</i>)
S_{DS}	Design spectral response acceleration (<i>ASCE 7</i>)
Δ	Elastic inter-story drift of the building (<i>ASCE 7</i>)
Δ_{fallout}	Minimum drift capacity to prevent glass fallout (<i>ASCE 7</i>)
I_p	Component importance factor (<i>ASCE 7</i>)
D_p	Component displacement amplification factor (<i>ASCE 7</i>)
C_d	Deflection amplification factor (<i>ASCE 7</i>)
δ_{max}	Maximum allowable inter-story shear displacement (<i>ASCE 7</i>)
F_{ph}	Horizontal seismic design force (<i>NZS 1170.5</i>)
C_p (T_p)	Spectral design coefficient (<i>NZS 1170.5</i>)
C_{ph}	Horizontal response factor (<i>NZS 1170.5</i>)
F_{pv}	Vertical seismic design force (<i>NZS 1170.5</i>)
C_{pv}	Vertical response factor (<i>NZS 1170.5</i>)
C_{vd}	Vertical acceleration coefficient (<i>NZS 1170.5</i>)
R_p	Part risk factor (<i>NZS 1170.5</i>)
W_p	Weight of the part (<i>NZS 1170.5</i>)
μ_p	Ductility of the part
P-wave	Primary wave
S-wave	Secondary wave
F_v	Vertical seismic force due to P-wave (<i>JASS 14</i>)

F_h	Horizontal seismic force due to S-wave (<i>JASS 14</i>)
W	Weight of the curtain wall component (<i>JASS 14</i>)
a_v	Vertical ground acceleration (<i>JASS 14</i>)
a_h	Horizontal ground acceleration (<i>JASS 14</i>)
E	Elastic Modulus
V	Poisson's Ratio
G	Shear Modulus
T	Shear Force
A	Bonded Area
K	Shear Stiffness
ρ	Displacement
γ	Shear Strain
ε	Diagonal Elongation Strain
d_0	Initial Diagonal Length
d'	Elongated Diagonal Length
Δx	Applied Displacement
α	Frame Rotation Angle
θ	Frame Distortion Angle
M_{3-3}	Bending Moment about Local Axis 3
σ	Normal Stress
τ	Shear Stress
σ_{VM}	Von Mises Stress
U_x	Horizontal Displacement along the X-axis
U_z	Vertical Displacement along the Z-axis
R_2	Rotation about the Y-axis
δx	Centroidal Displacement
ϕ	Glass Rotation
S_{max}	Maximum Principal Stress

List of Figures

Chapter 1

Figure 1- 1. PEER-PBEE standard four stage frameworks.	2
Figure 1- 2. Test setup comparison for standard and seismic glazing.	5
Figure 1- 3. Movement of a glass plane within window frame under seismic drift.	5
Figure 1- 4. Full-scale racking test of a unitized curtain wall under drift.	6

Chapter 2

Figure 2- 1. Core-formed fine glassware of the Hellenistic era.	9
Figure 2- 2. Production process of core-molded vessels.	9
Figure 2- 3. Rose window, Chartres Cathedral, France.....	10
Figure 2- 4. Interior glazing, Sainte-Chapelle, Paris.	10
Figure 2- 5. Crystal Palace exterior, London, 1851.	11
Figure 2- 6. Crystal Palace interior during the Great Exhibition.....	11
Figure 2- 7. Glass House, Philip Johnson, 1949.....	12
Figure 2- 8. Farnsworth House, Mies van der Rohe, 1951.....	12
Figure 2- 9. Generali Tower, Zaha Hadid Architects, Milan.....	13
Figure 2- 10. Shenzhen Bao'an Airport façade, Massimiliano & Doriana Fuksas, Shenzhen.....	13
Figure 2- 11. The Shard, Renzo Piano, London.	14
Figure 2- 12. Apple Park, Cupertino.....	15
Figure 2- 13. Interior façade at Apple Park.....	15
Figure 2- 14. Stress–strain curve of glass compared with steel.	16
Figure 2- 15. Breakage pattern of annealed glass.....	19
Figure 2- 16. Fracture pattern of heat-strengthened glass.	20
Figure 2- 17. Fracture mode of fully tempered glass.....	21
Figure 2- 18. Laminated glass composition.	22
Figure 2- 19. Laminated triple glazing unit section.	22
Figure 2- 20. Comparison of breakage patterns for glass types.	23

Figure 2- 21. Residual stress profiles through the glass thickness: (a) heat-treated glass; (b) chemically toughened glass.	24
Figure 2- 22. Fracture behavior in annealed, tempered and laminated glass types.	25
Figure 2- 23. Edge-initiated cracking pattern in monolithic glass under tensile stress. ..	26
Figure 2- 24. Glass façade damage on a Houston high-rise.	27
Figure 2- 25. Insulating-glass unit.....	28
Figure 2- 26. Spacer cross-section illustrating butyl rubber and silicone sealant.....	29
Figure 2- 27. EN AW-6063-T6 aluminum extrusion.	29
Figure 2- 28. Mullion–transom joint with gasketed glass.....	30
Figure 2- 29. Section of a curtain wall framing system supporting a double-glazed unit.	31
Figure 2- 30. Exploded view of the stick-system curtain wall façade.....	31
Figure 2- 31. Schematic representation of Performance-Based Design (PBD) procedure.	32
Figure 2- 32. Unitized Curtain Wall System Components.	34
Figure 2- 33. Unitized Curtain Wall systems.	36
Figure 2- 34. Unitized and Stick-Built Curtain Wall Systems maintenance process.....	37
Figure 2- 35. Maintenance process of Unitized Curtain Wall Systems.....	38
Figure 2- 36. Connection detailing adopted for the façade configurations.	40
Figure 2- 37. Unitized curtain wall glazing system (left); possible displacement lateral shape (right).....	41
Figure 2- 38. The Shard, London.	42
Figure 2- 39. Shanghai Tower, Shanghai.	43
Figure 2- 40. One World Trade Center, New York.....	43
Figure 2- 41. Apple Park, Cupertino.	44
Figure 2- 42. Fondation Louis Vuitton, Paris.	45
Figure 2- 43. Guangzhou Opera House, Guangzhou.....	45
Figure 2- 44. Time Warner Center Atrium, New York.....	46
Figure 2- 45. Hearst Tower Lobby, New York.	46
Figure 2- 46. 30 St Mary Axe, London.	47

Figure 2- 47. Intesa Sanpaolo Tower, Turin.	48
Figure 2- 48. Louvre Pyramid, Paris.....	48
Figure 2- 49. Seattle Central Library, Seattle.....	49

Chapter 3

Figure 3- 1. The Pacific Ring of Fire, with trenches marked with blue lines.....	51
Figure 3- 2. Diagram of the geological process of subduction.	51
Figure 3- 3. Kahramanmaraş, Turkey earthquake of 2023.	52
Figure 3- 4. Typical test specimen configuration.	64
Figure 3- 5. First 30 seconds of crescendo test (AAMA 501.6).	65
Figure 3- 6. Schematic of displacement time history for dynamic crescendo test.	65

Chapter 4

Figure 4- 1. Experimental setup study showing in-plane drift test configuration	69
--	----

Chapter 5

Figure 5- 1. Front view of the façade panel model.	74
Figure 5- 2. Aluminum rectangular hollow-section with dimensions.	75
Figure 5- 3. Detailed sectional diagram of a triple-glazed unit.....	77
Figure 5- 4. a) Spring layout on panel edges (front). b) Axonometric view, Y-axis orientation.....	78
Figure 5- 5. Glass–frame silicone connector cross-section.	79
Figure 5- 6. Silicone joint shear schematic with dimensions and forces.	80
Figure 5- 7. Boundary conditions, 24 mm top-corner displacement.	82

Chapter 6

Figure 6- 1. Elongation (ϵ) of the diagonal caused by in-plane shear.	84
Figure 6- 2. Rotation (α) of the vertical member due to lateral drift.	85
Figure 6- 3. Distortion (θ) of the internal angle reflecting racking deformation.....	86
Figure 6- 4. Moment distribution (M3-3) in the aluminum frame.	87
Figure 6- 5. Von Mises stress distribution in the aluminum frame.....	89

Figure 6- 6. Stress-strain curve of 6063-T6 aluminum alloy.	90
Figure 6- 7. a) SAP2000 model; b) Deformation under 24 mm in-plane displacement... 91	
Figure 6- 8. Joint 1-displacement output from SAP2000 (left-bottom corner).	92
Figure 6- 9. Joint 4-displacement output from SAP2000 (left-top corner).	92
Figure 6- 10. Joint 179-displacement output from SAP2000 (centroidal joint).	94
Figure 6- 11. The centroid (Joint 179) displacements, the SAP2000 results.	95
Figure 6- 12. Glass-panel kinematics under lateral drift.	95
Figure 6- 13. Maximum principal stress distribution in the glass.	96
Figure 6- 14. Stress-strain curve of laminated glass.	97

Chapter 7

Figure 7- 1. Moment distribution (M3-3) in the aluminum frame.	103
Figure 7- 2. Von Mises stress distribution in the aluminum frame.	105
Figure 7- 3. Type B-Deformed shape	107
Figure 7- 4. Type C-Deformed shape	107
Figure 7- 5. Maximum principal stress distribution in the glass panel.	108
Figure 7- 6. Comparison of principal tensile stress by connector stiffness.	111
Figure 7- 7. Frame Dimension Variants.	114
Figure 7- 8. Moment distribution (M3-3) in the aluminum frame.	116
Figure 7- 9. Von Mises stress distribution in the aluminum frame.	118
Figure 7- 10. Type 1 façade unit under 24 mm in-plane displacement.	120
Figure 7- 11. Joint 4-displacement output from SAP2000 (left-top corner).	120
Figure 7- 12. Joint 176-displacement output from SAP2000 (centroidal joint).	121
Figure 7- 13. Type 6 façade unit under 24 mm in-plane displacement.	121
Figure 7- 14. Joint 104-displacement output from SAP2000 (left-top corner).	122
Figure 7- 15. Joint 200-displacement output from SAP2000 (centroidal joint).	122
Figure 7- 16. Maximum principal stress distribution in the glass panel.	124
Figure 7- 17. Matrix of support configurations.	127
Figure 7- 18. Deformed SAP2000 model under COMB1.	130

Figure 7- 19. Moment distribution (M3-3) in the aluminum frame.	131
Figure 7- 20. Von Mises stress distribution in the aluminum frame.	133
Figure 7- 21. Type 3-Façade unit under COMB1.	135
Figure 7- 22. Type 3-Joint 4-displacement output from SAP2000 (left-top corner).	135
Figure 7- 23. Type 3-Joint 179-displacement output from SAP2000 (centroidal joint)..	136
Figure 7- 24. Type R-Façade unit under COMB1.	137
Figure 7- 25. Type R-Joint 4-displacement output from SAP2000 (left-top corner).	138
Figure 7- 26. Type R-Joint 179-displacement output from SAP2000 (centroidal joint)..	138
Figure 7- 27. Maximum principal stress distribution in the glass panel.	140

List of Tables

Chapter 1

Table 1- 1. PBEE loss variables for cost, downtime and casualty streams 3

Table 1- 2. Façade-specific decision variables. 4

Chapter 2

Table 2- 1. Comparative Mechanical Properties of Structural Glass Types 17

Table 2- 2. Component-level functions, quality-control checks and seismic roles within a unitized curtain wall cassette. 35

Table 2- 3. Key Distinctions Between Unitized and Stick-Built Curtain Walls. 38

Chapter 3

Table 3- 1. Seismicity matrix for façade design guidance. 53

Table 3- 2. Behavior Factors (q_a) for Non-Structural Elements (Eurocode 8). 56

Table 3- 3. Part Risk Classification..... 60

Table 3- 4. Part Response Factor, C_{ph} and C_{pv} 61

Table 3- 5. Seismic Performance Grades under JASS 14 63

Table 3- 6. Seismic Design Code Comparison Table 67

Chapter 5

Table 5- 1. Material properties for EN AW 6063-T6 aluminum..... 76

Table 5- 2. Material properties for laminated glass..... 76

Table 5- 3. Material properties for structural silicone. 78

Table 5- 4. Stiffness Calculation Steps of Silicone Rubber Connector. 80

Table 5- 5. Parameters for calculating Shear Stiffness (K). 81

Chapter 6

Table 6- 1. Glass corner-joint displacements by SAP2000. 92

Table 6- 2. Parameters for displacement and rotation calculations. 93

Table 6- 3. Shear Reactions for Silicone Connectors. 98

Table 6- 4. Shear-Stress Parameters for Silicone Connector Evaluation.....	98
Table 6- 5. Stress Results and Tensile Capacity.....	100

Chapter 7

Table 7- 1. Matrix of bonded area configurations for silicone connectors.....	102
Table 7- 2. Peak M3-3 Bending Moment in the aluminum frame by connector type.	104
Table 7- 3. Peak Von Mises stress in the aluminum frame by connector type.....	106
Table 7- 4. Glass centroidal translation and rotation outputs by connector type.....	107
Table 7- 5. Maximum principal tensile stress in the glass panel by connector type.	109
Table 7- 6. Link 2 – In-Plane Shear Forces (24 mm drift).	110
Table 7- 7. Silicone Connector Stress-to-Strength Check.	110
Table 7- 8. Structural response by silicone connector geometry.....	112
Table 7- 9. Matrix of panel geometry variations.	114
Table 7- 10. Frame kinematics by panel variant (24 mm drift).....	115
Table 7- 11. Peak M3-3 Bending Moment in the aluminum frame by panel variant.	117
Table 7- 12. Peak Von Mises stress in the aluminum frame by panel variant.	119
Table 7- 13. SAP2000 output parameters for glass-panel movement.	119
Table 7- 14. Glass centroidal translation and rotation outputs by panel variant.....	123
Table 7- 15. Maximum principal tensile stress in the glass panel by panel variant.....	125
Table 7- 16. Structural response by panel dimension variants.	126
Table 7- 17. Corner joint displacements (Ux, Uz) for Type 3 and Type R under COMB1.	129
Table 7- 18. Peak M3-3 Bending Moment in the aluminum frame by restraint variant. .	132
Table 7- 19. Peak Von Mises stress in the aluminum frame by restraint variants.	134
Table 7- 20. Glass centroidal translation and rotation outputs by restraint variant.	139
Table 7- 21. Maximum principal tensile stress in the glass panel by restraint variant. .	141
Table 7- 22. Structural response by restraint condition variants.	142

Chapter 1

Introduction

The role of glass in architecture has transformed greatly to become one of the most defining materials of contemporary buildings. In the modern day, glass is valued for both its aesthetic value and serving practical purposes. It serves as multi-functional architectural element as well as structural piece. Glass is now employed by architects in load-bearing façades, walkable floors and even whole transparent shells that respond to the demand for openness and daylight. Contemporary architects have marked landmark buildings demonstrating the dual role glass can play in architectural narratives.

The increase in the use of glass in architecture also corresponds to advances in production technology. The float glass process ensures uniform thickness and flawless surfaces, while thermal and chemical tempering increases strength and thermal resistance; safety, sound and blast insulation can also be achieved through lamination. Glass has also been transformed with the addition of insulated glazing units (IGUs), specialized coatings, as well as embedded sensors, which allow for environmental control, glare reduction and energy production. Passive glass has now become an active building envelope component that supports comfort, performance and well-being of occupants due to these advancements.

Nonetheless, the shift from cladding to structure requires an equivalent change in structural engineering and seismic design approaches. While the use of glass allows for greater visual transparency and reduction in material used, glass as a structural element poses problems as it is brittle in nature and does not tolerate inelastic deformation. Unlike wrought iron or reinforced concrete which can dissipate energy, glass fractures under tension or concentrated stress. This renders its performance unfavorably under seismic loads. In an earthquake, buildings undergo lateral floor displacements or inter-story drift which leads to rigid joint deformation that threatens the integrity of glass façade joints [1]. Insufficient accommodation of such movement may result in edge loading which can cause cracking or total panel fallout.

Façade failures in practice tend to be more complex, including hazards such as glass breakage, leaking fluids, thermal inefficiencies or even falling debris, all while the primary structure remains intact [2]. It highlights treating curtain walls as fully immersed in the building's intricate dynamic response as a system especially in critical operational environments in medical facilities, aviation hubs or high-rise structures. In contrast, conventional practice tends to treat façades as independent lines of non-structured elements, which results into obsolescence of detailed seismic protective measures governed by code-based frameworks.

In this regard, Performance-Based Earthquake Engineering (PBEE) is widely regarded as the most suitable framework for evaluating non-structural systems [1]. The work reported here tailors the existing PEER-PBEE procedure for glazing by: (i) constructing new fragility curves that relate inter-story drift and floor acceleration, drawing on recent shake-table tests; (ii) adding life-cycle carbon costs to the classic 3D's (dollars, downtime and deaths); and (iii) integrating these loss functions into a user-friendly tool that ranks retrofit and new-design options for high-rise buildings according to economic, environmental and social performance [3]. The Pacific Earthquake Engineering Research Center (PEER) has formalized this approach into a standard four-stage workflow, summarized in Figure 1-1.

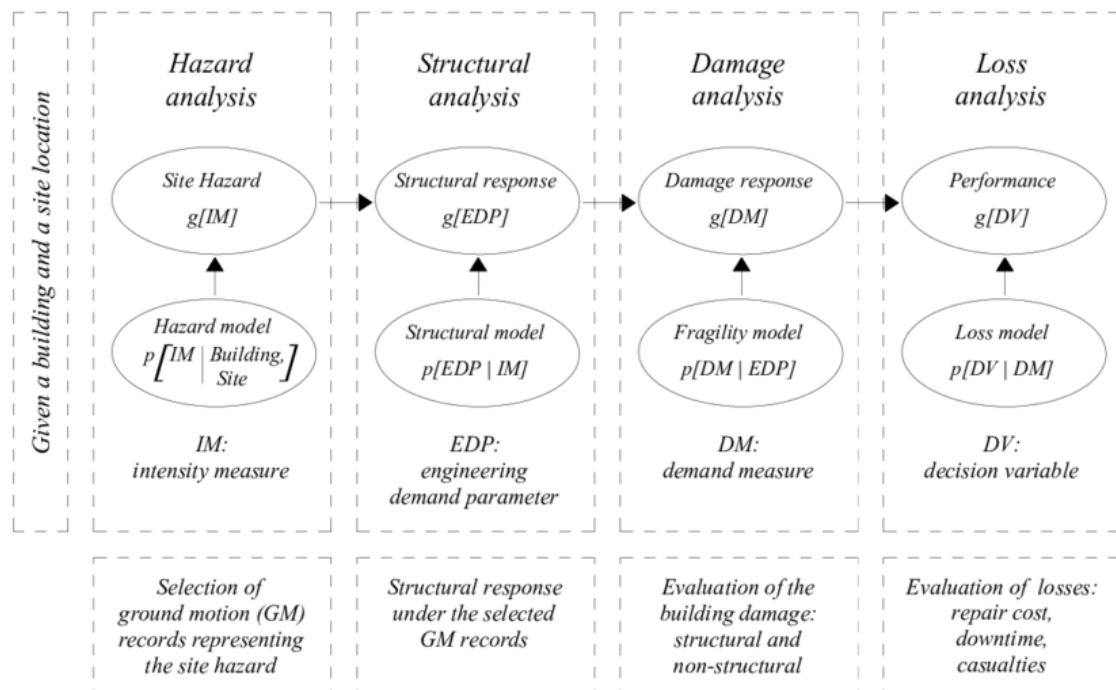


Figure 1- 1. PEER-PBEE standard four stage frameworks.

Figure 1-1. adapted from: https://www.researchgate.net/publication/283622415_Does_seismic_risk_affect_the_environmental_impact_of_existing_buildings

- **Hazard Analysis**, where the site-specific annual frequency of exceedance for each chosen intensity measure (IM) is computed;
- **Structural Analysis**, in which the prescribed IM is translated into engineering-demand parameters (EDPs) such as peak inter-story drift and floor acceleration;
- **Damage Analysis**, during which the fragility functions relate each EDP to observable damage measures (DMs);
- **Loss Analysis**, in which each DM is assigned physical, economic and social consequences (collectively termed decision variables (DVs), and the results are aggregated to produce risk metrics that are meaningful to owners, insurers and regulators.

Within the PBEE framework, façade systems are treated as clear performance goals instead of mere by-products of the structural layout. Probabilistic demand models translate earthquake intensity into inter-story drift patterns, while component fragility functions turn those drifts into damage odds for glazing, anchors and sealants.

Table 1- 1. PBEE loss variables for cost, downtime and casualty streams [4].

PBEE level	Damage-Cost	Downtime	Death
IM (intensity measure)	Ground-motion parameter	Ground-motion parameter	Ground-motion parameter
EDP (engineering-demand parameter)	Maximum drift	Maximum drift or floor acceleration	Maximum drift
DM (damage measure)	Extent of structural or non-structural damage	Extent of damage/repair required	Extent of damage and probability of collapse or debris impact
DV (decision variable)	Repair / replacement cost	Length of closure for repair	Probability and number of casualties

This step-by-step breakdown allows designers to set façade-specific thresholds and to measure in clear, monetary terms how different connections or materials lower risk for owners, insurers and regulators alike. Consequently, PBEE turns glass curtain walls from mere visual skin into engineered components that play a vital role in overall resilience of building system (Table 1-2.).

Table 1- 2. Façade-specific decision variables.

Decision Variables	Quantification for glass façades
Damage-Cost (Dollars)	Measure the area of broken glass or bent frames, multiply by the usual repair price per square meter, then add the cost of scaffolding and contractor fees.
Casualties (Deaths)	Take the chance that falling pieces kill or injure someone per square meter and multiply by how many people are normally in that spot.
Functional interruption (Downtime)	Add up the days repair crews need on site and the extra days spent on inspections, permits and getting equipment in place.

1.1. Seismic Behavior of Glazing Systems

Façade systems exhibit a distinctive line of seismic weakness in their incapacity to allow for in-plane drift. Standard glass infill systems employed in unitized curtain wall panels struggle with lateral movement due to their rigid connection along with assembly tolerances. On the other hand, seismic glazing systems are designed with flexible gaskets or connections that allow differential movement between the frame and glass without failure [2].

Figure 1-2. shows the behavioral difference between standard glazing systems (Type 1) and seismic glazing systems (Type 2). Standard systems are dominated by inter-story drift and fail under glass breakage due to stress concentration at the corners and edge. Seismic systems, however, permit relative displacement between the glazing frame and the outer seismic frame, which greatly reduces the chance of fracture [2].

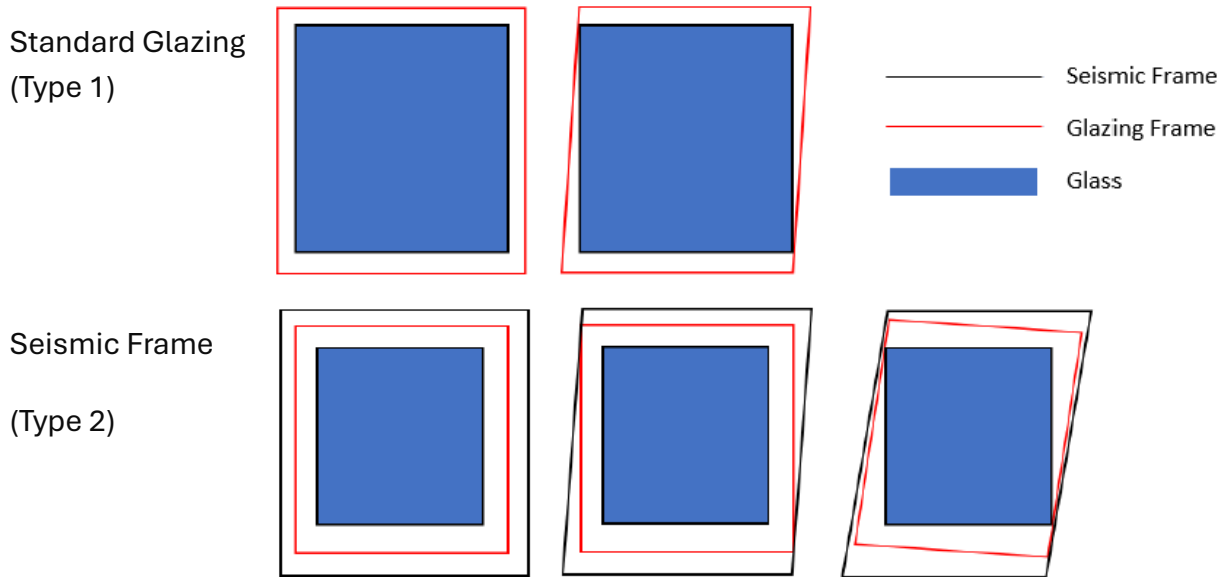


Figure 1- 2. Test setup comparison for standard and seismic glazing.

The mechanical behavior of a glass panel subjected to lateral movement is more complex than it appears. When inter-story drift is applied, the frame undergoes deformation that introduces both translational and rotational movement to the glass pane. A typical panel does not only undergo linear displacement as illustrated in Figure 1-3., but also considerable in-plane rotation, which induces diagonal stress paths leading to corner cracking [5].

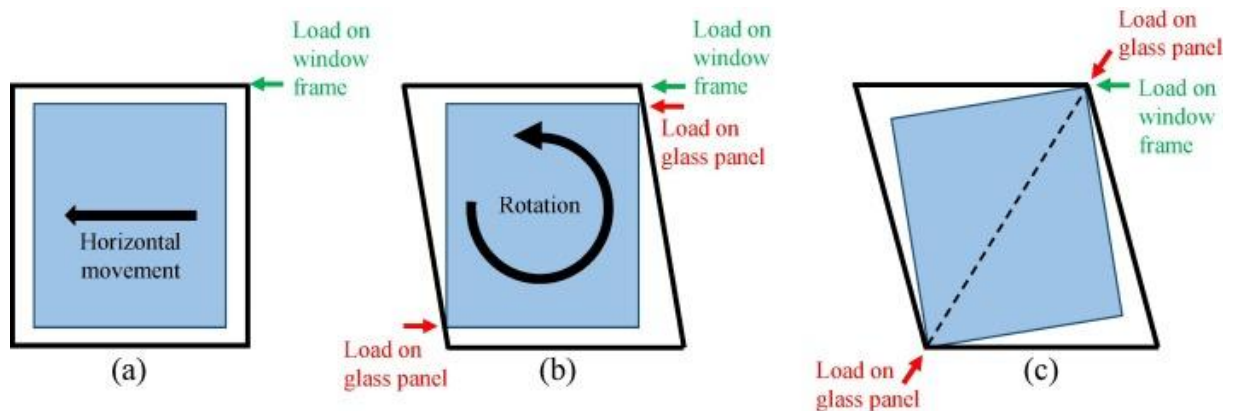


Figure 1- 3. Movement of a glass plane within window frame under seismic drift.

Figure 1-2. adapted from: https://www.researchgate.net/publication/352414726_Performance_comparison_of_standard_and_seismic_glazing_systems

Figure 1-3. adapted from: <https://www.sciencedirect.com/science/article/pii/S2352012423001133>

To understand these behaviors, full-scale test setups simulating seismic loading through racking simulations are conducted (Figure 1-4.). These setups use horizontal actuators to apply displacement to the glazed façade specimens mounted between floor beams, simulating inter-story drift [6]. Experimental results validate that glass panel failure frequently initiates at locations where rigid fixation occurs against setting blocks or where edge gaps are insufficient to permit in-plane motion. This highlights the critical role of connection detailing, tolerances and restraint design in reducing damage during an earthquake [6].

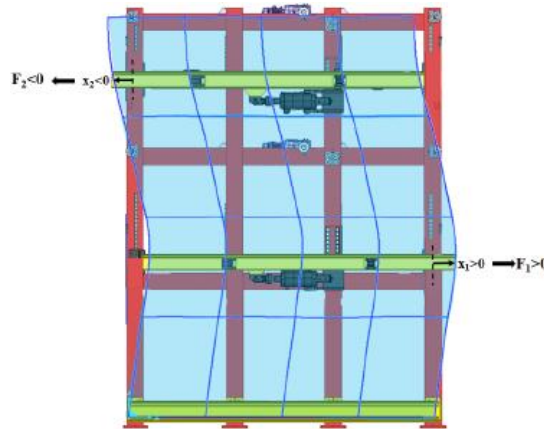


Figure 1- 4. Full-scale racking test of a unitized curtain wall under drift.

1.2. Research Foundation and Aim

This thesis explores the unitized curtain wall panels structural behavior with respect to seismic drift, enhancing the field's understanding. The focus lies on panel systems with triple glazed insulated glass, aluminum supporting frames and structural silicone joints connecting them. The research methodology involves a full-scale experimental study performed by Permasteelisa Group, one of the world's leading façade engineering and contracting companies, in collaboration with TU Delft University [7].

This research further extends the experimental framework with numerical simulation performed in Structural Analysis Program (SAP2000), a finite element analysis (FEA) software with prominence in structural and façade engineering. The work starts with digitally replicating Type 3 reference panel model, a unitized glazed façade bonded within an aluminum frame using structural silicone connectors, which acts as the baseline model.

Figure 1-4. adapted from: https://www.researchgate.net/publication/333396140_The_Role_of_Details_for_Seismic_Performance_of_a_Full_Scale_Glass_Façade

1.3. Relevance and Thesis Structure

The relevance of this research is in the gap it bridges between the physical testing and modeling of a façade system digitally as it is under seismic loading. While experimental studies are essential for collecting empirical data on the failure modes and mechanical responses of unitized glazing systems, numerical simulation helps explore a broader and more flexible exploration of design parameters, enabling more accurate performance predictions across numerous configurations by engineers and architects.

This thesis aims to refined strategies for designing based on the performance of non-structural façade elements, particularly for regions prone to earthquakes where envelope integrity is critical for occupant safety and building functionality. This study enhances understanding on optimization of resilience of unitized curtain wall systems by providing insights through the systematic evaluation of connector design, panel size and restraint conditions relative to realistic displacement. The results foster architectural creativity and innovation in design as well as the evolution of international standards like Eurocode 8 [8], ASCE 7 [9] and CEN/TS 19100 [10] which are embracing the active role of dynamic façades in seismic safety.

Thesis Structure:

Chapter 2 starts with the basics of structural glass, its evolution and outlines its mechanical properties, associated treatments such as tempering and lamination and manufacturing processes relevant to façade systems. Furthermore, it analyzes the architectural reasoning for employing glass as a structural material and how transparency, lightness and innovation define its use in modern building envelopes.

Chapter 3 focuses on the non-structural elements of a building, primarily the curtain walls, and their seismic response to earthquake loading. It describes inter-story drift, racking effects and glass panel failure mechanisms and discusses some of the key regulations and PBPD (performance-based design) concepts relevant to façade design from a seismic perspective.

In Chapters 4 to 7, the analytical core of the thesis is presented, documenting parametric modeling carried out in SAP2000. Each chapter focuses on a specific set of parameters, including connector geometry and panel proportions and boundary restraint conditions and presents their corresponding structural responses. The analysis also covers displacement patterns, stress distribution in the glass and aluminum components, bending moment development and shear behavior of the connectors under lateral drift coupled with self-weight.

In Chapter 8, the thesis has been concluded with an overview of the major outcomes from all the simulation scenarios. It analyzes the most important elements determining the seismic performance and gives precise instructions on how to improve the design of unitized curtain wall systems.

Within this framework, the thesis builds a comprehensive understanding of how structural glass façades perform during seismic events, offering both theoretical knowledge and practical guidance for architects, engineers, and industry professionals.

Chapter 2

Structural Glass in Architecture

2.1. Evolution and Architectural Role of Glass

Each stage in the development of glass showcases a society's values, technological advancements and artistic ambitions. The use of glass as a luxury item dates back over four millennia to ancient Egypt and Mesopotamia, where craftsmen shaped vessels of glass and stone into opaque containers utilizing the core-forming method. This technique involved heating glass to a liquid state and then cooling it while shaping into simplistic figures that served ritual and ornamental purposes (Figure 2-1.). Glass began to be used more widely in construction by the Romans during the 1st century BCE as it became easier to produce thinner and more translucent glass using the glassblowing technique. The more decorative use of public infrastructures like bathhouses and villas by Roman builders included the first small glass panes, a step towards the use of transparent enclosures, though expensive glass was still considered a luxury (Figure 2-2.) [11][12].

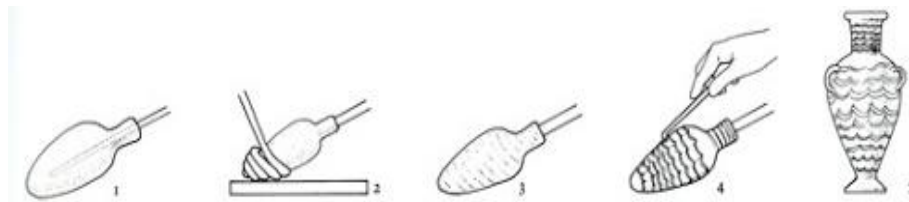


Figure 2- 1. Core-formed fine glassware of the Hellenistic era.

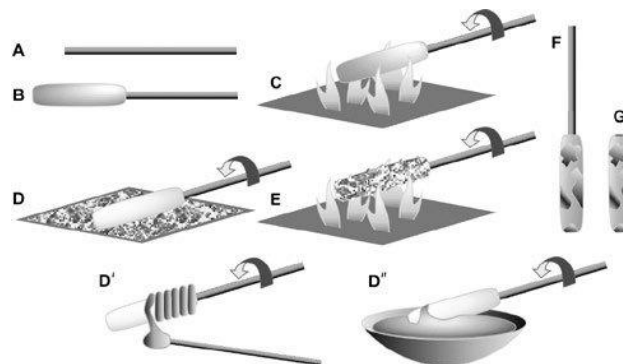


Figure 2- 2. Production process of core-molded vessels.

Figure 2-1. adapted from: <https://storymaps.arcgis.com/stories/66349c9dcd994bd4be52e37115ce34e0>

Figure 2-2. adapted from: https://www.researchgate.net/figure/Production-of-core-molded-vessels-A-metal-or-wooden-rod-B-formation-of-core-form_fig3_335528649

The use of glass in Gothic architecture in Europe signified a new form of artistic expression. Glass became a medium for divine storytelling through stained glass windows, which adorned sacred spaces with colorful narrative scenes. Glass was transformed from a material into a message in works, such as the rose window of Chartres Cathedral in France (Figure 2-3.) and the full-height-stained glass walls of Sainte-Chapelle in Paris (Figure 2-4.). While these large-scale glazed elements are often seen as structurally passive, they only became possible due to stone engineering advancements like flying buttresses and pointed arches. These structural innovations permitted immense vertical voids to be filled with light in cathedral walls, firmly establishing glass as a spiritual and architectural element [13].

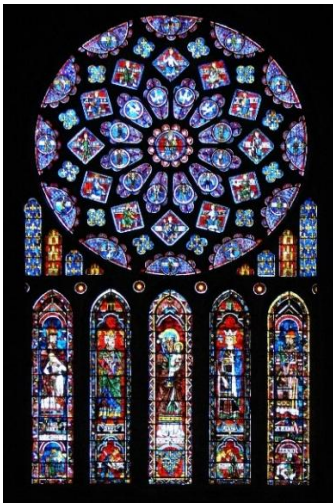


Figure 2- 3. Rose window, Chartres Cathedral, France.



Figure 2- 4. Interior glazing, Sainte-Chapelle, Paris.

The 19th century brought about a major turning point with the introduction of new techniques such as cylinder, crown, and later the plate glass method during the Industrial Revolution. These techniques made the production of glass cheaper, easier and more efficient, paving the way for its use in monumental public buildings. The most iconic of these was the Crystal Palace, designed by Joseph Paxton for the Great Exhibition of 1851 in London. The structure was remarkable as it consisted of over 300,000 factory-made glass panes which were bolted onto a cast-iron frame that was assembled off-site. It was completed in less than nine months, with a floor area exceeding 77,000 square meters. It was the largest enclosed space on the planet at that time.

Figure 2-3. adapted from: <https://www.worldhistory.org/article/1277/the-stained-glass-windows-of-chartres-cathedral>

Figure 2-4. adapted from: <https://www.sainte-chapelle.fr/en/discover/history-of-the-sainte-chapelle>

The Crystal Palace was the first building constructed with industrial glass, which later became a fundamental characteristic of modern architecture (Figures 2-5. and 2-6.). The building not only used glass extensively but also set new standards for its transparency as well as the use of prefabrication connected to modular architectural design, laying the foundation for contemporary façade systems [14].



Figure 2- 5. Crystal Palace exterior, London, 1851.



Figure 2- 6. Crystal Palace interior during the Great Exhibition.

With the rise of architectural modernism in the 20th century, glass was embraced as a symbol of transparency, rationalism and openness. The float glass invention by Pilkington in 1959 allowed for the production of long and perfectly flat glass sheets. This embraced modernist glass ideals since it enabled architects to dissolve barriers between the interior and the exterior spaces of the building.

Figure 2-5. adapted from: <https://www.wadhursthistorysociety.org/the-story-of-the-crystal-palace/>

Figure 2-6. adapted from: <https://www.britannica.com/topic/Crystal-Palace-building-London>

Glass became the façade of the building instead of simply filling the openings. This change can be seen in Philip Johnson's Glass House (1949) in Connecticut (Figure 2-7.) which is fully immersed in the landscape while providing complete structural visual immersion. They transformed the role of glass in architecture: instead of filler, it is incorporated as an integral part of architectural expression. Another example is Ludwig Mies van der Rohe's Farnsworth House (1951) in Illinois (Figure 2-8.) which is one of the most radical examples of minimalist living, a structure made entirely of glass and steel [15].



Figure 2- 7. Glass House, Philip Johnson, 1949.



Figure 2- 8. Farnsworth House, Mies van der Rohe, 1951.

In the contemporary era, the use of glass has evolved to include structural functions and responsive features. The ability of glass to bear loads, resist impacts and meet rigid thermal and acoustic demands has been possible due to advanced technologies such as tempering, lamination and insulating glazing units. The design of walkable glass floors, glass bridges, glass columns and even glass beams is now possible. The static and dynamic mechanical behavior of glass is also enhanced by structural silicone, spider

Figure 2-7. adapted from: https://www.reddit.com/r/ArchitecturePorn/comments/13xh4dn/farnsworth_house_plano_il_mies_van_der_rohe_1951/

Figure 2-8. adapted from: <https://www.architecturaldigest.com/story/architect-philip-johnson-glass-house-modernism-article>

systems and hybrid assemblies. In addition, windows are incorporating glass as part of intelligent façades that include photovoltaic layers, electrochromic coatings and sensor-based shading systems, thus redefining the envelope as an active environmental regulator. This combination of glass's transparency, adaptability and performance makes it a key material for sustainable and high-performance architecture today [16].

Leading façade contractors such as Permasteelisa Group have helped achieve large-scale innovations, and their projects demonstrate the modern curtain wall systems' aesthetic and technical integration [17]. Notable examples include Generali Tower in Milan by Zaha Hadid Architects with its curved glass panels mounted on a twisted skyscraper body (Figure 2-9.). Another example is Shenzhen Bao'an International Airport by Fuksas, which showcases unitized glass façades set within complex double-curved surfaces (Figure 2-10.).



Figure 2- 9. Generali Tower, Zaha Hadid Architects, Milan.

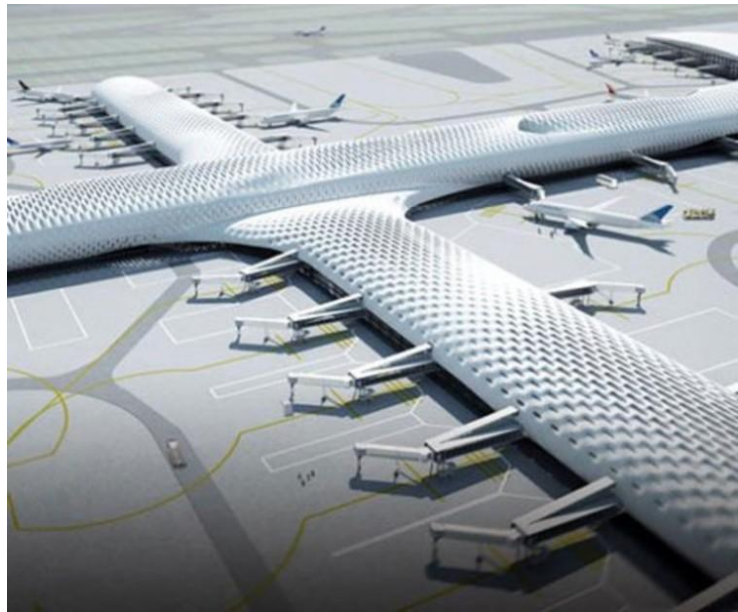


Figure 2- 10. Shenzhen Bao'an Airport façade, Massimiliano & Doriana Fuksas, Shenzhen.

Figure 2-9. adapted from: <https://glassforeurope.com/generali-tower/>

Figure 2-10. adapted from: <https://www.archdaily.mx/mx/02-8463/aeropuerto-internacional-de-shenzhen-terminal-3-massimiliano-doriana-fuksas>

The Shard in London by Renzo Piano (Figure 2-11.) soaring over 300 meters exemplifies low-emissivity and laminated glazing's environmental, structural and architectural advantages. The tower's sharply tapering, soaring form is clad with 11.000 individual glass panels mounted in angled planes that change the light reflection as the day progresses, enhancing the crystalline effect. More than just stunning visuals, the glass façade incorporates high-performance triple glazing with selective solar coatings engineered to reduce heat gain while maximizing daylight. These systems are integrated into the unitized curtain wall that also accommodates wind load, movement, thermal bridging and façade solar gain. Thus, the glass becomes more than a visual envelope and instead a multi-layered façade system that contributes to the energy performance, indoor environmental quality, structural expression and comfort of the building.



Figure 2- 11. The Shard, Renzo Piano, London.

Another noteworthy example is Apple Park located in Cupertino, California, which was designed by Foster + Partners (Figure 2-12. and 2-13.). The main ring-shaped headquarter building contains the world's largest curved structural glass panels, each measuring over 14 meters and weighing multiple tons. These panels perform more functions than clad portions of the building. They are essential for the building's thermal and seismic response. The installation of vertically curved glass around the building ensures unobstructed panoramic view while withstanding lateral forces and differential movement.

Figure 2-11. adapted from: <https://www.giftround.co.uk/blog>

The engineering is astonishing especially considering the seismic nature of the area. Both The Shard and Apple Park showcase a new era of architecture where glass must perform under structural, environmental and aesthetic criteria. These projects prove that glass, which was once limited to ornament and infill, is now a fully integrated, multifunctional building material, capable of defining and enhancing the resilience of large-scale architecture.



Figure 2- 12. Apple Park, Cupertino.



Figure 2- 13. Interior façade at Apple Park.

This shift from ornamental and symbolic to performative and structural use of glass history provides important context to this thesis. The boundaries of glass used in architecture have shifted from purely aesthetic or daylighting purposes. With the increasing height and complexity of buildings, glass is expected to take on roles usually attributed to steel or concrete, such as in seismic design. This thesis works on that line by studying the structural performance of glass in unitized curtain wall systems under seismic loading, connecting centuries of evolution with the most modern engineering techniques focused on performance.

2.2. Mechanical Properties of Glass

Glass is an example of an amorphous, non-crystalline solid material, which is distinguished by compressive strength and brittleness with a high elastic modulus. Unlike ductile construction materials like steel or aluminum, glass does not deform plastically. From the viewpoint of a structural engineering, glass has a linear-elastic response up to failure after which it breaks suddenly. This behavior stems from the lack of a crystalline lattice in the atomic structure of glass, which means no dislocation mechanisms for accommodating plastic flow. Therefore, tensile stress approaching a material's maximum threshold results in instantaneous fracture without warning or residual deformation [18][19].

Figure 2-12. and 2-13. adapted from: <https://www.fosterandpartners.com/projects/apple-park>

Modulus of elasticity (E), Poisson's ratio (V), tensile and compressive strength, shear modulus (G) and other fundamental mechanical properties of glass differ with manufacturing process and treatment type. However, for most types of soda-lime silicate glasses (used in architectural applications), the Elastic Modulus (E) is relatively stable at approximately 70.000 MPa and the Poisson's Ratio (V) is around 0,23 [20].

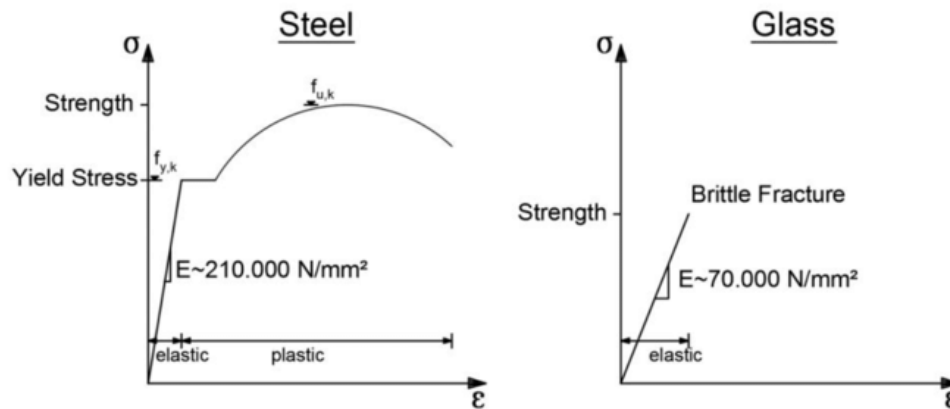


Figure 2- 14. Stress–strain curve of glass compared with steel.

Figure 2-14. illustrates the stress-strain behavior of annealed glass in comparison to structural steel. The glass curve exhibits linear behavior until it shatters suddenly and catastrophically, showing no plastic deformation zone or yielding plateau. On the other hand, steel shows an elastic phase, followed by plastic deformation and strain-hardening, allowing ductility and energy dissipation. This comparison underscores the importance of compensatory methods, such as lamination and flexible joints in structural design that incorporates glass in earthquake-prone areas [21].

Glass is characterized by being strong in compression but weak in tension, which is governed by tensile strength values. In most scenarios, bending-induced tensile stresses become critical especially at edges, openings and points of mechanical restraint. Surface flaws, micro-cracks and residual stresses from cutting or thermal treatment make tensile failure of glass highly sensitive [22].

Figure 2-14. adapted from: https://www.researchgate.net/figure/Stress-strain-curves-of-steel-and-glass-for-an-uniaxial-tensile-loading-scenario-redrawn_fig50_313662114

It is critical to understand that the characteristic strength values given in EN 16612 and ASTM E1300 standards are probabilistic. This is very important in the design practice and in the evaluation of the seismic performance of the structures, these values incorporate partial safety factors due to the reliability of the glass and safety of life calculations. Therefore, the design strength of glass is not a constant value, but rather a probabilistic value which depends on numerous factors such as load duration, glass type, thickness, edge treatment and environmental factors [23].

Table 2- 1. Comparative Mechanical Properties of Structural Glass Types [20][22][23].

Properties	Unit	Annealed Glass	Heat-Strengthened Glass	Fully Tempered Glass	Laminated Glass	Chemically Tempered Glass
Elastic modulus (E)	MPa	70.000	70.000	70.000	70.000	70.000
Poisson's ratio (V)	-	0,23	0,23	0,23	0,23	0,23
Shear modulus (G)	MPa	28.455	28.455	28.455	28.455	28.455
Yielding Strength (fyi)	MPa	45	70	120	45	150
Post-Fracture Behavior	-	Brittle Shards	Large Cracks	Cubes	Retains integrity through	Local cracks
Safety After Failure	-	None	Low	Moderate	High (through interlayer)	High

The key mechanical properties of structural glass are summarized in Table 2-1. It also includes the properties of laminated glass which were used as input data in the SAP2000 numerical modeling for this thesis.

Formula of Shear Modulus:

$$G = E / [2(1+V)]$$

Within this thesis, a laminated triple-glazing unit is employed following the full-scale Permasteelisa–TU Delft experimental study. The numerical models of these assemblies are done in SAP2000, which allows for parametric studies of the glass–frame–connector elements and their interaction under lateral drift loading. Moreover, platforms like ABAQUS are recognized in literature for their simulations of complex stress distributions, fractures or energy dissipation in seismic events. These software tools enable engineers to analyze façade systems and assess their mechanical response with regard to deformation, stress-damage and the safety margins against failure, which provides invaluable information on critical structural response processes. Consequently, the mechanical behavior of glass framed structures guides the simulations performed in this research and informs the creation of strategies for building envelopes that withstand extreme conditions.

2.3. Glass Types for Façade Systems

The selection of glass type for architectural façades is very important to their performance concerning the environment, structure and seismic activities. Each glass possesses varying degrees of strength and safety, and their post-breakage behavior and fabrication traits differ. In terms of seismic design, these differences are critical, the glazing systems have to endure inter-story drift, dynamic acceleration and post-fracture retention without hazardous fallout. This section describes the five primary glass types used in façade systems: annealed, heat strengthened, fully tempered, laminated glass and chemically tempered, and used in modern curtain walls, with emphasis on their structural and seismic performance.

2.3.1. Annealed Glass

One of the most common types of glass used in construction is annealed glass, which is also referred as float glass. It is the result of a float process where molten glass is poured over a pool of molten tin and cooled in a controlled furnace called an annealing Lehr. This process encourages slow cooling which relieves thermal stresses, resulting in flat panes of glass with high optical clarity.

An overview of brittle fracture characteristics of glass materials is imbedded in Figure 2-15. With regard to safety and hazard risk, it's important to note that glass materials which undergo catastrophic breakage are mostly unsuitable for applications where safety is a priority. This is also true for buildings that are subject to dynamic loads, such as wind pressure, impacts or seismic motions.



Figure 2- 15. Breakage pattern of annealed glass.

Unlaminated annealed glass is normally excluded in areas with high seismic risk or where building codes require enhanced occupant protection. However, glass is still commonly used in non-load-bearing partitions, internal glazing and protected external applications, where safety concerns related to mechanical glass breakage are not primary [20].

2.3.2. Heat-Strengthened Glass

Heat-strengthened glass is a type of semi-tempered glass created through a thermal procedure that improves its mechanical strength and thermal stress resistance while retaining some fracture characteristics of annealed glass. From a mechanical perspective, heat-strengthened glass has about twice the strength of standard annealed glass, having a bending strength of 70 MPa and an unchanged elastic modulus.

As with other glass types, heat-strengthened glass has a failure mode, however it differs from fully tempered glass by not shattering into small granular pieces. Instead, it cracks into larger and more predictable fragments, which generally remain held in place (Figure 2-16.). This reduces the risk of immediate panel fallout during seismic events or vibrations induced by wind. Therefore, the glass is suitable for laminated applications where post-breakage safety is critical [24].

Figure 2-15. adapted from: <https://ggames.com/glass/toughening-and-heat-treating>

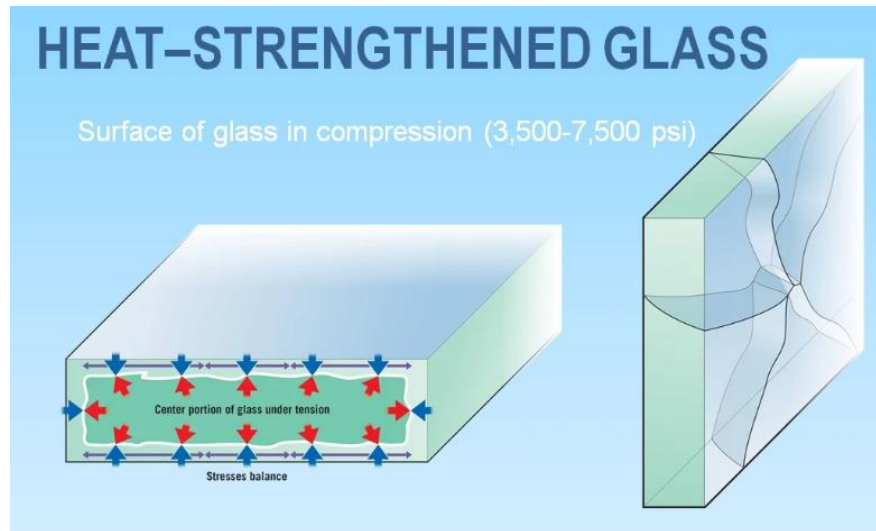


Figure 2- 16. Fracture pattern of heat-strengthened glass.

Although heat-strengthened glass cannot be used solely as safety glass on its own due to the size and sharpness of its fragments, it performs well in laminated form for seismic applications. In-plane drift and dynamic loading are more resilient, especially when bonded with ductile structural silicones or when installed in unitized frames intended for movement absorption. This combination aids in delaying panel fallout while preserving façade integrity during seismic excitation.

2.3.3. Fully Tempered Glass

Fully tempered glass, also called as toughened glass, is made by heating annealed glass to about 620-650°C, then cooling it quickly to create high surface compressive stress. This allows the glass to achieve a bending strength of up to 120 MPa which is nearly four times what annealed glass can achieve. The higher strength and better tempered thermal resistance of toughened glass makes it an ideal material for high-performance applications, like safety-critical applications [21].

Tempered glass is categorized under safety glass because of its unique behavior after breaking. It breaks into small, blunt edged granular particles (Figure 2-17.). This behavior is particularly helpful for overhead, railing or high-occupancy façade systems. However, unlike laminated glass, it does not retain any load-bearing capacity after breakage, which can be a disadvantage in seismic applications unless employed in a laminated or bonded assembly.

Figure 2-16. adapted from: <https://glassed.vitroglazings.com/topics/heat-strengthened-vs-tempered-glass>

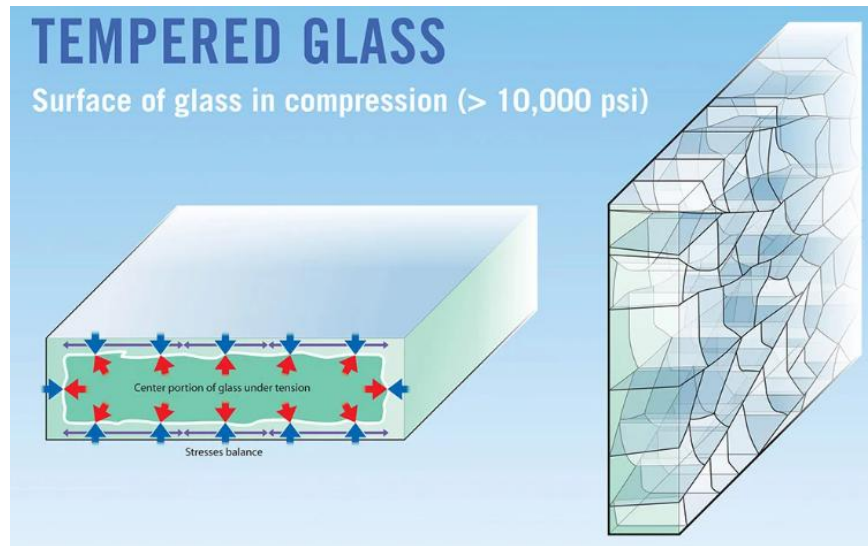


Figure 2- 17. Fracture mode of fully tempered glass.

Along with its advantages, fully tempered glass cannot be altered by cutting, drilling or modification of any type after tempering. Any post-processing must occur before the tempering cycle. In unitized curtain walls, especially in seismic regions, this glass is often combined with structural silicone bonding or lamination to address the lack of post-breakage integrity.

2.3.4. Laminated Glass

Laminated glass is produced by bonding two or more panes of glass with an interlayer, which makes it a safety glass product. Laminated glass is one of the most reliable glazing solutions for areas that are prone to seismic activity, high traffic zones and blast resistant façades due to its impact resistance and structural strength.

When glass breaks, the interlayer holds the fractured glass pieces and adds some level of protection against loading. This is important for seismic protection where glass can break due to in-plane drift and racking. Laminated IGUs (insulated glazing units) provide support with silicone structural adhesives to the frame, which helps prevent fallout and preserve the building envelope during earthquake-induced movements [23].

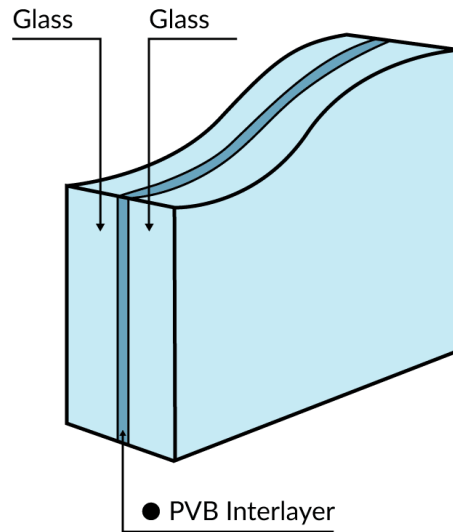


Figure 2- 18. Laminated glass composition.

Laminated glass provides additional insulation of acoustic, UV protection and explosions. Its flexible nature allows for embedding coatings, mesh or photovoltaic films between the layers without compromising the glass's structural integrity. For safety reasons, laminated glass is commonly used in performance-based curtain walls, railings, canopies and floor systems.

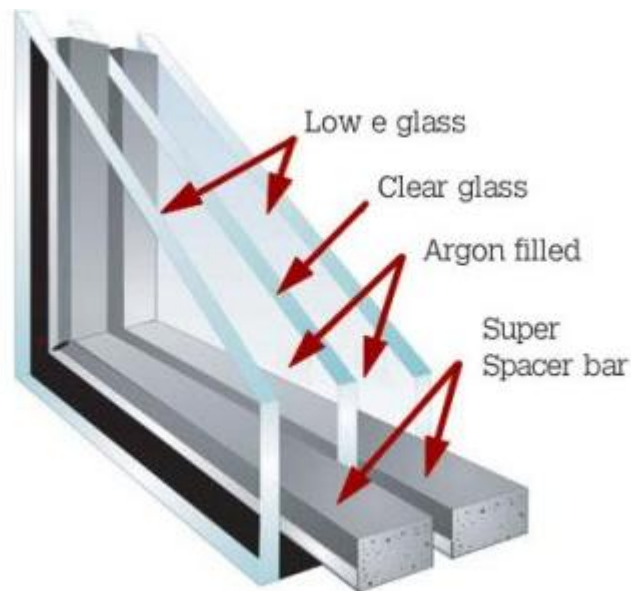


Figure 2- 19. Laminated triple glazing unit section.

Figure 2-18. adapted from: <https://dynamicfenestration.com/laminated-glass-benefits/>

Figure 2-19. adapted from: <https://www.comparegardenroomsuk.co.uk/triple-glazed/>

For this study, laminated triple glazing is used in unitized curtain wall panels subject to seismic drift simulations. This multilayer arrangement increases performance due to the laminated safety glass with insulating features of two heat-treated glass panes and a third separated by an inert gas cavity. The advantage of using laminated units is crucial in regards to post-breakage integrity and for thermally shattering, acoustically silencing and withstanding impacts on the façade, which are increasingly critical in advanced building envelopes.

The glass composition depicted in Figure 2-19. includes coatings and fillings of low-emissive layers, argon gas, along with structural spacer bars. This configuration aids realistic modelling of stress concentration as well as the deformation behavior over time under seismic loading. With the SAP2000 software, lateral drift and gravity load simulations are run using the glass system to predict façade response and safety performance.

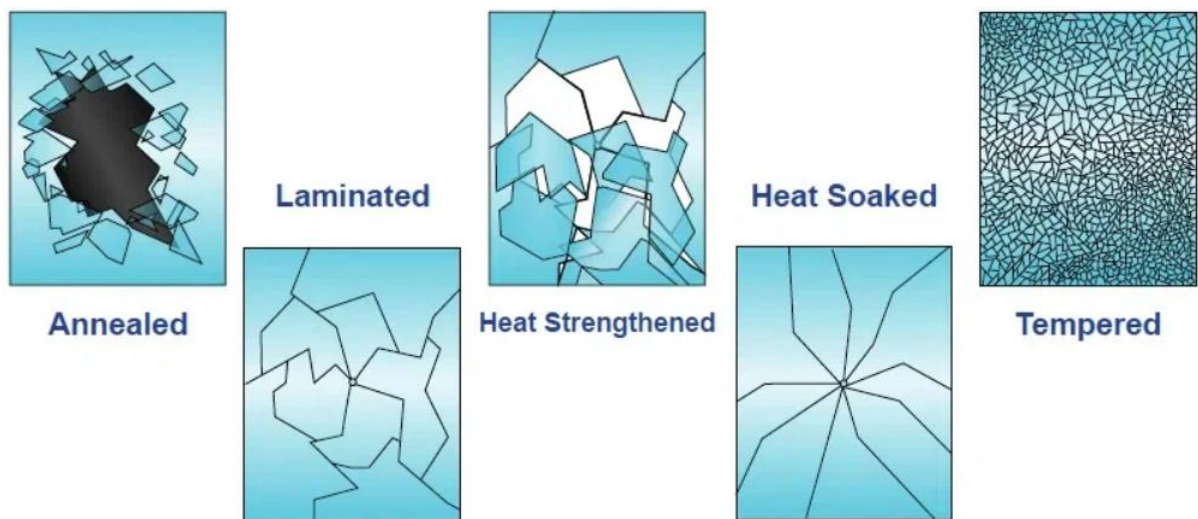


Figure 2- 20. Comparison of breakage patterns for glass types.

Figure 2-20. adapted from: <https://www.migoglass.com/info/the-difference-between-heat-strengthened-and-t-75795203.html>

2.3.5. Chemically Tempered Glass

Chemically tempered glass is obtained from an ion-exchange process where smaller sodium ions in the glass surface are exchanged for larger potassium ions while the glass is in a molten salt bath. As a result of this treatment, the surface of the glass undergoes a high compressive stress layer which increases the glass's mechanical strength without causing any optical distortion or thermal deformation. The compressive stresses can go beyond 800 MPa and the flexural strength can be as high as 150 MPa [20][24].

Even though surface strength is high for chemically tempered glass and ideal for thin and complex shapes, it remains brittle and breaks sharp fragments. This is a key safety drawback for comparison with thermally tempered glass. Due to this reason the application of chemically tempered glass in earthquake-prone areas is often restricted to laminated versions, which is where an interlayer retains shattered fragments and enables better performance after breaking.

Figure 2-21. compares the residual stress distribution of glass that has been chemically toughened to glass that has been heat treated (thermally tempered). The grillage structure shows that heat treated glass has a gradual compressive stress profile that extends deeper into the glass body. On the other hand, chemically strengthened glass exhibits a distinct sharp, compressive zone concentrated close to the surface. This provides an edge over fortified façade panels that require tight tolerances or low optical distortion as the glass can remain more dimensionally precise [25].

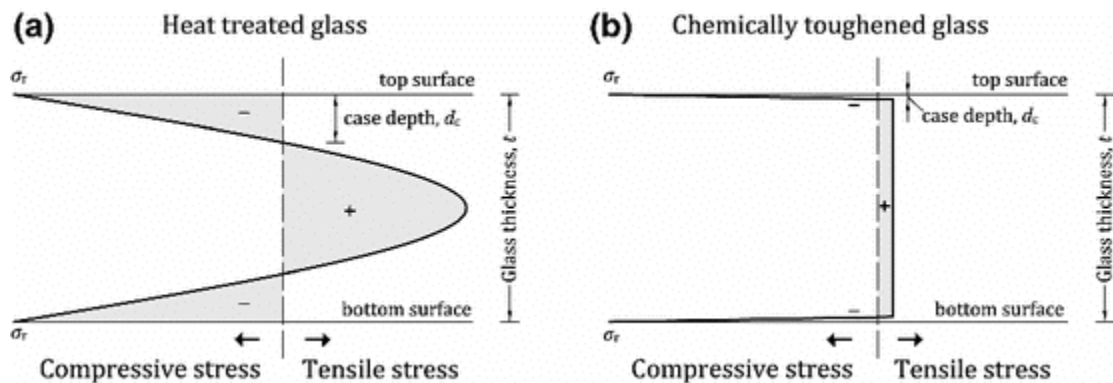


Figure 2- 21. Residual stress profiles through the glass thickness: (a) heat-treated glass; (b) chemically toughened glass.

Figure 2-21. adapted from: https://www.researchgate.net/figure/Residual-stress-profile-through-the-glass-thickness-for-a-heat-treated-and-b-chemically_fig1_318291365

2.4. Safety and Design Considerations

Ensuring safety in the application of structural glass in a building's curtain wall involves more than just picking a particular glass type. Although each glass variant has its own strength profile, real-world performance hinges on how edges are treated, panes are supported, frame restrain moves, connections allow flexing and the system handles broken glass during shaking, strong wind or thermal expansion [26][27][28].

The way each glass types break remains a primary concern for architects, engineers and occupants. Annealed glass shatters into large, sharp shards that can cause serious injury risk. Heat-strengthened panes crack into fewer but still sharp pieces, while fully tempered units crumble into small, cube-like granules that lower the risk of injury. Laminated panels, held together by a tough polymer, stay mostly intact even after impact, an extra safeguard in seismic areas. Figure 2-22. shows each breakage pattern side by side and notes the safety risks tied to them [26].

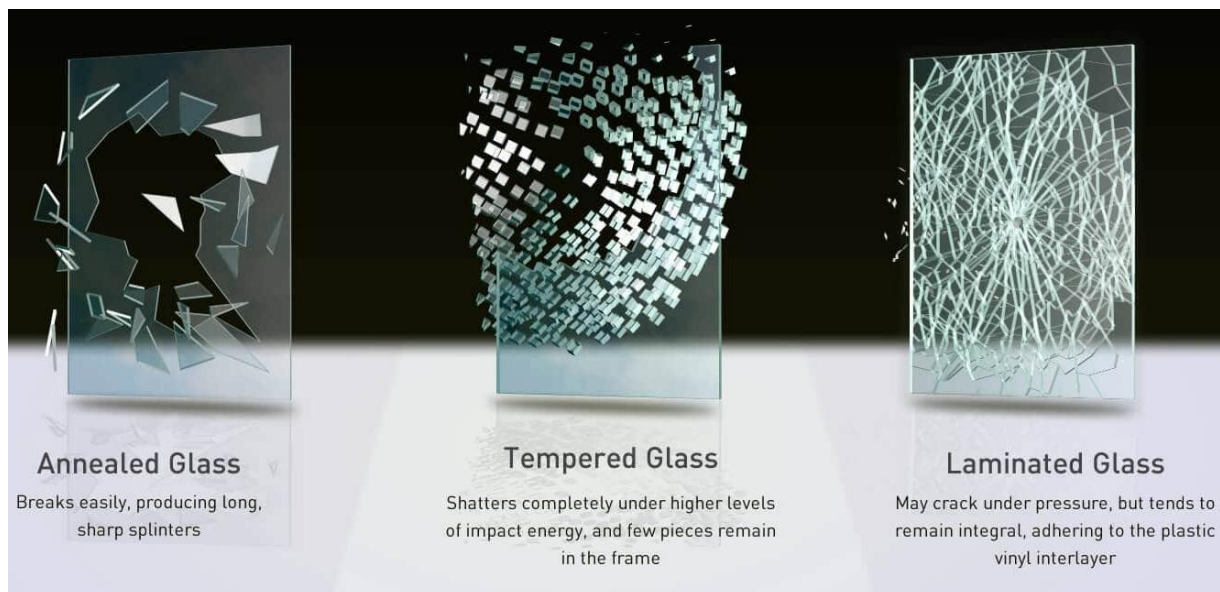


Figure 2- 22. Fracture behavior in annealed, tempered and laminated glass types.

Figure 2-22. adapted from: <https://www.trueblueglass.com.au/common-types-of-glass/>

The quality of an edge largely determines how much tensile strength a component has and how well it endures over time. Small scratches or micro-sized cracks on cut or unpolished edges often start breaks when the glass is pulled, bent or moved unevenly (Figure 2-23.). Guidelines such as EN 16612 and ASTM E1300 therefore emphasize that designers clearly identify each edge type-ground, polished or seamed-before finalizing plans. In addition, subjecting tempered glass to a heat soak lowers the chance of sudden failure from nickel sulfide particles, failures which may appear months after the glass is installed [28].



Figure 2- 23. Edge-initiated cracking pattern in monolithic glass under tensile stress.

The shape and detail of the framing system directly affects the forces move through the building and how safe the outer skin remains. Stiff aluminum frames, for instance, can concentrate stress at corners or anchorage points, whereas joints designed to move let those forces spread more evenly. When the substructure can bend, panels are able to sway during an earthquake instead of cracking right away, a behavior that noticeably boosts seismic durability.

In unitized curtain walls, structural silicone sealants act as a vital safety mechanism. The sealant not only transfer the load from glass to frame; it also absorbs the small or large gaps that shifting heat or shaking ground might create. Its performance hinges on key properties (shear stiffness, stretch limit and long-term aging), which determine whether the joint can bend, store energy and survive without peeling apart or losing bond [29]. Clear guidelines such as ETAG 002 and ASTM C1184 specify dimensions, curing and surface prep so that every joint performs reliably across the whole service life of the façade [21][31].

Both the dimensions and aspect ratio of a glass panel significantly govern its overall behavior and mode of failure. Narrow panels, or those with excessive width compared to height, tend to develop high stress concentrations at the corners and free edges, particularly under seismic loading. Numerical models run in SAP2000 or ABAQUS capture these regions as peak stress zones, indicating the need for extra framing, thicker lamination or increased interlayer thickness [27][29].



Figure 2- 24. Glass façade damage on a Houston high-rise.

An illustrative example appeared during recent post-storm inspections, including the severe glazing failure on a high-rise downtown building in Houston, Texas on May 17, 2024 (Figure 2-24.), when many large panels of differing aspect ratios failed because of differential movement and stress build-up. The event underscores how crucial thoughtful geometry is to keeping building's façade safe.

Post-breakage behavior is frequently ignored however it is crucial for safety and reducing damage. Laminated glass, because of its interlayer, holds shattered pieces and avoids hazardous shards, which is particularly important in atriums and sidewalks. In contrast to fully tempered monolithic glass that can completely dislodge after breaking, laminated glass designs reinforced with structural silicone retain their form and some load-bearing capacity even during cyclic movement. Bianchi et al. verified that laminated units using tested sealants could stay intact during 2%–3% inter-story drift cycles, preventing failure modes such as pull-out or edge tearing [26][27].

Figure 2-24. adapted from: <https://www.theguardian.com/us-news/2025/feb/21/hurricane-proof-skyscrapers-derechos-study>

Curtain-wall designs now routinely incorporate back-up elements like safety clips, holding gaskets and load-sharing anchors. These components work together to prevent panel ejection and limit progressive damage during earthquakes. Guidance for incorporating such features at the design stage can be found in FEMA E-74 and Japans JASS-14 [29][30].

Safety, however, is also tied to the broader environment. Thermally efficient interlayers, UV-blocking coatings, fire-rated glass and pressure-equalized profiles help maintain strength and occupant protection under multiple hazards. Although these features do not carry load directly, they lower thermal gradients and internal pressures that might otherwise weaken the panes [28].

2.5. Glass Façade Components

Structural glazing is now widely viewed as a three-material design in which glass, silicone sealant and aluminum frame act as one coordinated system. In a modern curtain wall, the glass panel carries most wind and inertia forces; the silicone bonds transmit those loads to the frame while allowing thermal expansion and racking; and the aluminum channels spread edge reactions to the buildings main structure. Examining any component in isolation almost always overlooks key load paths and hides failure modes that post-event inspections and full-scale tests have documented. Figure 2-25. presents the complete insulated glass unit, and Figure 2-26. provides a close-up of the spacer with its two-seal detail [30].

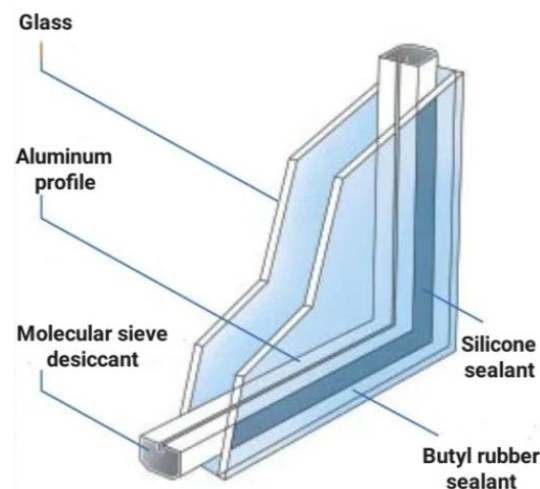


Figure 2- 25. Insulating-glass unit.

Figure 2-25. adapted from: <https://www.ljglassmachinery.com/more-glass-deep-process-articles/how-to-select-the-secondary-sealant-for-insulating-glass-the-structural-adhesive>

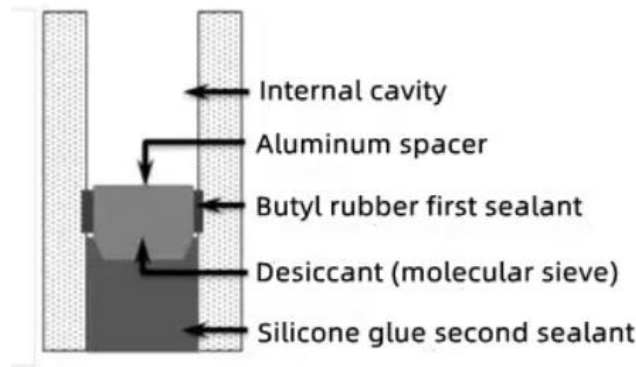


Figure 2- 26. Spacer cross-section illustrating butyl rubber and silicone sealant.

Selection of the glass type still sets the upper limit for load capacity and post-breakage performance; after a suitable plate is chosen, the focus of serviceability shifts to edge finish and sealant compatibility. Polished and beveled edges reduce the number of surface defects; the glass can carry stresses closer to nominal code limits; such edges also offer a clean chemical surface that maximizes primer wetting with one-part neutral-cure silicone.

Aluminum mullions and transoms (Figure 2-27.) are usually extruded from EN AW-6063-T6 or comparable alloys, as the magnesium-silicon heat treatment supplies an excellent stiffness-to-weight ratio and a uniform anodized surface that resists weathering. At the scale of a panel, the torsional rigidity of either box or I profile limits the amount of edge rotation the system can absorb before the bite starts to slip [33].



Figure 2- 27. EN AW-6063-T6 aluminum extrusion.

Figure 2-26. adapted from: <https://www.ljglassmachinery.com/more-glass-deep-process-articles/how-to-select-the-secondary-sealant-for-insulating-glass-the-structural-adhesive>

Figure 2-27. adapted from: https://www.theworldmaterial.com/6063-aluminum-alloy/#google_vignette

Modern curtain-wall design uses thick, thermally broken box sections joined with a precise male-female stacking system held together by pinned connections. These pins permit slight rocking during seismic drift, dissipating energy as the panels slide and reducing the peak bending moments at the corners of the glass [31]. Figure 2-28. illustrates the details, highlighting the slip-prone joint and the gasket that seals each glass panel.

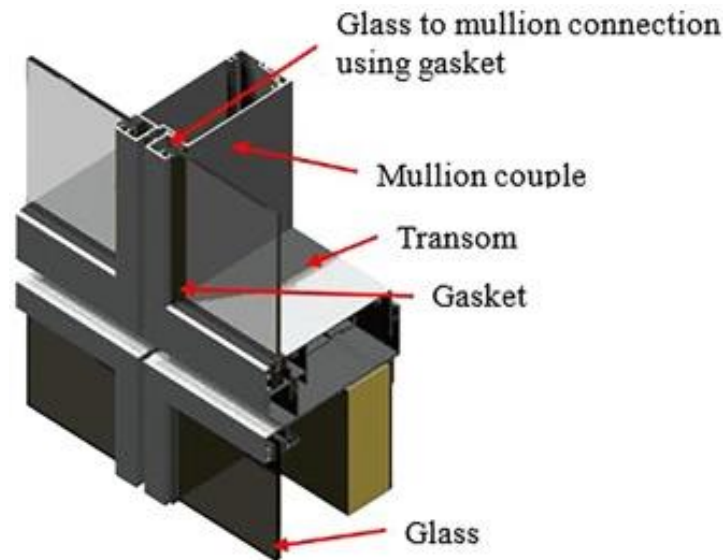


Figure 2- 28. Mullion–transom joint with gasketed glass.

Structural silicone acts as the critical adhesive seal between aluminum and glazing. If the bond is overly rigid, bending moments concentrate in the frame and tensile stress rises at the glass edge; if it is too soft, the panel rotates excessively and the gasket may pull loose [34]. Testing standards such as ETAG 002 and ASTM C1184 attempt to balance these opposing risks by setting minimum aspect ratios and mandating full-scale peel, dynamic-movement, and residual-adhesion assessments.

Since aluminum grows almost twice as fast as soda-lime glass for any given temperature increase, their differing expansion is a key concern even in temperate climates. When a horizontal run of unitized panels elongates, axial displacement pushes movement toward the edges; without a flexible seal, the built-up strain energy is released almost instantly by edge chips or a sudden tear failure in the silicone.

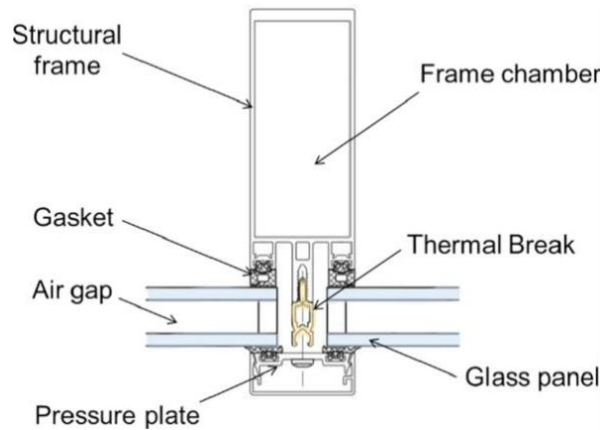


Figure 2- 29. Section of a curtain wall framing system supporting a double-glazed unit.

Modern cassette systems therefore move the structural silicone outboard of the thermal break and locate the glass on sliding, multi-directional supports (Figure 2-29.). These stainless-steel hooks or pintles let each panel shift independently, permitting inter-story drift and overall frame shortening to convert into in-plane shear instead of peeling at the bond line (Figure 2.30.) [35].

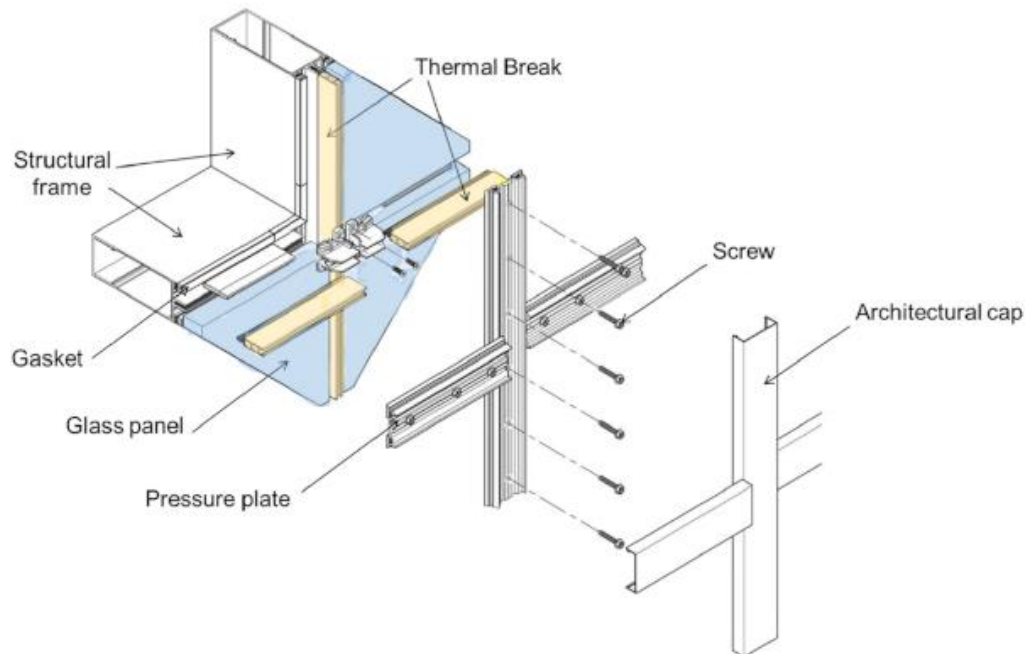


Figure 2- 30. Exploded view of the stick-system curtain wall façade.

Figure 2-29. adapted from: <https://www.glassonweb.com/article/thermal-response-curtain-wall-framing-system-under-fire-conditions>

Figure 2-30. adapted from: <https://www.glassonweb.com/article/thermal-response-curtain-wall-framing-system-under-fire-conditions>

When these elements are assembled within a performance-based design process, façade engineers usually employ a three-layer modelling approach. During the concept phase, simplified beam-spring models give an early estimate of joint slip and frame deflection. At design-development, full three-dimensional finite element analysis (Figure 2-31.) predicts local glass edge stresses, silicone strain and plastic hinges in the aluminum under extreme displacements. Ultimately, façade-specific mock-ups are tested for racking, air pressure and water tightness, which allowing designers to match analytical forecasts with on-site behavior before full production-fabrication [36].

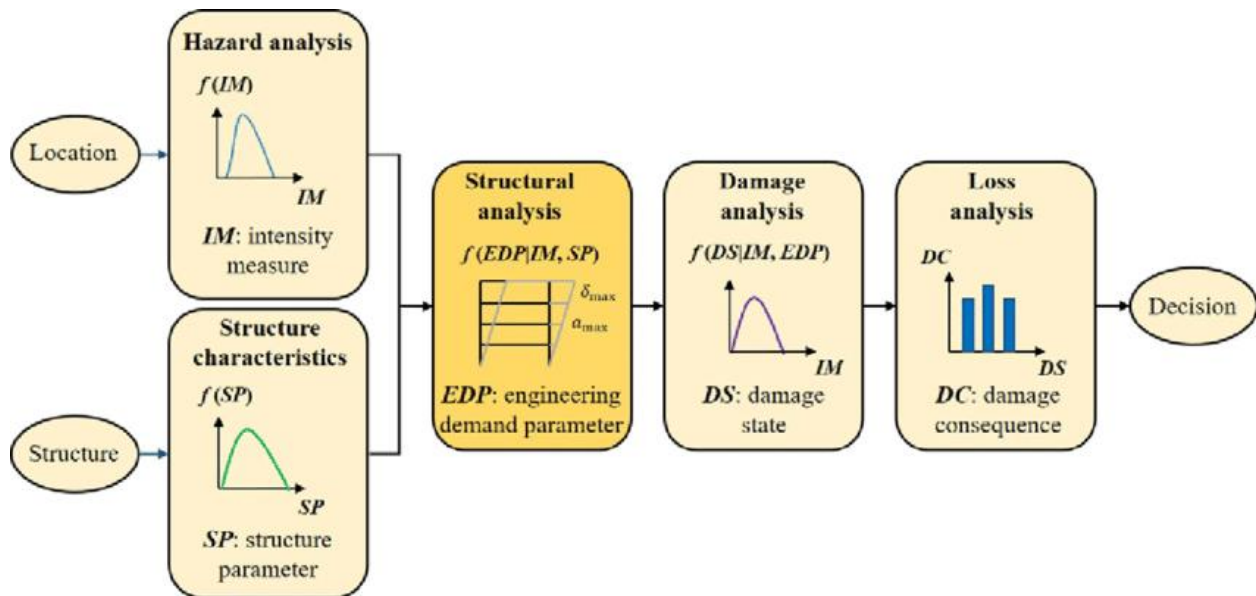


Figure 2- 31. Schematic representation of Performance-Based Design (PBD) procedure.

Recent architectural trends, such as double-curved skins, floor-to-ceiling glazing and mixed-material façades, have pushed designers to merge structure and façade more than ever before. Designers now specify hybrid cassettes that blend carbon fiber pultrusion with aluminum flanges or add tuned-silicone mass dampers at stack joints to limit noticeable motion in tall, slender towers. Such advances still depend on the material synergy outlined earlier: glass brings transparency and diaphragm action; silicone adds resilience and energy dissipation; aluminum offers precision, modularity and load redistribution.

2.6. Unitized Curtain Wall Systems

Unitized curtain wall systems (UCWs) consist of full-story panels that are glazed, gasketed, insulated and assembled in the factory so they arrive on site ready to plug directly into the buildings frame. Since glass, structural silicone, aluminum cassettes, thermal breaks and pressure-equalized drainage are all assembled under controlled factory conditions, each unit is made to millimeter precision and shipped as a nearly finished element [36]. This industrial assembly method provides three key benefits:

- **Architectural control:** Designers can choose large insulated glass units, sharp shadow joints and continuous interior reveals without fearing that distracted site trades will add stray sealant or misalign sight lines.
- **Predictable performance:** Factory conditions allow constant quality checks (optical clarity, bead thickness, gasket crush), making sure each panel meets air and water-tightness targets such as EN 12153 or AAMA 501.
- **Compressed schedules:** After the steel frame is verified, a tower crane or mast climber can set an entire fabric stack at the pace of one floor per shift, letting interior crews start weeks sooner than with stick-built walls.

2.6.1 Component Roles

A unitized curtain-wall (UCW) panel functions acts like a micro, self-sufficient building skin and it is built to factory tolerances, arrives on-site as a stiff box and mounts to pre-set anchors in minutes. Each cassette carries its own aluminum frame, glass units, structural-silicone seal, thermal break, vapor barrier, drainage channels and mounting brackets. It eliminates the scaffold assembly common to stick systems, where mullions, transoms, pressure plates and infills are linked one by one.

The engineering order can therefore be outlined hierarchically: (i) the glass itself spans wind and inertia loads as a membrane, (ii) structural silicone transfers those loads into the outer frame while allowing shear movement, (iii) the aluminum sub-frame relays reactions to the building anchors, (iv) stack joints between neighboring panels isolate inter-story drift and frame shortening, thus preventing stress build-up at corner points [38].

System components

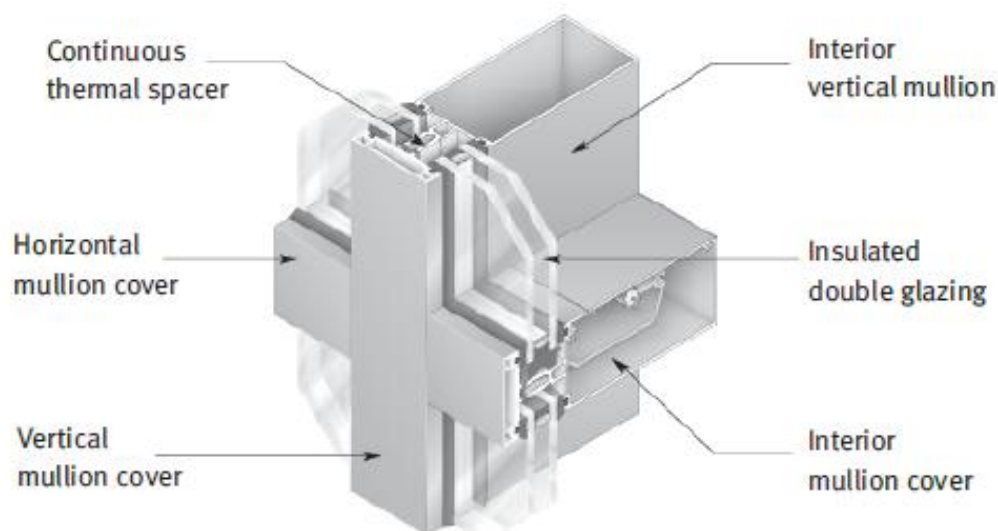


Figure 2- 32. Unitized Curtain Wall System Components.

Since every load in a unitized curtain wall passes through an identical, factory-tested chain of pieces, the design team can quickly adjust details (joint width, gasket durometer or anchor drift allowance-to meet site-specific demands) such as seismic movement, slab sag or daily thermal expansion (Figure 2-32. and 2-33.). For architects, the setup yields exceptionally narrow sight-lines, without external pressure plates, the glass aligns nearly flush with only a slim silicone or EPDM shadow joint. For façade contractors, the cassette method cuts installation time, sidesteps weather hold-ups and shifts most quality checks to the shop floor. Table 2-2. identifies each part and illustrates its role within the system.

The table illustrates how every component bear weight and still permits movement, a dual duty that gives UCW its strength. Structural silicone sits outside the thermal break so it mostly shears rather than stretches during seismic sway, and hook-and-slot anchors let each cassette drop into place yet slide sideways as the concrete floors grow or shrink [39].

Table 2- 2. Component-level functions, quality-control checks and seismic roles within a unitized curtain wall cassette.

Sub-component	Core Function	Secondary Benefit	Seismic Contribution	Typical QC Check*
Glass pane (monolithic / laminated / IGU)	Resists out-of-plane wind & live loads through plate action.	Day-lighting, acoustic damping, solar control.	Membrane stretches; corners rotate.	Optical distortion, edge polish.
Structural silicone element	Transfers glass loads into frame while permitting differential movement.	Acts as flexible gasket against air and water.	Shear-dominant energy absorption; prevents hard-spot forces.	H-pull adhesion test.
Aluminum cassette and stack joint	Distributes reactions to anchors; forms thermal-break cavity.	Hosts gaskets, sun-shades, BIPV clips.	Allows panel rocking via slotted pins; dissipates drift.	Mullion deflection mock-up.
Anchor set (gravity bracket and head restraint)	Couples panel to slab edge; carries self-weight to structure.	Horizontal adjustment for survey tolerance.	Sliding head allows inter-story drift without prying.	Slip-load rig test.

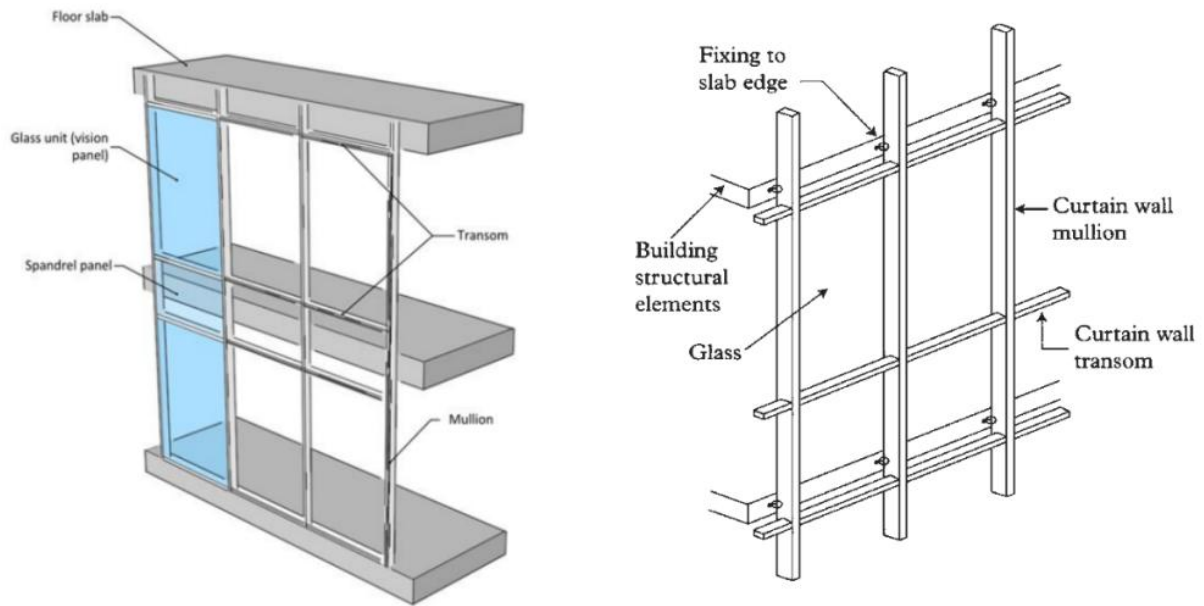


Figure 2- 33. Unitized Curtain Wall systems.

2.6.2. Unitized and Stick-Built Curtain Wall Systems

Unitized curtain wall technology has transformed the logistics, risk profile and design possibilities of high-rise building façades. In this approach, each cassette departs the factory as a sealed unit: insulated glass units (IGUs), drainage baffles, gaskets, thermal break and even internal blinds are installed to precise tolerances indoors. On site, the crew simply cranes the cassette onto a pre-leveled bracket, locks a gravity hook and seals a dry EPDM rubber or silicone joint with the adjoining panel [37] [39].

Stick-built walls take a different path. Installers bolt vertical mullions to the slab edge, cut transoms to fit and splice them in the air, then glaze each pane behind swinging safety nets. The approach stays cost-effective on low-rise buildings and irregular plans-curved atria, saw-tooth ribbons, retrofits, where every panel differs and the capital for a cassette line cannot be spread across enough units. On-site freedom, however, invites extra movement: shim packs settle, sealant cures slower in the rain and under different weather conditions and alignment depends on crews. From a structural perspective; the long, uninterrupted mullions act like vertical beams. That continuity helps the frame resist story shear, yet high bending forces appear at the glass edge if slip splices or anti-buckling pins do not limit inter-story drift [40].

Figure 2-33. adapted from: https://qstuts.com/curtain-wall-systems-types-benefits-design-and-trends/#google_vignette

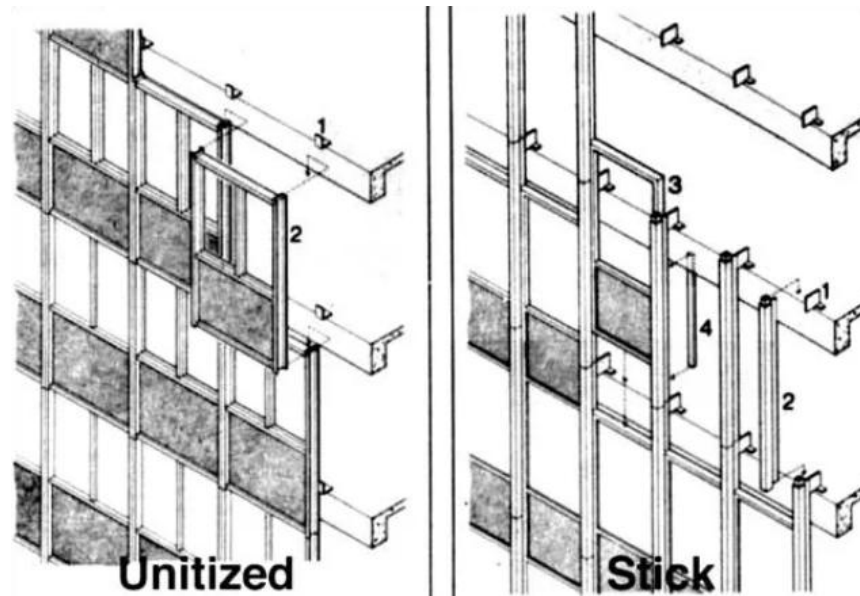


Figure 2- 34. Unitized and Stick-Built Curtain Wall Systems maintenance process.

Seismic tests highlight the differences even more clearly. Contemporary factory-made anchors now work in two stages: a gravity hook that carries routine loads and a slotted plate or spring bolt that locks in only during extreme sway. PTFE shims are set between stories, letting them slide with very little friction instead of bending the glass edge. Large-scale racking tests TU Delft and the National Research Council show unitized panels surviving 2-3% inter-story drift without losing glass, while comparable stick façades often lose gaskets or suffer edge bite at barely half that value [7].

From an architectural point of view, these unitized modules yield the all-glass aesthetic: external pressure plates disappear, mullions can hide inside the spandrel and the joint shrinks to a shadow gap. By contrast, stick systems need visible cover caps to clamp each slab, resulting in heftier sight lines. A stick wall, however, can step in and out freely, which eases the addition of shading fins, stone spandrels or other ventilated units (Figure 2-34.).

Developers are now mixing the two, pairing unitized vision units with site-hung terracotta slats or aluminum fins, a move that balances schedule gains with broader design latitude and highlights how adaptable the unitized model can be when supported by smart connections and BIM-led shop processes [40].

Figure 2-34. adapted from: <https://www.mannleecw.com/stick-vs-unitized-curtain-wall/>

Table 2- 3. Key Distinctions Between Unitized and Stick-Built Curtain Walls.

Attribute	Stick-Built Curtain Wall	Unitized Curtain Wall	Commentary
Fabrication	Site-based, weather-dependent.	Factory-based.	UCWs benefit from controlled climate and repeatable tolerances [2].
Installation speed	Sequential mullion, transom, glass.	Pre-glazed panels craned into place.	A 40-story tower can be air or watertight months earlier.
Panel size	Limited by site glazing logistics.	Limited by transport envelope.	Both accept large IGUs, but UCW avoids high-rise hoisting.
Seismic detailing	Project-specific detailing required.	Drift-rated stack joints pre-engineered.	UCW joints shake-table-tested to 3–4 % drift [5].
Maintenance mode	Individual glass replacement	Whole cassette swap or indoor reglaze.	Life-cycle strategy set during concept design.

Table 2-3 highlights the differences between the stick built and unitized curtain wall systems, focusing on ease of fabrication, speed of installation, comprehensive seismic detailing and maintenance efficiency over time. Figure 2-35. illustrates how unitized curtain wall systems enhance high-rise building performance by enabling whole cassette replacement maintenance or indoor re-glazing.

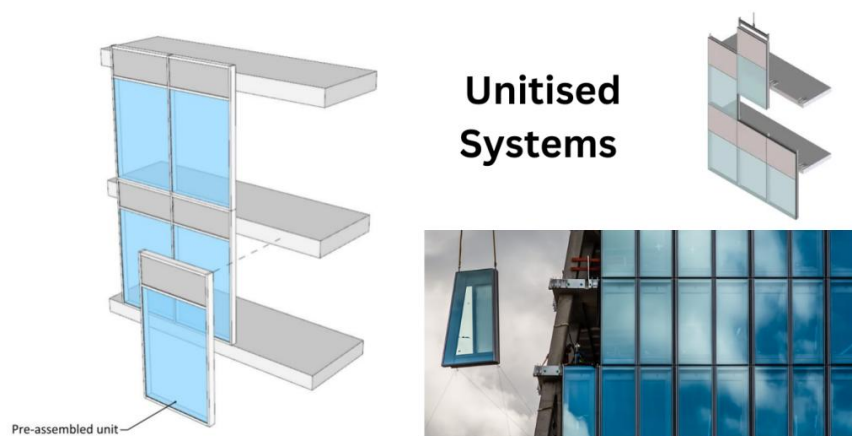
**Figure 2- 35.** Maintenance process of Unitized Curtain Wall Systems.

Figure 2-35. adapted from: <https://qstuts.com/curtain-wall-systems-types-benefits-design-and-trends/>

2.6.3. Seismic Behavior

Recent full-scale studies have advanced knowledge of unitized curtain-wall (UCW) performance far beyond the early single-story racking tests. Multi-directional shake-table experiments at UC Berkeley, TU Delft and the Colloquiate consortium show that cassette-based façades remain airtight and watertight at drift ratios that would damage stick-built glazing [26]. Three key observations appear in every test series:

- **Stack-joint mobility:** Engineered compression seals and male-female connectors absorb several centimeters of shear displacement without bending stress, passing to the insulating glazing unit. When drift forces relax, the elastomer recovers, automatically restoring the primary water barrier.
- **Fuse-plate anchors:** Consist of thin stainless-steel strips designed to fail in shear, and they are routinely slid between each curtain-wall cassette and the supporting structure. When the building is pushed hard sideways, these strips bend first, sparing the fragile glass corners and stopping the metal frame from ripping apart. Because the fuses are inexpensive, easy to check from inside, and quick to swap out after an earthquake, they add resilience without a heavy maintenance burden.
- **Captive laminated IGUs:** Rely on deep gaskets, continuous sealant and specially shaped edge blocks. When all three fit together perfectly, broken laminated layers cling to the frame and keep part of their strength. This property is vital for fire escape and exit paths, which is why modern design standards in quake-prone cities prefer laminated glass rather than monolithic, fully-tempered panels.

Since the load path follows a clear set of joints, engineers can fine-tune joint gaps, sealant shape and anchor clearances to suit inter-story drift, slab-edge sag or uneven thermal expansion. Architects gain a benefit: without external pressure plates, the glazing is shown as a single, continuous, interrupted skin broken only by a narrow shadow line.

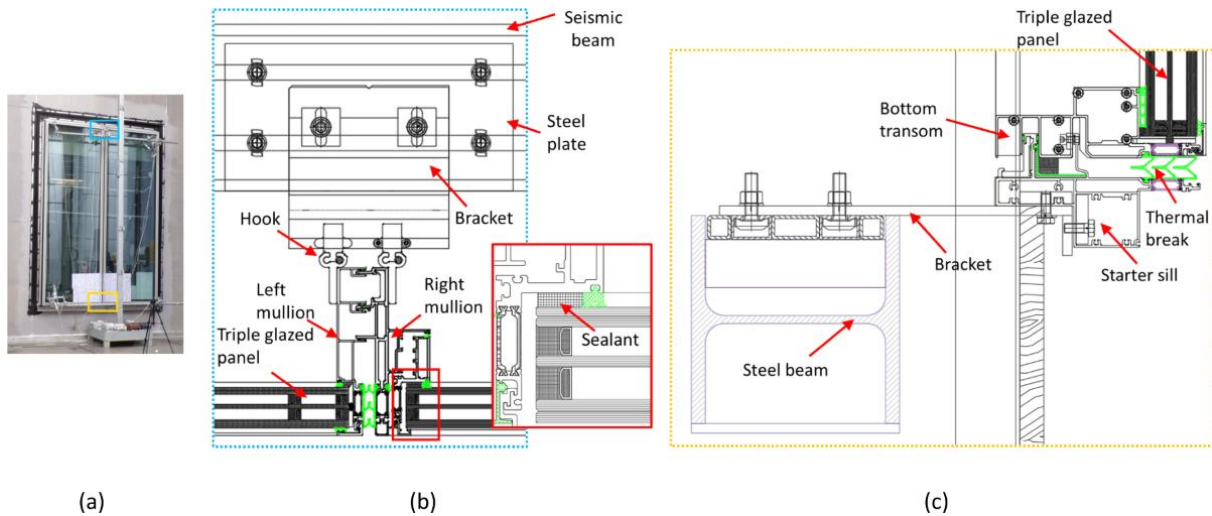


Figure 2- 36. Connection detailing adopted for the façade configurations.

Figure 2-36. illustrates this advantage in practice. It shows a two-story unitized curtain-wall mock-up mounted on a testing rig and pushed through sideways displacements while the hidden cassette anchors quietly manage drift [7].

- **In diagram (a)**, the entire cassette hangs from a steel seismic beam, while onboard sensors record side-to-side motion and monitor the airtight seal.
- **View (b)** zooms in on the hook-and-bracket junction: its elongated slot lets the panel tip a few millimeters before contact occurs, so the glass edge stays evenly pressed.
- **Diagram (c)** highlights the starter sill bracket, which resists vertical shear yet slides freely sideways; when the main frame returns to center, gravity nudges the cassette upright and the stack-joint gaskets self-close.

Figure 2-37. provides a façade-bay-scale snapshot showing how a unitized panel grid bends when story-shear is applied. The left panel displays the undeformed, gravity-only form and highlights a single cassette (in red shaded) whose width and height set the tributary area for both wind and seismic demand. The right panel, by contrast, the same grid accepts a sideways load, so mullions slide and curve, transoms twist, and the once squared cassette shears into a parallelogram. Most of that movement happens through smooth arcs in the aluminum and slight give at the panel joints, yet the glass sheets stay nearly flat [42].

Figure 2-36. adapted from: <https://doi.org/10.1007/s40940-024-00255-2>

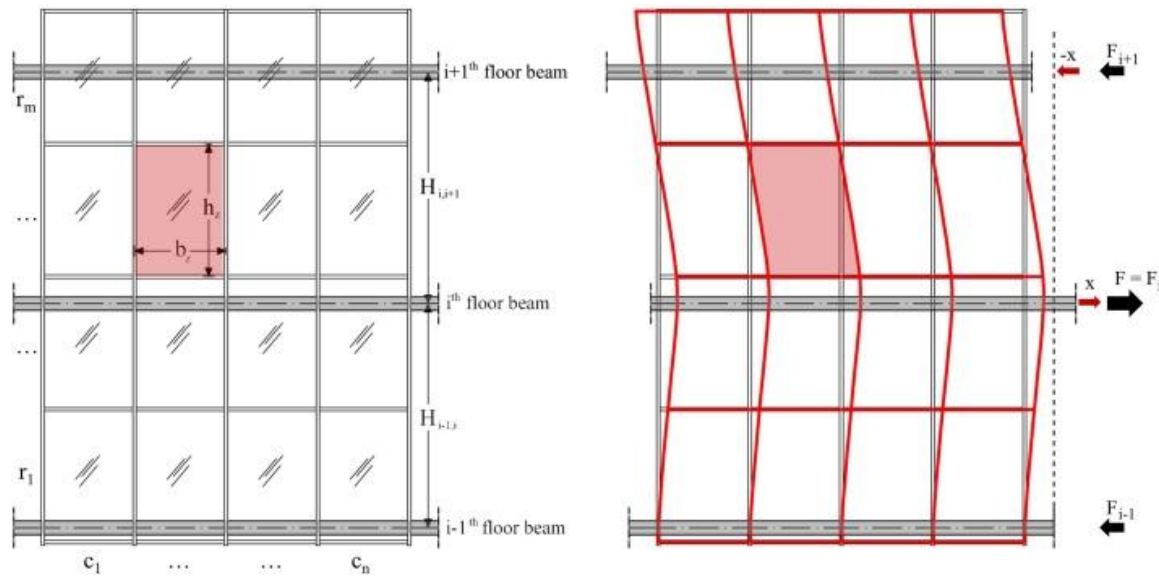


Figure 2- 37. Unitized curtain wall glazing system (left); possible displacement lateral shape (right).

Insights from these and similar programs have been woven into AAMA 501.4, ETAG 002 and JASS 14, which now require a representative unitized curtain wall mock-up to endure cyclic racking before production starts. As a result, design teams outline drift envelopes at the concept stage and demand that air and water paths, as well as façade plane tolerances, meet residual serviceability thresholds.

2.7. Architectural Applications of Glass Façades

Over the last years, the glass skin of a building has shifted from a neutral weather-barrier into a primary vehicle for architectural expression, environmental strategy and cultural meaning. One way to map this shift is by looking at how the glass behaves itself;

- Planar,
- Curved,
- Cable-Net,
- Climate-Adaptive,
- Point-Supported;

and following landmark projects on every continent that stretch each behavior to its technical edges.

2.7.1. Planar Curtain-Wall Façades

The planar curtain wall remains the most common glass envelope on today's high-rise buildings. Its clean, flat appearance conveys corporate openness, and engineering exactitude while allowing engineers to tune the system for local weather, security needs and earthquake sway.

- The Shard (London, 2012, Renzo Piano Building Workshop) leans eight angled panes against one another, forming vertical shards that seem to vanish into the clouds (Figure 2-38.). Scheldebouw-Permasteelisa designed and installed the stick-built units while managing double-skin winter gardens in the gaps between the panels [43].
- Shanghai Tower (Shanghai, 2016, Gensler) escalates the planar language of skyscrapers to the mega tall realm (Figure 2-39.). A gently twisting double curtain wall, anchored by thousands of rectangular lites supplied and installed by Yuanda, balances wind load with continuous sky-lobby gardens [44].
- One World Trade Center (New York, 2014, SOM) wraps its tapering prism in bomb-blast-rated, unitized panels by Benson Industries; the slight twist in each facet scatters light from the Hudson River light while meeting tough security rules and keeping views clear (Figure 2-40.) [45].



Figure 2- 38. The Shard, London.

Figure 2-38. adapted from: <https://www.permasteelisagroup.com/project-detail?project=791&utm>



Figure 2- 39. Shanghai Tower, Shanghai.



Figure 2- 40. One World Trade Center, New York.

Figure 2-39. adapted from: <https://www.yuandacn.com/index.php/en/projects-cn-2/103-domestic/shanghai/216-shanghai-center-building-2.html>

Figure 2-40. adapted from: <https://www.architectmagazine.com/design/one-world-trade-center>

2.7.2. Curved-Form Glass Façades

Many recent landmarks echo fluid or aerodynamic shapes by bending the glass itself. Where flat walls project sharp clarity, curving skins signal continuity, movement and high-tech bravado.

- Apple Park (Cupertino, 2017, Foster + Partners) surrounds a central orchard with a 2600-foot ring made of thousands of cold-bent lites supplied by Sedak, yielding an unbroken horizon of shimmering reflection (Figure 2-41.) [46].
- Fondation Louis Vuitton (Paris, 2014, Gehry Partners) drapes its galleries with twelve sweeping glass sails, each pane uniquely shaped and installed by RFR and Permasteelisa, evoking a vessel gliding through the Bois de Boulogne (Figure 2-42.) [47].
- Guangzhou Opera House (Guangzhou, 2010, Zaha Hadid Architects) wraps a ribbed granite shell around inclined fins of glass that vanishes in daylight yet sparkles at night like stones rinsed by a river, announcing the city's cultural quarter (Figure 2-43.) [48].

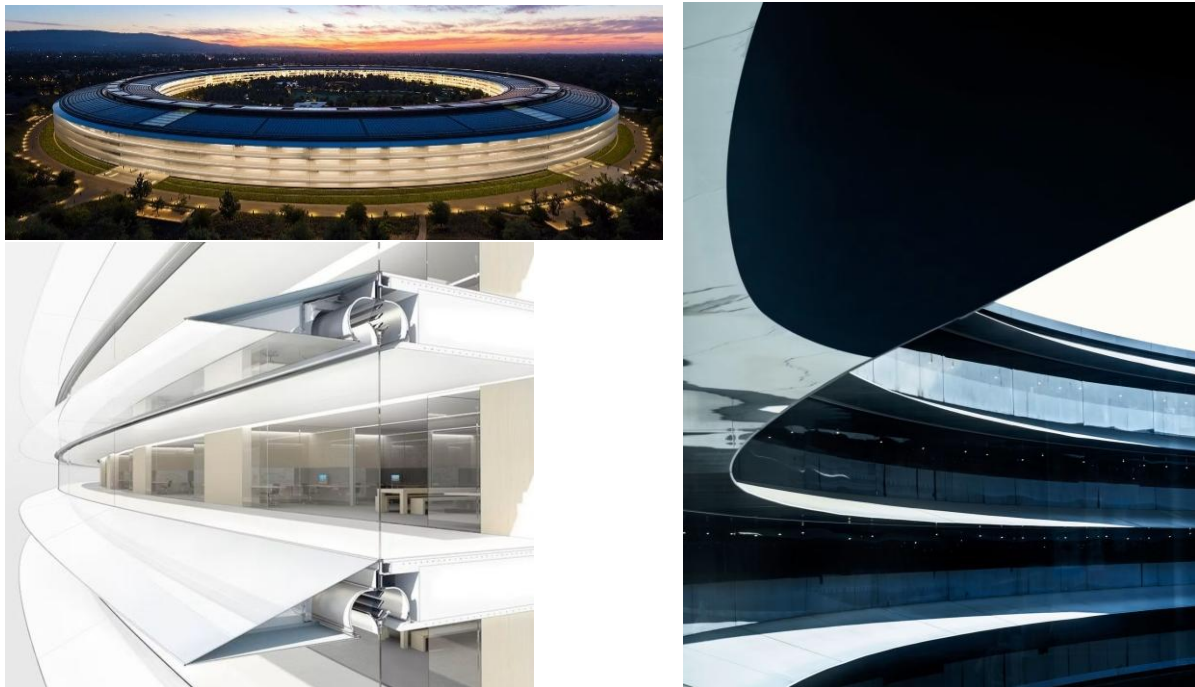


Figure 2- 41. Apple Park, Cupertino.

Figure 2-41. adapted from: <https://architizer.com/blog/inspiration/stories/architectural-details-apple-park-windows/>



Figure 2- 42. Fondation Louis Vuitton, Paris.

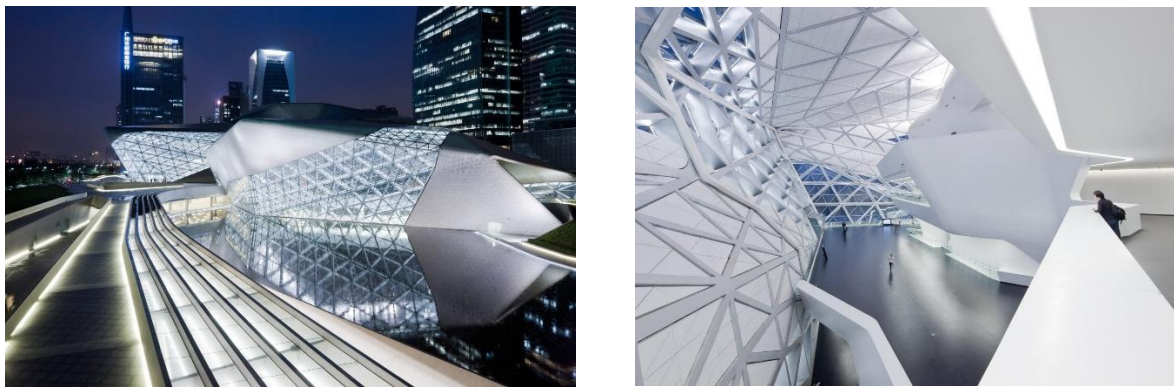


Figure 2- 43. Guangzhou Opera House, Guangzhou.

2.7.3. Cable-Net Glass Façades

When designers seek the boundary between inside space and outside air, tensioned cables and clear glass fins replace heavy mullions with an almost invisible steel and lattice of silica.

- Time Warner Center Atrium (New York City, 2003, SOM) drapes Columbus Circle in a four-story cable net façade engineered by Schlaich Bergermann Partner, transforming a busy intersection into an all-weather urban living room (Figure 2-44.) [49].

Figure 2-42. adapted from: https://www.architectmagazine.com/design/buildings/fondation-louis-vuitton-designed-by-gehry-partners_o

Figure 2-43. adapted from: <https://www.zaha-hadid.com/architecture/guangzhou-opera-house/>

- Hearst Tower Lobby (New York City, 2006, Foster + Partners) links its historic solid stone base to Norman Foster's glass and steel diagrid tower with a 12-story, Gartner-Permasteelisa cable wall that floods the lobby with sun while remaining nearly invisible from the street (Figure 2-45.) [50].



Figure 2- 44. Time Warner Center Atrium, New York.

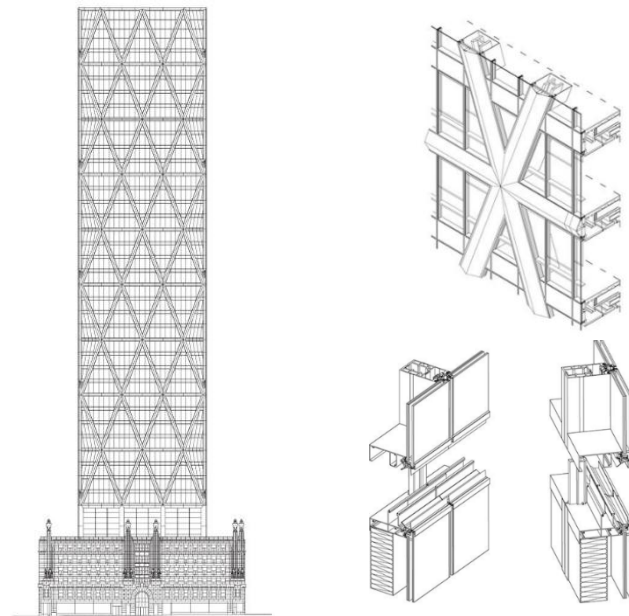


Figure 2- 45. Hearst Tower Lobby, New York.

Figure 2-44. adapted from: <https://pixels.com/featured/inside-time-warner-center-nyc-antonino-bartuccio.html>

Figure 2-45. adapted from: <https://www.permasteelisagroup.com/project-detail?project=8&>

2.7.4. Climate-Adaptive (Double-Skin) Glass Façades

When daylighting, energy savings, and comfort top the brief, architects turn to smart stacked-glass skins. A ventilated gap regulates heat gain, allows fresh air to move and even captures energy, all while preserving views.

- 30 St Mary Axe (London, 2004, Foster + Partners) spirals a narrow, naturally ventilated channel around its core offices; the outer layer, built by Schmidlin-Permasteelisa, forms shaded winter gardens that vent hot air through a lantern at the roof (Figure 2-46.) [51].
- Intesa Sanpaolo Tower (Turin, 2015, Renzo Piano Building Workshop) nests full-height winter gardens between twin glass layers; Permasteelisa fitted photovoltaic blades and operable vents, enabling mixed-mode operation for much of the year (Figure 2-47.) [52].

Across these cases, the double skin acts like an adaptive buffer, both their static and movement behavior, allowing designers and manufacturers like Permasteelisa to balance transparency with strict comfort and energy targets without giving up the sculptural quality of glass.

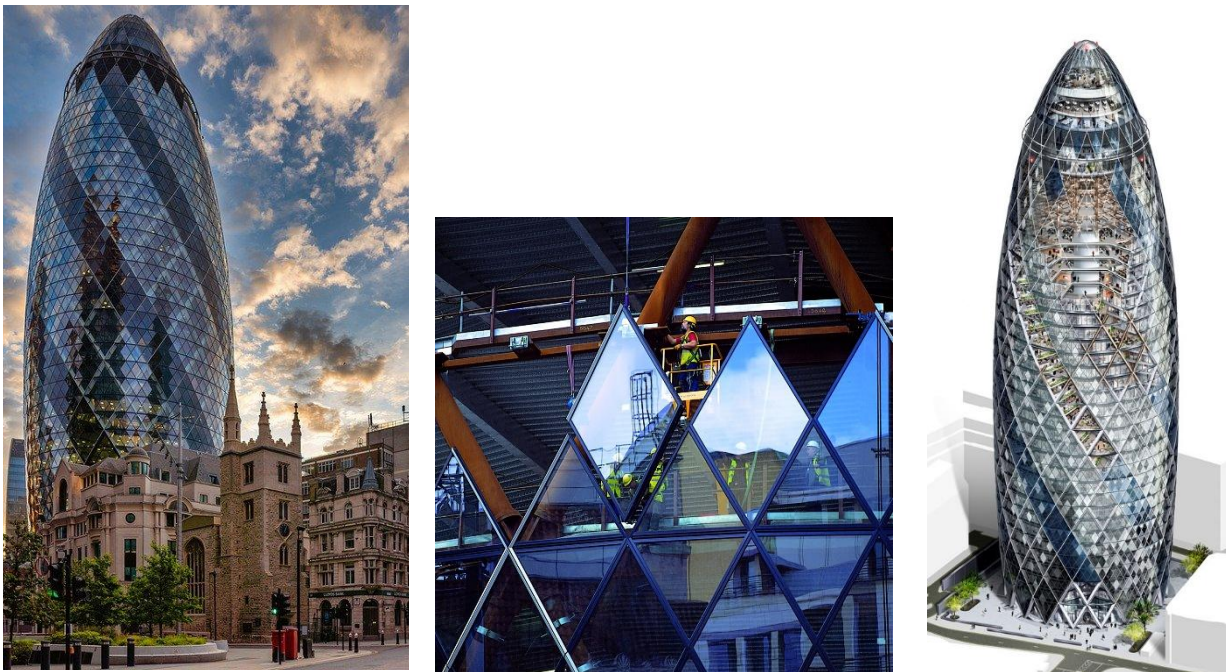


Figure 2- 46. 30 St Mary Axe, London.

Figure 2-46. adapted from: <https://www.fosterandpartners.com/projects/30-st-mary-axe>

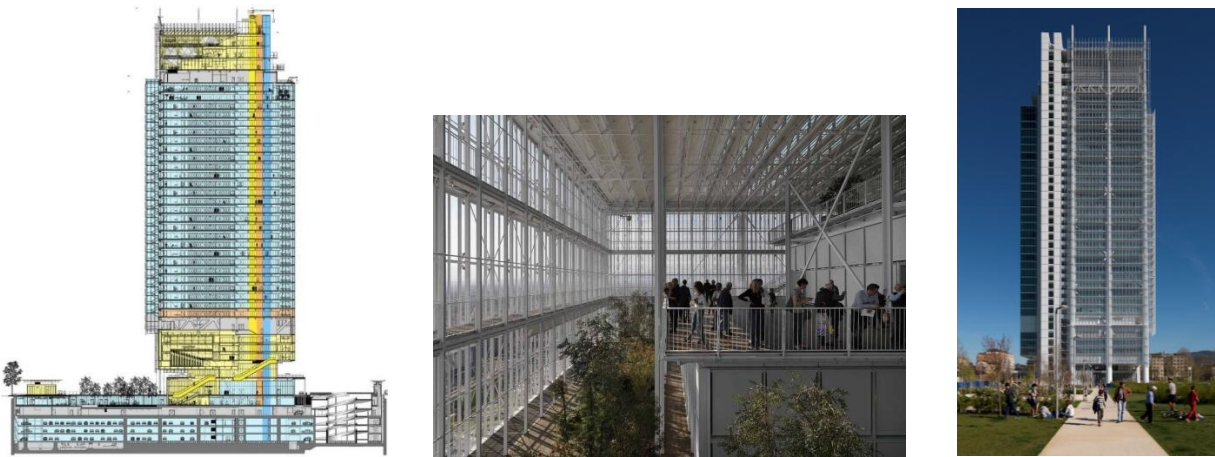


Figure 2- 47. Intesa Sanpaolo Tower, Turin.

2.7.5. Point-Supported Glass Façades

When a project demands almost invisible support, designers specify point-supported façades, largely glass panels anchored by discrete spider or ball joint fittings that nearly disappear from view.

- Louvre Pyramid (Paris, 1989, I. M. Pei & Partners) serves as the archetypal spider wall: its 673 diamond panes affixed to stainless-steel nodes create a glass lantern that both honors and visually contrasts the 17th-century palace (Figure 2-48.) [53].
- Seattle Central Library (Seattle, 2004, OMA + LMN) encloses its stacked platforms within a rhomboid steel grid and point-supported insulated panels, letting the arrangement glow like an urban lantern once the sun goes down (Figure 2-49.) [54].



Figure 2- 48. Louvre Pyramid, Paris.

Figure 2-47. adapted from: <https://www.fosterandpartners.com/projects/30-st-mary-axe>

Figure 2-48. adapted from: <https://www.rostarchitects.com/articles/2023/1/6/the-louvre>



Figure 2- 49. Seattle Central Library, Seattle.

Chapter 3

Seismic Design and Regulations

Seismic forces are different from wind or gravity loads; because they include fast reversals, simultaneous in-plane racking, out-of-plane jolts and many cycles that can push the structure that may past elastic-limit of the building. Data from recent subduction and strike-slip quakes show ground velocities that create roof drifts of 0,5 to 2 % in a fraction of a second, out-pacing the response of glass, sealants and rigid aluminum anchors [55].

During these brief pulses the whole curtain wall acts like a chain of fuses. Glass panels must bend like thin diaphragms, silicone joints must shear without tearing and aluminum cassettes must slide or yield at planned edges, so that brittle parts avoid sudden failure. Shake-table tests reveal that damage rarely starts from average membrane stresses predicted by plate theory but instead appears at weak spots such as corner bites, over-tightened anchors or stiff gaskets.

Non-structural components now produce most of the direct and indirect losses that commercial buildings suffer in quakes, making the stakes unusually high. Repairing curtain walls, installing makeshift weather seals and absorbing occupancy losses can easily cost several times the price of any visible frame damage, especially in tall, all-glass towers where every broken panel threatens waterproofing and emergency exits. Surveys following the 2011 Christchurch quake, the 2017 shake in Mexico City, and Kumamoto in 2016 all point to falling glass, loosened spandrels and ripped seals as the main reasons streets were cordoned and prolonged business interruption [56][57].

As a result, current performance-based codes treat the building façade as a life-safety system in its own right; it must stay bonded to the frame, keep debris from falling and, if possible, hold a minimal level of air and water seal after the main shock. Meeting that goal requires thinking holistically about glass strength, silicone flexibility, anchor play and back-up pathways.

3.1. Global Seismic Context

Earthquakes are far from random events; their distribution closely mirrors the movements of tectonic plates. About 90 % of the world quakes and nearly all great shocks with $M_w \geq 8$ or larger-pack into the roughly 40.000-kilometer Ring of Fire that circles the Pacific (Figure 3-1. and 3-2.), while another 5 to 6 % align along the trans (Mediterranean, Himalayan, Alps belt); only a small fraction occurs along mid-ocean ridges or deep inside continents [58].

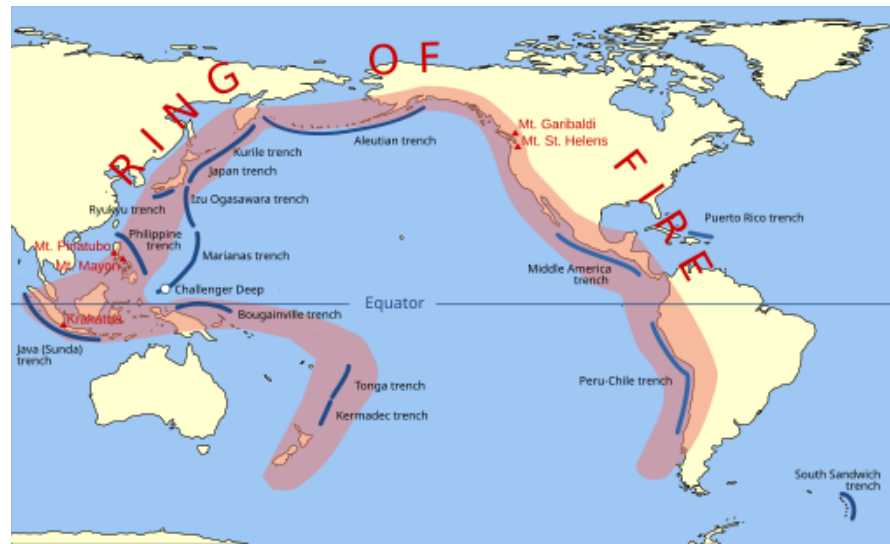


Figure 3- 1. The Pacific Ring of Fire, with trenches marked with blue lines.

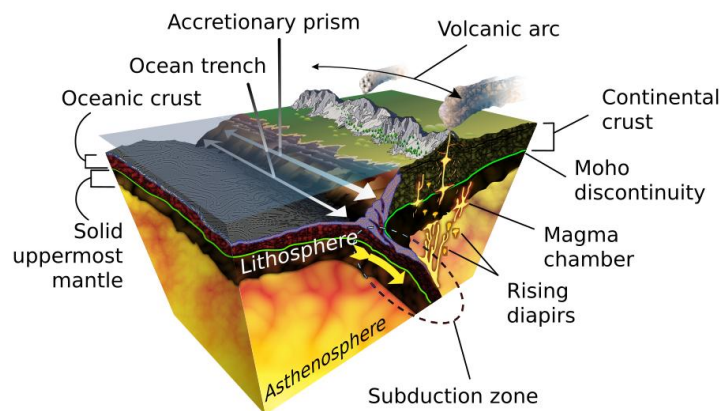


Figure 3- 2. Diagram of the geological process of subduction.

Figure 3-1. and 3-2. adapted from: https://en.wikipedia.org/wiki/Ring_of_Fire?utm_source

Long-term records maintained by the U.S. Geological Survey indicate an annual average of roughly sixteen major earthquakes of $M_w \geq 7.0$ or greater set against thousands of moderate shocks and millions of micro-quakes logged by dense monitoring networks [59]. On the basis of this data, seismologists classify future building sites into four broad hazard bands, summarized in Table 3-1.

- **Very-High Seismicity:** plate-boundary regions such as Chile, Japan, Alaska, Sumatra and New Zealand routinely face M_w 7-9 earthquakes that release concentrated short-period spectral energy. Laboratory tests on full-scale curtain-wall prototypes reveal that these sudden velocity spikes can force cassette joints apart by 1-2 % of inter-story drift within a single pulse, endangering glass edge bite and ripping shallow silicone seals [60].
- **High Seismicity:** California, Mexico, Türkiye (Figure 3-3.), Greece, Italy and Taiwan experience frequent strike-slip and subduction quakes (M_w 6,5-7,5) that repeatedly over a building's service life. Surveys of Christchurch after 2011 and Mexico City 2017 in post-earthquakes show that unitized curtain walls anchored with slotted brackets and deep gaskets endured 2-3% inter-story drift without glass loss, while stick-built assemblies leaked at roughly half that movement [61].

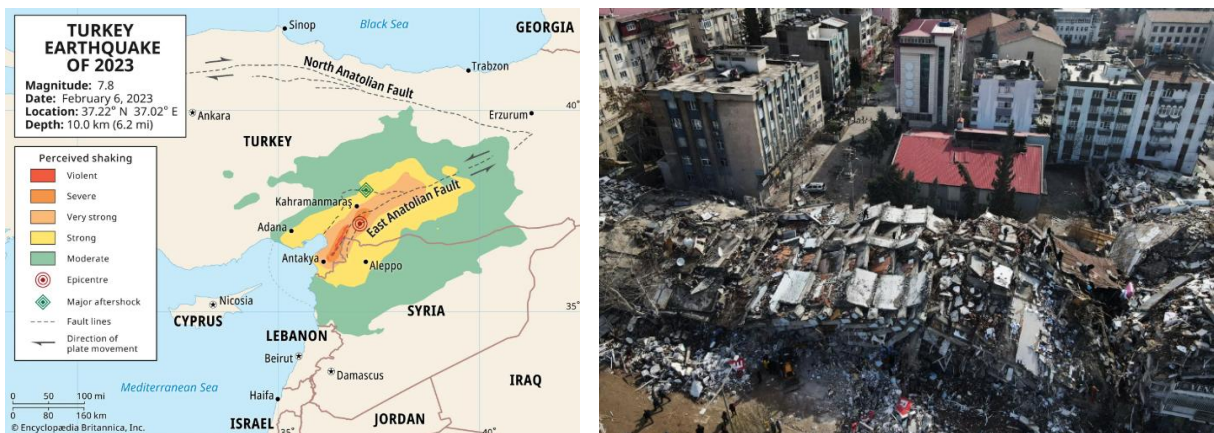


Figure 3- 3. Kahramanmaraş, Türkiye earthquake of 2023.

- **Moderate seismicity:** Areas such as the U.S. Pacific Northwest, parts of Spain, Iran, China and India generate lower peak accelerations but shaking lasts far longer. Soft-soil basins extended shaking beyond 60 seconds, exhausting gasket recovery and sliding-anchor travel well before maximum drift.

Figure 3-3. adapted from: <https://www.britannica.com/event/2023-Turkey-Syria-earthquake>

- **Low Seismicity:** Around Northern Europe, most of Australia and the Arabian Peninsula magnitude events remain rare so façade design is driven mainly by wind loads. Nevertheless, techniques that proved effective in higher-risk places, such as laminated glass for post-breakage retention, are steadily adopted in local baseline codes.

Table 3- 1. Seismicity matrix for façade design guidance.

Band	Representative regions	Typical demand on façades
Very High	Chile, Japan, Alaska, New Zealand	1–2 % drift in a single pulse; high accelerations
High	California, Mexico, Türkiye, Italy	Multiple M_w 6.5–7.5 events; cumulative cyclic drift
Moderate	Pacific NW, Spain, Iran	Long-duration shaking on soft basins
Low	Northern Europe, Australia	Wind governs; rare low-magnitude quakes

Table 3-1 shows seismic demand levels (very high, high, moderate and low) across global regions, helping guide façade design by drift expectations with geographic seismicity.

In modern high-rise buildings, the budgetary weight of the building shifts away from the structural frame to what engineers label the other 80 %”: cladding, glazing, ceilings, pipes, HVAC, furnishings and the contents that line every floor. Studies of recent earthquakes show that these non-structural elements can match or even outstrip the cost of the steel or concrete skeleton and they are the main reason firms lose income while repairs drag on [48].

The 2023 Turkey sequence illustrated the point clearly: twelve hospitals that remained structurally stable were still partly closed because façades shattered, ceilings sagged and power or water lines failed, leaving emergency services short-handed [62].

Recent studies have shown that drift capacity of a curtain wall is unusually sensitive to seemingly minor façade-system parameters. A 2024 parametric test of unitized curtain walls assemblies found that slight changes to:

- the bending stiffness of mullion-splice joints,
- the depth of the silicone sealant bite,
- the height-to-width ratio of panels,

can double or halve the drift limit at which visible damage appears. Parallel models indicate that adding sliding or self-centering connectors largely separates the cladding from the main frame and keeps joints leak-proof even when in-elastic drifts near 2%.

Collectively, these results imply that earthquake behavior of a glass curtain wall depends far more on the craft of its brackets and seals than on strength of the glass. Careful tuning of joint stiffness, seal geometry and connection motion thus offers a practical, performance-driven way to turn a fragile building envelope into a robust part of its seismic shield.

3.2. Code Requirements for Façade Systems

Traditional building codes have been concerned with the strength, ductility and stability of beams, columns, shear walls and foundations as distinct structural units. While these elements do not contribute to the lateral or gravity load resistance of the building, they are crucial from the standpoint of safeguarding occupants, ensuring operational continuity during crises and supporting post-earthquake habitability [63].

Façade systems, glazing units, ceilings partitions, elevators, HVAC ducts, plumbing and fire protection lines along with lighting fixtures are included under non-structural components. There is increased focus about their performance during seismic events as evidence consistently shows that damage to these non-structural elements leads to disproportionately greater financial losses alongside longer recovery times in comparison to structural damage especially prominent in high-rise towers and critical infrastructure facilities.

As a result, international building codes and testing standards have developed in concern with the seismic behavior of façade systems. Here is a summary analysis of all important nations pertaining to the curtain walls testing and design for seismic activity including Europe, America, New Zealand, Japan along with some specialized façade tests like AAMA 501.4 and 501.6.

3.2.1. European: Eurocode 8 (EN 1998)

In the Europe regulatory framework earthquake risk is covered by Eurocode 8 (EN 1998-1:2004). It focuses mostly on structural parts; however, within Section 4.3.5. Non-structural Components Eurocode has a separate subsection for “appendages” which incorporates curtain walls, cladding systems, parapets, antennae, gables, railings, mechanically mounted equipment and similar features [8].

Despite their secondary structural role, these elements are subject to seismic design verification when:

- They are likely to result in injury hazards to people,
- Their detachment endangers vital building functions especially in critical-use like hospitals or emergency shelters [8][64].

Eurocode 8 states that all non-structural elements “shall, together with their supports, be verified to resist the design seismic action” (EN 1998-1. S.4.3.5). This requirement covers not only the integrity of the element itself but also its anchorage systems, which may include brackets, bolts and adhesive joints. Weaknesses in these components are usually responsible for what is seen post-earthquake façade shedding in damage surveys.

Failure modes associated with a critical designation due to a specific function or considerable mass and hazard potential necessitate more sophisticated modeling which creates response spectra from the main structural system. For all other cases, a simplified static method will work without an issue.

Simplified Method for Seismic Force Calculation:

Non-structural elements are subjected to seismic forces that can be represented by a horizontal static equivalent force S_a acting at the element’s center of mass. Eurocode 8 provides the following formula:

$$F_a = \gamma_a \cdot \frac{S_a}{q_a} \cdot W_a$$

Where:

- F_a : Seismic design force acting in the most unfavorable direction
- W_a : Weight of the non-structural element
- γ_a : Importance factor, reflecting safety or operational criticality

- q_a : Behavior factor, expressing ductility and energy dissipation
- S_a : Seismic coefficient, dependent on building and site parameters

The seismic coefficient S_a is further defined by:

$$S_a = \alpha \cdot S \cdot \left(\frac{3 \cdot (1 + \frac{z}{H})}{\sqrt{1 + (1 - \frac{T_a}{T_1})^2}} \right)$$

Where:

- α : Design ground acceleration ratio a_g/g
- S : Soil amplification factor
- T_a : Period of the non-structural component
- T_1 : Period of the building
- z : Height of the component above the seismic base
- H : Total height of the building

According to EN 1998, S_a must not be less than αS to avoid underestimating seismic forces.

Behavior and Importance Factors:

The behavior factor q_a measures how much energy can be absorbed by ductile deformations within a component inelastic range of response. Eurocode specifies these default values in Table 3-2.:

Table 3- 2. Behavior Factors (q_a) for Non-Structural Elements (Eurocode 8).

Type of Non-Structural Elements	Behavior Factor (q_a)
Parapets, signs, chimneys (unbraced)	1.0
Curtain walls, partitions and façades	2.0
Suspended ceilings, equipment anchors	2.0

The importance factor γ_a is generally taken as 1.0. However, for components essential to life safety or containing hazardous materials, it must not be lower than 1.5.

Eurocode 8 does not require an assessment for the ability to sustain in-plane rigid body motion (inter-story drift) of a component's displacement capacity.

This is particularly critical for curtain wall systems as they are influenced by racking movement between floor slabs during seismic activity. As Nardini and Doebeel (2016) remarked, “no requirements are provided by EN 1998 about the capability of the non-structural elements to accommodate the displacements that the main structure experiences during the earthquake” [64].

As a result, façade designers are assumed to fill in this gap with additional performance criteria mock-up testing to guarantee:

- Glass panels remain within safe stress limits,
- Sealants and joints sustain non-excessive strain,
- Anchors permit differential movement associated with flexing without risk of becoming detached.

3.2.2. American: ASCE 7-16 and FEMA 460/461

In the United States, a comprehensive multidisciplinary approach for mitigating seismic risk at both structural and non-structural levels is provided under the framework of the National Earthquake Hazards Reduction Program (NEHRP). Coordinating through FEMA, NIST, NSF, USGS and NEHRP seeks to enhance resilience to earthquakes in buildings and infrastructure. Such strategies include reducing loss of life and property damage along with post-earthquake downtime by enforcing performance-based design criteria on structural and non-structural elements of the building.

NEHRP's recommendations have been directly used in designing *ASCE/SEI 7-16 Minimum Design Loads and Associated Criteria for Buildings and Other Structures* which serves as the basis for seismic design incorporated in U.S. building codes [9]. In this standard, non-structural components such as curtain walls, suspended ceilings, partitions, cladding systems, parapets, mechanical and electrical equipment are required to be designed not only to withstand lateral seismic forces but inter-story drift caused relative motion between stories.

The horizontal seismic force F_p imposed on a non-structural component is given by the following expression [9]:

$$F_p = a_p \cdot S_{DS} \cdot \left(1 + \frac{z}{h}\right) \cdot \frac{I_p}{R_p} \cdot W_p$$

Where:

- F_p : Seismic design force
- W_p : Weight of the component
- I_p : Importance factor (typically 1.0 or 1.5 depending on the component's function)
- z : Height of the component above the base
- h : Total building height
- a_p : Component amplification factor
- R_p : Component response modification factor
- S_{DS} : Design spectral response acceleration (short period)

The minimum and maximum values of F_p are also regulated:

$$F_{p,min} = 0,3 \cdot S_{DS} \cdot I_p \cdot W_p$$

$$F_{p,max} = 1,6 \cdot S_{DS} \cdot I_p \cdot W_p$$

These forces act in both orthogonal directions on the component's center of mass and must be considered alongside applicable vertical loads and wind forces. Moreover, design compatibility of drift requirements must be satisfied; inter-story displacements from ground shaking are endured without compromising façade systems or their points of anchorage. For glass curtain walls and glazed partitions, the drift limit is specified as:

$$\Delta_{fallout} \geq (1,25 \cdot I_p \cdot D_p, 13 \text{ mm})$$

Where:

- $\Delta_{fallout}$: Allowable inter-story drift to prevent glass fallout
- I_p : Importance factor of the non-structural component
- D_p : Amplified displacement demand on the component due to seismic drift

This criterion mitigates the risk of brittle failures such as glass fallout or detaching from anchorages during significant seismic activities.

ASCE 7-16 provided offset inter-story shear demands on façades that allowed individual floors to slide under each other during seismic shaking. The maximum allowable inter-story shear is specified as follows:

$$\delta_{max} = C_d \cdot \Delta$$

Where:

- Δ : Elastic inter-story drift of the building
- C_d : Deflection amplification factor depending on the lateral force-resisting system

This requirement assurance that differential movement between brackets, sealants and joints within curtain wall assemblies does not compromise structural safety nor waterproofing integrity. Reconnaissance of earthquakes stemming from Northridge (1994) and Mexico City (2017) has shown these failures often result in glass fallout, sealant rupture or water intrusion; even in buildings that remained unaltered structurally [65].

Along with balance force and drift techniques, FEMA 460 and FEMA 461 provide more detailed experimental guidelines. While FEMA 460 provides specific guidance on general considerations for the performance of components and systems within a structure to seismic loads, FEMA 461 defines cyclic racking protocols that simulate earthquake drift, which is often used to test curtain wall mock-ups under displacement control [66] [67].

3.2.3. New Zealand: NZS 1170.5

NZS 1170.5:2004 titled “*Structural Design Actions – Part 5: Earthquake Actions – New Zealand*” serves as the backbone of earthquake design in New Zealand. This standard outlines processes for evaluating seismic effects on structural and non-structural building components within a framework of defined boundaries. In relation to the building codes of New Zealand, non-structural elements are referred to as “parts” and their design is described in *Section 8* of the standard, which encompasses façades, curtain walls, cladding systems partitions as well as service equipment and mechanical systems set to the primary structural frame [68].

All parts must be designed to resist specified seismic actions proportional to their hazard level and particular response dynamics. The regulation places criteria not only on horizontal and vertical forces acting simultaneously on a part's centroid, but also inter-story drift and deflection coordination between adjacent floors (story levels).

Design actions are derived through formulas incorporating characteristics of the part, its location within the structure and other regional seismic factors.

The horizontal seismic force is calculated by:

$$F_{ph} = C_p (T_p) \cdot C_{ph} \cdot R_p \cdot W_p \leq 3,6 \cdot W_p$$

Where;

- $C_p (T_p)$: Spectral design coefficient (period-dependent)
- C_{ph} : Horizontal response factor (depends on ductility)
- R_p : Part risk factor
- W_p : Weight of the part.

Table 3- 3. Part Risk Classification.

Category	Criteria	Part Risk Factor R_p	Structure Limit State
P.1	Part representing a hazard to life outside the structure.	1.0	Ultimate Limit State
P.2	Part representing a hazard to a crowd of greater than 100 people within the structure.	1.0	ULS
P.3	Part representing a hazard to individual life within the structure.	0.9	ULS
P.4	Part necessary for continuing function of the evacuation and life safety systems within the structure.	1.0	ULS
P.5	Part required for operational continuity of the structure.	1.0	Serviceability Limit State
P.6	Part for which the consequential damage caused by its failure are disproportionately great.	2.0	SLS
P.7	All other parts.	1.0	SLS

**Table adapted from NZS 1170.5:2004 Table 8.1. [68].*

Table 3-3. outlines the part risk classification according to NZS 1170.5 where risk factors are assigned based on possible threats, use and occupancy and the function of the structure which has an impact on design limit states for non-structural components.

The vertical seismic design actions must also be evaluated using:

$$F_{pv} = C_{pv} \cdot C_{vd} \cdot R_p \cdot W_p \leq 2,5 \cdot W_p$$

Where;

- C_{pv} : Vertical response factor
- C_{vd} : Vertical acceleration coefficient
- R_p : Part risk factor
- W_p : Weight of the part.

Table 3- 4. Part Response Factor, C_{ph} and C_{pv} .

Ductility of the part (μ_p)	C_{ph} and C_{pv}
1.0	1.0
1.25	0.85
2.0	0.55
3.0 or greater	0.45

**Table adapted from NZS 1170.5:2004 Table 8.2. [68].*

As shown in Table 3-4., the specific part response factors C_{ph} and C_{pv} are used to trim down horizontal and vertical seismic forces in accordance with the component's ductility capacity. The more ductile an element is, the lower the response factor assigned to it. This minimizes the design seismic demand in NZS 1170.5.

For façade systems connected over several levels, zoning rules require that upper-level components withstand forces from lower levels due to inter-story dimension changes provided by leading stage braces along multiple anchorage lines.

The considerations restated in the serviceability (SLS) and ultimate (ULS) limit states of NZS 1170.5 are ensuring for performance and life safety preservation during moderate to high seismic events. The minimum ductility requirement specifically designed to $\mu_p = 1.25$, which reflects a conservative approach to design that safeguard connections and attachments, especially for heavy or elevated components.

Partial structural ductility and classification is treated with more attention while accounting for vertical seismic actions in comparison to the quasi-static approach outlined in Eurocode 8. NZS 1170.5 is one of the stricter international standards for non-structural seismic design because of its comprehensive approach and well-defined response and risk factors.

3.2.4. Japan: JASS 14

Japan is located on the Pacific Ring of Fire which is one of the world's most active areas for earthquakes and volcanic eruptions, making it essential for architects and engineers to develop seismic design methodologies providing adequate protection against these hazards. Among other regulatory frameworks enhancing safety resilience during an earthquake is captured by the standard JASS14 developed by The Architectural Institute of Japan (AIJ), which governs the performance based structural design focusing on curtain wall systems influenced by seismic actions [64].

The JASS 14 standard acknowledges that curtain walls, although non-structural elements of a building, need to endure considerable inertial and displacement forces during an earthquake. These forces are divided into two main categories: vertical accelerations due to P-wave (primary wave) energy and horizontal accelerations from S-wave (secondary wave) activity. The standard summarizes the seismic effects on curtain walls with the following equations:

- **P-wave Loading:** $F_v = W \cdot a_v$
- **S-wave Loading:** $F_h = W \cdot a_h$

Where W is the weight of the curtain wall component, a_v and a_h represent vertical and horizontal ground accelerations. These equations, along with permissible short-term stresses for brackets, anchors, and support systems, determine safety against inertia failure modes.

JASS 14 subdivides seismic demands into three performance grades, each associated with a maximum allowable story drift ratio (a fraction of the floor height H) and corresponding to particular earthquake intensity levels and anticipated damage thresholds. This captures Japan's advanced performance-based approach where the expectation for curtain walls is not only their clean attachment to the structure but also their accommodation of the building deformation in a safe and functional manner.

Unlike Eurocode 8 or ASCE 7-16 which uses force-based approaches, JASS 14 uses a displacement design criterion where drifts have upper limits that relate to inter-story height. It ensures compatibility control (mainly at joints, brackets, glazing) concerning failure mechanisms as a result of local displacement differences is critical. Through mock-up simulation and mechanical validation, JASS 14 guarantees façade systems are safe (structurally and seismically tested) to overcome the expected loads.

Table 3- 5. Seismic Performance Grades under JASS 14 [64].

Grade	Inter-Story Drift Limit	Seismic Event Type	Performance Requirement
Grade 1	H/300	Frequently occurring earthquakes.	No visible damage to internal or external components.
Grade 2	H/200	Largest historical earthquakes	No component failure; resealing permissible.
Grade 3	H/100	Maximum considered event (100-year return period)	No glass breakage or component fallout.

3.2.5. American Testing Standards: AAMA 501.4 and AAMA 501.6

In addition to international seismic design standards such as Eurocode 8, ASCE 7, and JASS 14, the American Architectural Manufacturers Association (AAMA) provides essential testing guidelines specifically for evaluating the seismic performance of curtain wall systems. Two protocols that stand out are AAMA 501.4-09 and AAMA 501.6-09 which cover dynamic and displacement-based verification of building façades.

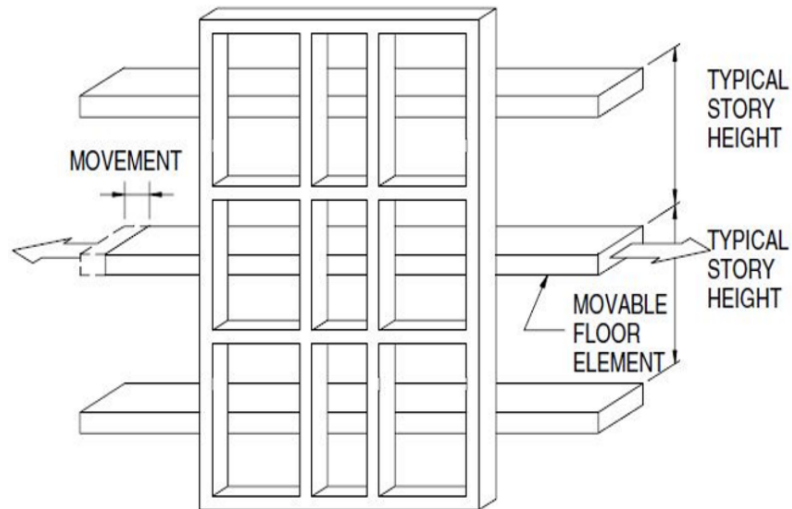


Figure 3- 4. Typical test specimen configuration.

AAMA 501.4, *“Recommended Static Test Method for Evaluating Curtain Wall and Storefront Systems Subjected to Seismic and Wind Induced Inter-Story Drift”*, outlines a procedure to evaluate serviceability of storefront systems with horizontal in-plane displacements, simulating inter-story drift during seismic activity. The tests are performed on full-scale multi-story mock-ups and measure degradation of air and water infiltration performance due to imposed drifts over time. This involves conducting air and water leakage tests before and after racking to determine assessed serviceability changes, enabling classification of designed performance by occupancy type: essential, high-occupancy or standard. The goal is to simulate the slow lateral racking resulting from seismic forces while mitigating testing velocity distortions due to acceleration-related impacts.

AAMA 501.6 bypasses the static evaluations performed in AAMA 501.4 and introduces a dynamic rack test that simulates the oscillatory effects of seismic loading to evaluate shear walls subjected to shear forces. The curtain wall specimen undergoes horizontal cyclic displacements due to programmable actuators simulating earthquake forces. This testing rigorously evaluates the seals and connection anchors for fatigue damage, sealant function, hierarchical joints performance and overall integrity under repetitive drift cycles. An important part of the standard is crescendo testing where displacement amplitude increases progressively via sinusoidal cycles until glass fallout occurs, which then determines inter-story drift limit (Δ_{fallout}) crucial for optimization mid and high-rise buildings glazing systems.

Figure 3-4. adapted from: https://www.researchgate.net/figure/Test-methods-in-the-AAMA-5014-standard_fig1_353406808

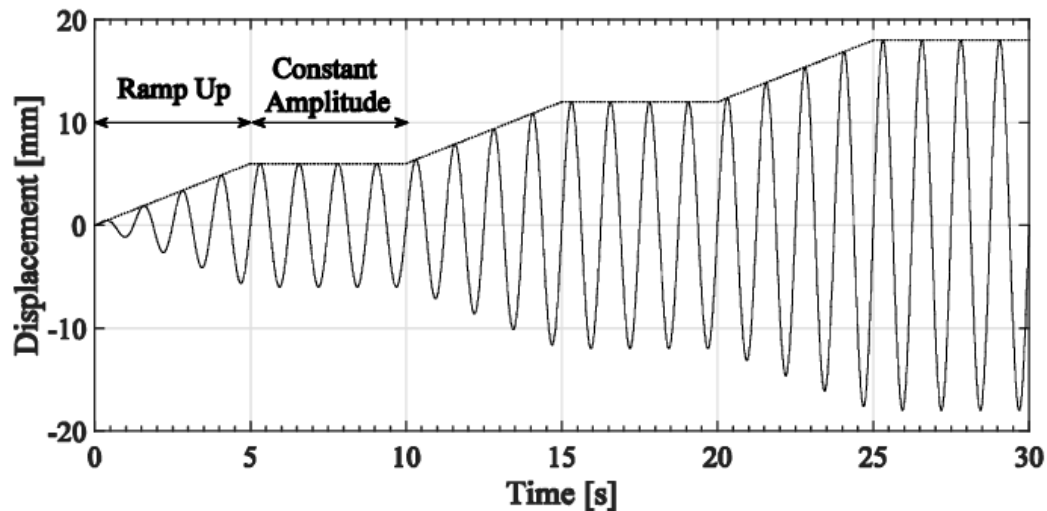


Figure 3- 5. First 30 seconds of crescendo test (AAMA 501.6).

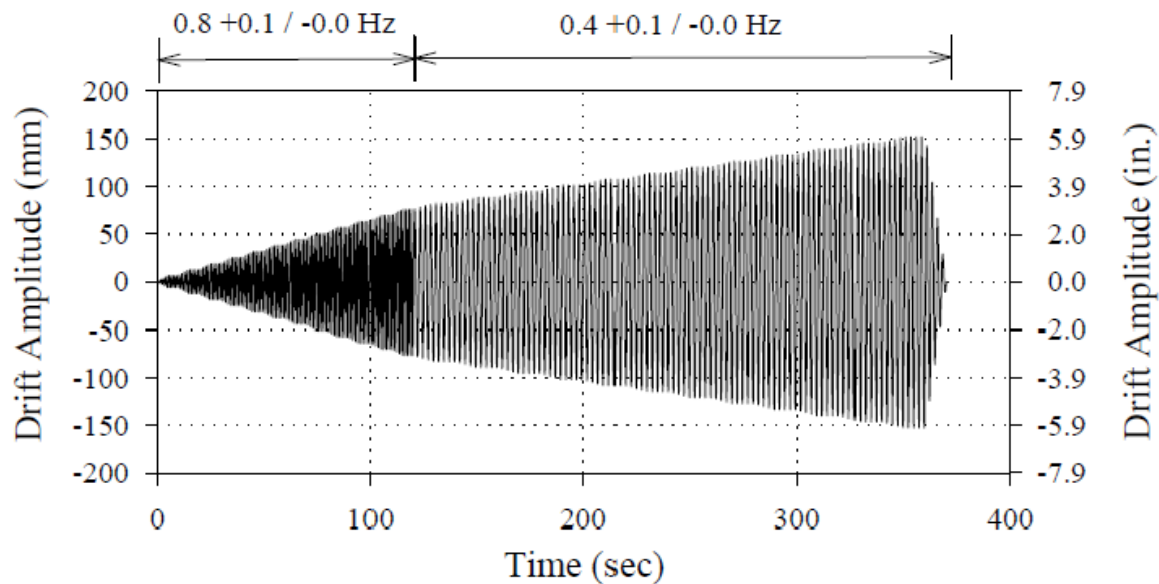


Figure 3- 6. Schematic of displacement time history for dynamic crescendo test.

To sum up, AAMA 501.4 addresses serviceability performance through controlled controllable lateral displacement while AAMA 501.6 shifts focus towards ultimate performance by finding failure points glazed systems are able to withstand during seismic drifts. In combination, these standards build a robust experimental foundation for understanding and validating the seismic behavior of complex curtain wall systems, thus promoting safer, more resilient architectural façades.

Figure 3-5. adapted from: https://www.researchgate.net/figure/First-30-seconds-of-crescendo-test-AAMA-5016_fig1_351102087

Figure 3-6. adapted from: https://www.researchgate.net/figure/Schematic-of-displacement-time-history-for-dynamic-crescendo-test-2_fig1_289815810

3.3. Seismic Code Comparison

The approach to seismic design in each region with regard to risk optimization and construction culture is observable in Eurocode 8, ASCE 7-16, NZS 1170.5 and JASS 14.

Based on EN 1998-1:2004, Eurocode 8 adopts a force-based design methodology. As an example of simplifications to structural computations provided by Eurocode 8, there is a static formula for determining horizontal seismic forces on façade systems and other non-structural components. Eurocode does not make provisions for checking in-plane drifts for these components. This lack of compatibility requirements means that a Eurocode-based design must be supplemented by performance evaluation or advanced simulation testing for flexible or brittle non-structural components such as glazing.

ASCE 7-16 (USA) is a hybrid model which uses force-based seismic load estimation alongside inter-story drift restrictions. It defines a permissible maximum drift (Δ_{fallout}), where glass fallout would potentially occur, particularly in relation to mock-up tests like AAMA 501.6. Also, horizontal and vertical seismic actions are both considered while paying special attention to detailing when there is insufficient clearance or ductility.

NZS 1170.5 (New Zealand) has a dual-action holistic approach by requiring horizontal as well as vertical seismic forces for the design of elements such as curtain walls deemed as “parts.” In addition, it requires components that are provided with multi-floor axial attachments to be checked for deformation-induced effects at every level. This standard contains additional specific coefficients including one focused on ductility response factors which makes it one of the most comprehensive in action combination. An important feature is the need for checking vertical acceleration which many other codes neglect.

JASS 14 (Japan) is a purely displacement-based design method. Rather than calculating seismic forces, it sets acceptable grades of performance based on inter-story drift measured as a fraction of the floor height (H). This standard is unique among the four in that it completely relinquishes reliance on force-based formulas and emphasizes practical seismic behavior. It also requires deconstruction compatible façade systems to preserve their structural and functional integrity under specified structural displacements.

As shown in Table 3-6., the seismic codes reviewed differ in their treatment of non-structural façade design. In Eurocode 8, non-structural system performance assessment relies on a simplified force approach without drift verification. It is worth noting that ASCE 7-16 and NZS 1170.5 have a more unified approach that includes vertical acceleration as well as some detailing based on forcing and displacement. JASS 14 stands out because all its methods are fully displacement-based; it focuses on inter-story drift compatibility with specified performance gradation levels. These variations collectively emphasize the need for design standardization and heightened focus on multifunctional criteria, especially concerning deformation-sensitive glazing systems.

Table 3- 6. Seismic Design Code Comparison Table [7].

Standard	Design Approach	Horizontal Action	Vertical Action	Drift Verification	Performance-Based Levels
Eurocode 8	Force-based	Yes	No	No	Not defined
ASCE 7-16	Force + Drift	Yes	Yes	Yes (Δ_{fallout} and more)	Defined by FEMA levels
NZS 1170.5	Force + Drift	Yes	Yes	Yes	Defined with mass and deflection
JASS 14	Displacement-based	Yes	Yes (P and S waves)	Yes (graded: H/300, H/200, H/100)	3 performance grades

3.4. Future Directions and Research Gaps

While considerable advancements have been made through Eurocode 8, ASCE 7-16, NZS 1170.5 and JASS 14, existing standards governing design details for non-structural façade systems continue to fall short in addressing dynamic loading conditions encountered in practice. Each standard offers varying approaches (force-based, displacement-based or hybrid) but challenges remain regarding consistent resilience across different façade geometries, materials, anchoring conditions and complex dynamic loads.

One of the critical gaps is the lack of full-scale experimental data on curtain wall systems exposed to seismic in-plane drift. Some testing procedures, such as dynamic racking (Δ_{fallout}) as noted in AAMA 501.6, are introduced, but their findings are not fully embraced by design codes. It is essential to establish validated performance-based design guidelines correlating test data with numerical simulation results and establishing a strong correlation.

Another important gap lies within modeling façade–structure interaction. Current design practices apply simplistic support boundary frameworks or completely ignore the nonlinear and deforming character of the connections, gaskets and silicone sealants that join frames with building walls.

Furthermore, numerous codes neglect to address vertical seismic actions decisively. NZS 1170.5 is one of the rare standards that explicitly expects parts to consider vertical load, but there is an international agreement on this matter. The behavior type related to materials like laminated glass or chemically tempered glasses concerning their role in the resilience to seismic forces need further study too for modern high-rise and unitized systems.

As a final point, consistency in performance grading and damage tolerance assessment within different operational areas remains an issue. Although JASS 14 incorporates a tiered performance-based system (H/300, H/200, H/100), similar stratification is absent in European codes. There is potential for greater collaboration across borders to create universal façade benchmarking for resilience and safety.

To summarize, further efforts should be put into façade seismic design to ensure the approaches are integrated, experimentally validated and harmonized. Focus should shift towards developing computational models and testing frameworks that enable dynamic tests of components while aligning global performance standards with life safety, system dependability and reparability after seismic events.

Chapter 4

Reference Experimental Study

This study builds on “*Influence of Design Variables on Seismic Performance of Unitized Curtain Walls: A Parametric Experimental Study*” by Bianchi et al., published in 2024. The research conducted by TU Delft together with Permasteelisa Group set up an experimental benchmark study considering these aspects and employed full-scale in-plane cyclic displacement tests on unitized curtain wall panels, altering geometrical and mechanical properties systematically to evaluate façade response to lateral seismic demands [7].

One specific panel configuration, Type 3, serves as the model prototype for numerical implementation in this thesis. This configuration consists of an insulated glass unit adhesively bonded within an aluminum frame. Such a unit could be a representative modular unit from a curtain wall system. In the TU Delft test setup, this unit was subjected to in-plane cyclic drift to mimic inter-story seismic displacements. This design also serves as the starting point for further analyses scoped in this research.

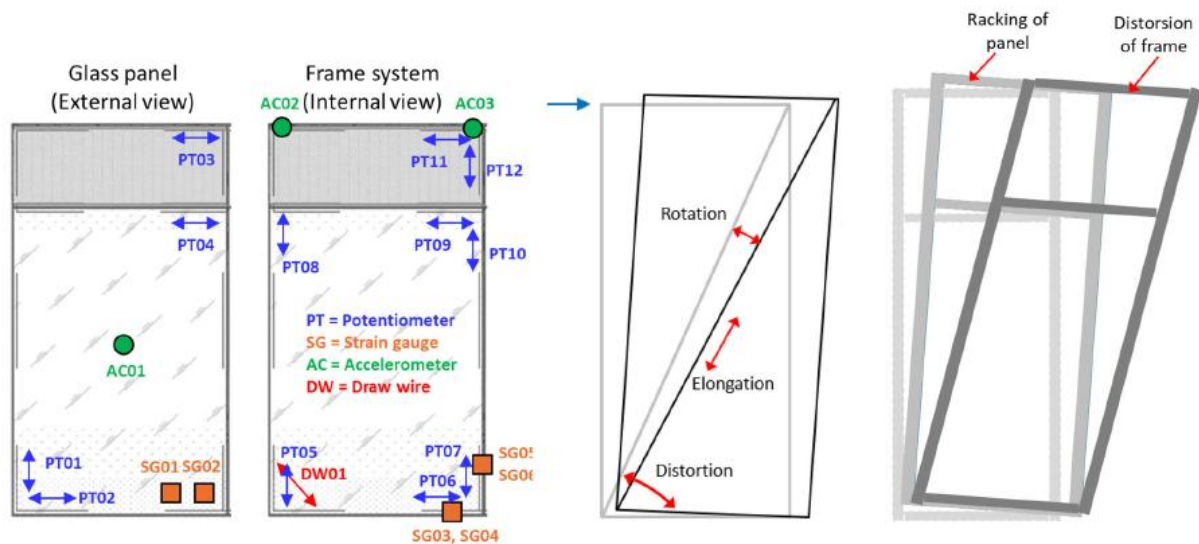


Figure 4- 1. Experimental setup study showing in-plane drift test configuration [7].

Figure 4.1. adapted from: <https://doi.org/10.1007/s40940-024-00255-2>

The testing environment was designed to replicate realistic in-plane drift scenarios typically encountered in seismic events. Each unit was mounted on a steel reaction frame and laterally loaded via displacement-controlled actuators. The instrumentation layout included displacement sensors and strain gauges to monitor both global panel response and localized effects near connectors and corners. A visual overview of the experimental configuration used in the TU Delft study is presented in Figure 4-1.

The simulations were conducted using SAP2000, a finite element analysis (FEA) platform capable of modeling nonlinear connections, advanced material behaviors, and complex support conditions. In the numerical model, the glass pane is represented with shell elements, the aluminum profiles with beam (frame) elements and the structural silicone adhesive with nonlinear spring connectors. The primary loads included an in-plane displacement at the top corners of 24 mm to simulate seismic drift demands. Gravity (self-weight) is considered in comparison models as Type R later on.

The modeling and analysis workflow is structured across three main chapters:

- Chapter 5 details the numerical environment, including software selection, mesh and element types, geometric parameters and loading and boundary conditions for the reference model.
- Chapter 6 presents the structural response of the reference Type 3 panel, including joint displacements, deformation profiles, connector forces, bending moments, and stress fields in both the frame and the glass.
- Chapter 7 works on three major parametric investigations:
 - Influence of silicone connector geometry (Chapter 7.1.),
 - Influence of panel dimension (Chapter 7.2.),
 - Influence of boundary restraint conditions (Chapter 7.3.).

Each individual component of the study enhances the understanding regarding the responsiveness such as global response (displacement, rotation) and local performance (stress concentration and the forces of the connectors) placed to have a wide understanding of the sensitivity to design of unitized curtain wall systems.

The main objectives of the presented modeling work are as follows:

- Validation of the numerical methodology which references the experiments performed by TU Delft while abstracting their results as observations and checking if the mechanics interact of the aluminum glass systems derivatively aligned considering the drift laterally.
- Evaluation of deformation details, also known as evaluation, including the bending of the aluminum frame, torsional rotation of the glass panel and inter-story slip between seismic levels.
- Stress quantization aims to analyze the frame for Von Mises forces in tension and the main force for the tension of the glass panels. The aim is to find areas with high risk and critical load paths.
- Connector performance assessment, through the simulation of nonlinear spring elements representing silicone adhesives, focusing on their stress accumulation under cyclic in-plane displacement.
- Identification of parameters influencing performance, for example, effects of aspect ratio, component shear stiffness, boundary restraint conditions, all applied toward developing flexible and safe designs for curtain walls.

This study contributes towards developing new transparent façade design protocols for seismic considerations by reinforcing them with experimental data alongside advanced finite element analysis. The results are beneficial to architects, structural engineers and façade consultants focused on improving the safety, reliability and strength of unitized systems constructed using glass.

Chapter 5

Numerical Modeling Strategy and Tools

5.1. Software and Modeling Environment

The current study's numerical modeling and simulation was executed using the Structural Analysis Program 2000 (SAP2000). This computer program is widely used in both academic research and engineering practice. SAP2000 offers an advanced capabilities for performing finite element analysis (FEA) on a wide range of structural systems. The interface of the software is suitable for façade work as it provides the ability to adjust custom material properties, displacement-controlled loading and complex interactions between connectors and structural elements.

In the TU Delft–Permasteelisa experimental study, a single unitized glass panel with an aluminum frame was model as finite element in detail. The glass parts were represented by shell elements, the aluminum sections had frame elements, while structural silicone connectors were modeled by linear link springs with given stiffness values that dwarf compared to overall stiffness of the assembly.

Boundary conditions and loading were aligned to the physical tests. 24 mm in-plane lateral displacement could be administered and monitored during evaluation of seismically induced drift collapse. Geometrical and mechanical elastic simplifications were made for computer simulations concerning system primary behaviors allowing optimization studies without introducing behavioral complexity from non-linearity.

By focusing on a single panel and using consistent boundary conditions, the study isolates the role of frame stiffness, connector flexibility and glass behavior under drift conditions. This methodology is consistent with the experimental framework and enables the construction of a controlled environment for the subsequent comparative simulations where changes in material properties or geometry will be introduced.

5.2. Element Types and Modeling Approach

Frame Elements for the Aluminum Structure

The façade unit perimeter is framed with an aluminum profile which was modeled using frame elements that resist axial forces and bending moments. Each edge of the rectangular frame was idealized as a member to the side with hollow rectangular cross section, which is common to use in curtain walls due to their efficiency. The corners were simulated to have pinned joints and were described as mechanically fastened hinges which allows rotation due to the connection's flexibility. Assigning material properties according to EN AW 6063-T6 aluminum alloy matched well with the Type 3 reference configuration.

Shell Elements for the Glass Panel

The glass panel was modeled using shell elements that can simulate thin surfaces subjected to in-plane and out-of-plane forces. In this case, glass panel was represented as a single-layer shell with an effective thickness of 28 mm which corresponds to the stiffness of triple laminated insulating glass units. This approach streamlines modeling within SAP2000 while maintaining structural accuracy. The panel was offset by 10 mm in the Y-direction relative to the frame's centerline to reflect real assembly conditions.

Spring Elements for the Silicone Connectors

The interface of the glass panel and its supporting frame is executed with link (spring) elements simulating the behavior of structural silicones. A total of 48 springs were uniformly distributed: 15 per vertical edge and 11 per horizontal edge. Each spring was defined with in-plane translational stiffness in the X and Z axes, while allowing rotational degrees of freedom to be released which permits relative movement of the panel to the frame.

Using shear deformation theory, spring stiffness values were derived from silicone bonded area and silicone thickness. With this bonding strategy, a realistic representation of the load transfer and deformation flexibility, which are the key properties of façade sealants during seismic shear, was achieved.

5.3. Geometric and Mechanical Properties of the Model

This section defines the physical dimensions and mechanical characteristics of each part of the model. The goal is to capture the real-life inputs of the model, including sizes, cross-sections, material stiffnesses and configuration of elements. These factors were chosen to depict typical construction standards in curtain wall systems and were intended to be in accordance with the Type 3 experimental configuration used as reference.

5.3.1. Overall Panel Geometry

The façade unit is modeled as a rectangular frame surrounding a single glass panel, the dimensions are derived from the experimental reference.

- **Panel Height:** 3430 mm
- **Panel Width:** 2535 mm
- **Glass offset from frame plane (Y-direction):** 10 mm

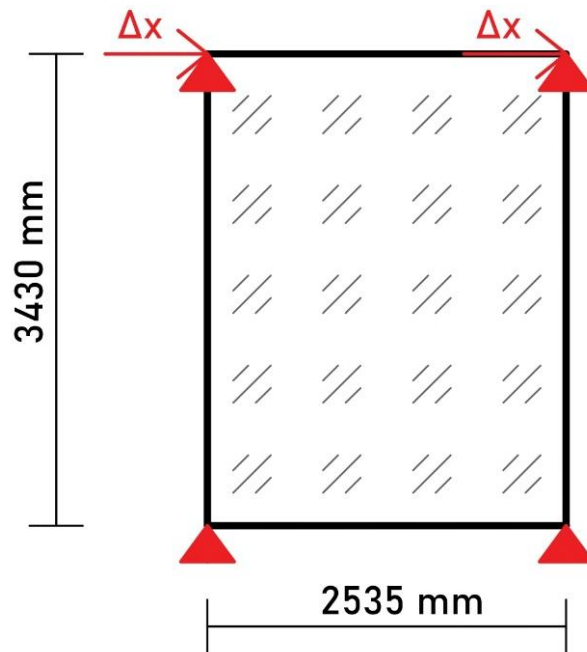


Figure 5- 1. Front view of the façade panel model.

Schematic representation of the façade panel with the frame dimensions and in-plane movement are detailed in Figure 5-1. Δx designs as the in-plane displacement, applied at the top corners. The bottom corners are fully restrained against movement.

5.3.2. Aluminum Frame Properties

The profile of the aluminum frame used in the model is characterized as a hollow rectangular section as it is a conventional standard of curtain wall construction for its high strength to weight ratio and its higher performance under bending. As shown in Figure 5-2., the profile has an outer width of 100 mm, an outer height of 185 mm and a wall thickness of 3 mm (Figure 5-2.).

These parameters were not only selected for their optimal structural performance but also according to Type 3 configuration from the prior reference experimental study. That guarantees correspondence between the numerical simulation and the experimental testing conditions.

- **Outer width:** 100 mm
- **Outer height:** 185 mm
- **Wall thickness:** 3 mm

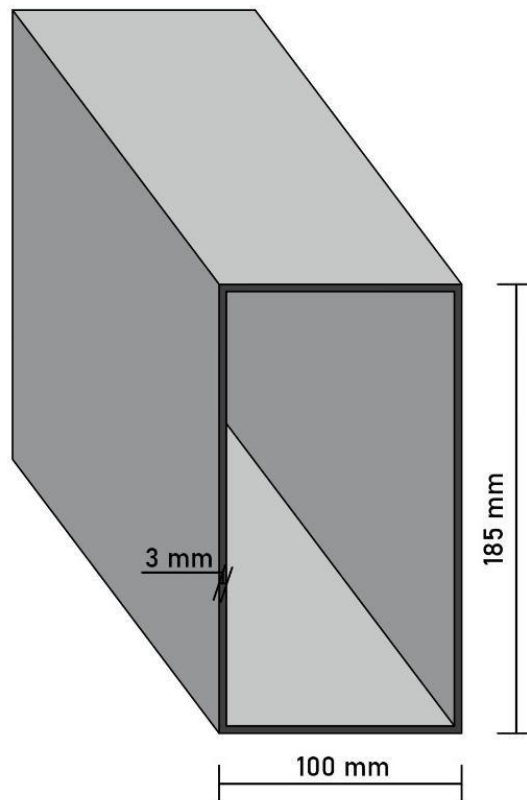


Figure 5- 2. Aluminum rectangular hollow-section with dimensions.

Table 5- 1. Material properties for EN AW 6063-T6 aluminum.

Parameters	Unit	6063-T6 Aluminum Alloy
Elastic modulus (E)	MPa	69.000
Poisson's ratio (V)	-	0,33
Shear modulus (G)	MPa	25.940
Yielding Strength (fyi)	MPa	260

5.3.3. Glass Panel Properties

The glass panel was modeled using shell elements to represent a monolithic unit with the stiffness of a triple-glazed insulating glass unit (IGU). In reality, the panel is made up of three individual glass panes: two outer panes of 10 mm and a middle pane of 8 mm thickness. The spaces between the disks are filled with gas and are 16 mm wide (Figure 5-3.). However, to simplify the process in SAP2000, the model was created as a single shell with an effective thickness of 28 mm, as opposed to three separate panes, which captures the stiffness characteristics while reducing model complexity.

- **Panel thickness in total:** 60 mm
- **Gap between Glasses:** 16 mm
- **Width:** 2535 mm
- **Height:** 3430 mm
- **Offset from frame center:** 10 mm in Y-axis

Table 5- 2. Material properties for laminated glass.

Parameters	Unit	Laminated Glass
Elastic modulus (E)	MPa	70.000
Poisson's ratio (V)	-	0,23
Shear modulus (G)	MPa	28.455
Yielding Strength (fyi)	MPa	45

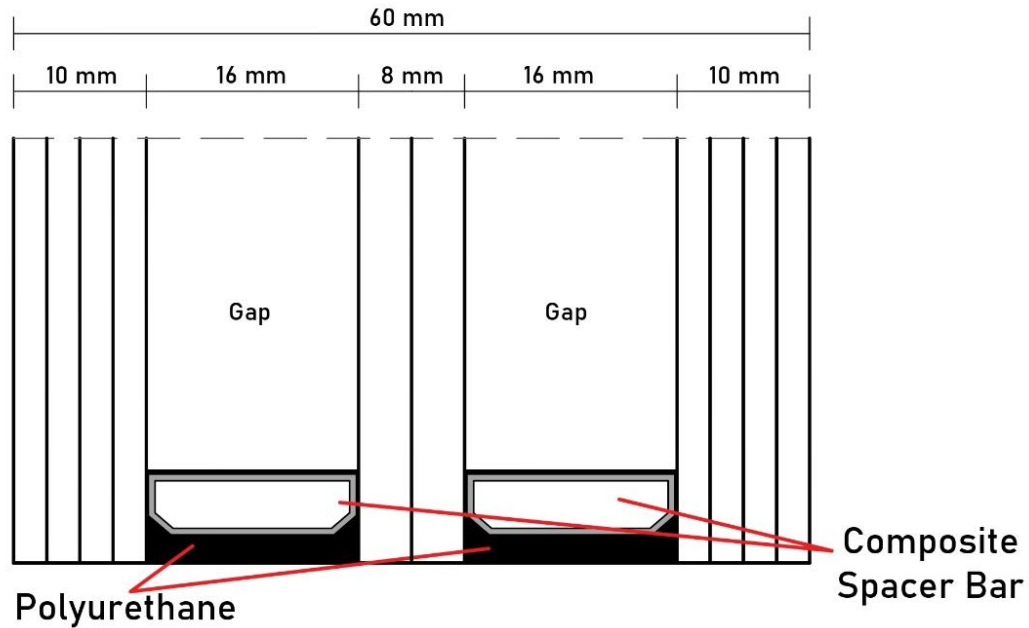


Figure 5- 3. Detailed sectional diagram of a triple-glazed unit.

5.3.4. Silicone Connector Properties

The bond between the glass and the frame was modeled with spring/link components to capture the mechanical behavior of structural silicone rubber. These connectors permit flexible load transfer with control over deformation during seismic drift.

Although the main displacement occurs within the X-Z plane, the springs were set in the Y-direction, perpendicular to the panel face. This position captures the compensating rotation due to the 10-mm offset between the centerline of the aluminum frame and the glass panel, which enables the springs to capture out-of-plane force transfer along with rotational effects due to eccentric connection.

Distribution of Springs:

- 11 per horizontal edge, 253,5 mm per gap (a)
- 15 per vertical edge, 245 mm per gap (b)
- Total: 48 springs

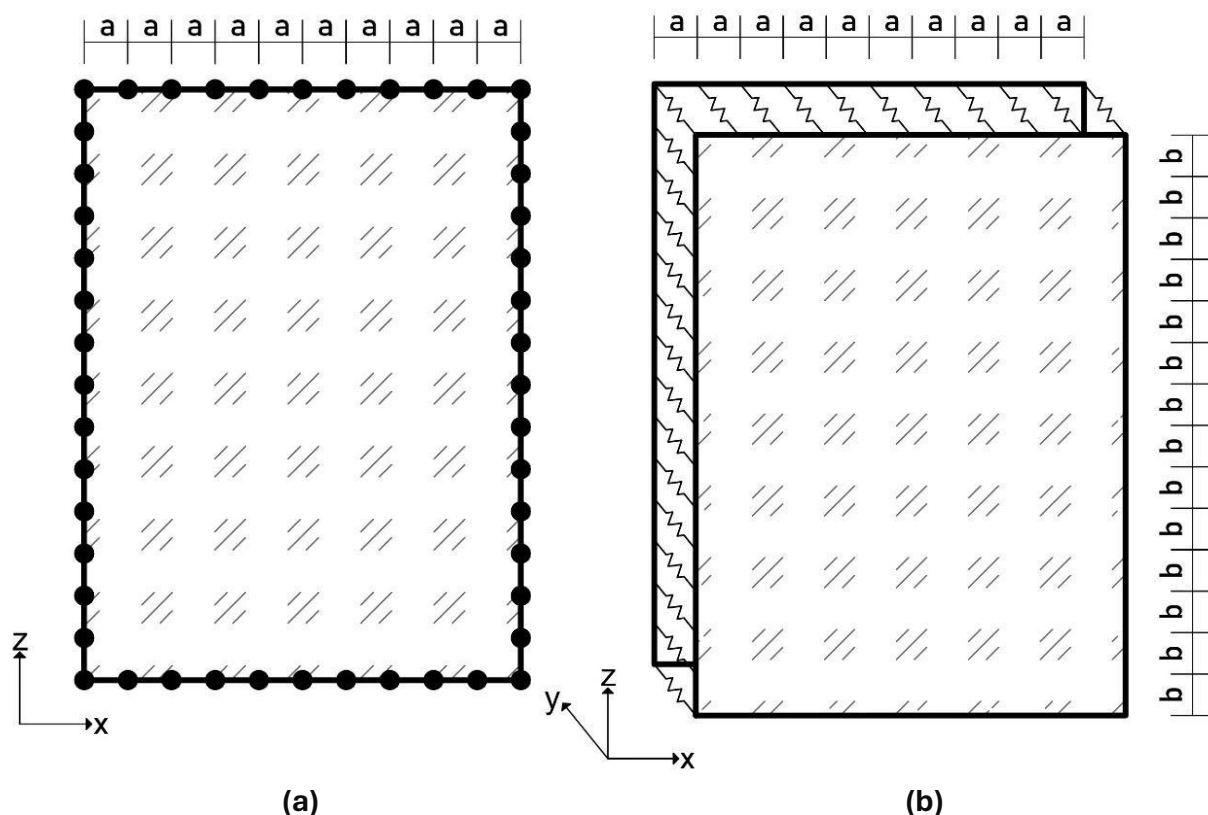


Figure 5- 4. a) Spring layout on panel edges (front). **b)** Axonometric view, Y-axis orientation.

Spacing: $a = 245$ mm (vertical), $b = 253,5$ mm (horizontal).

Figures 5-4. a) and 5-4. b) depict both the front and axonometric views of the spring configuration, showing the gaps, arrangement and spring directions used to construct the structural silicone in the numerical model.

Table 5- 3. Material properties for structural silicone.

Parameters	Unit	DOWSIL™ 993 Silicone
Elastic modulus (E)	MPa	2
Poisson's ratio (V)	-	0,45
Shear modulus (G)	MPa	0,7
Tensile Strength	MPa	0,95

The cross-sectional drawing in Figure 5-5. shows the bonded interface between the aluminum frame and the glass panel, connected by structural silicone. The spring is applied continuously along the edge of the glass as a side view shows, with a defined silicone bite (b) of 25 mm, bonding length (i) of 250 mm (which is unviewable on the side view) and silicone thickness (th) of 8 mm. All of these parameters are critical for estimating the stiffness of links and their ability to support shear forces during lateral drift.

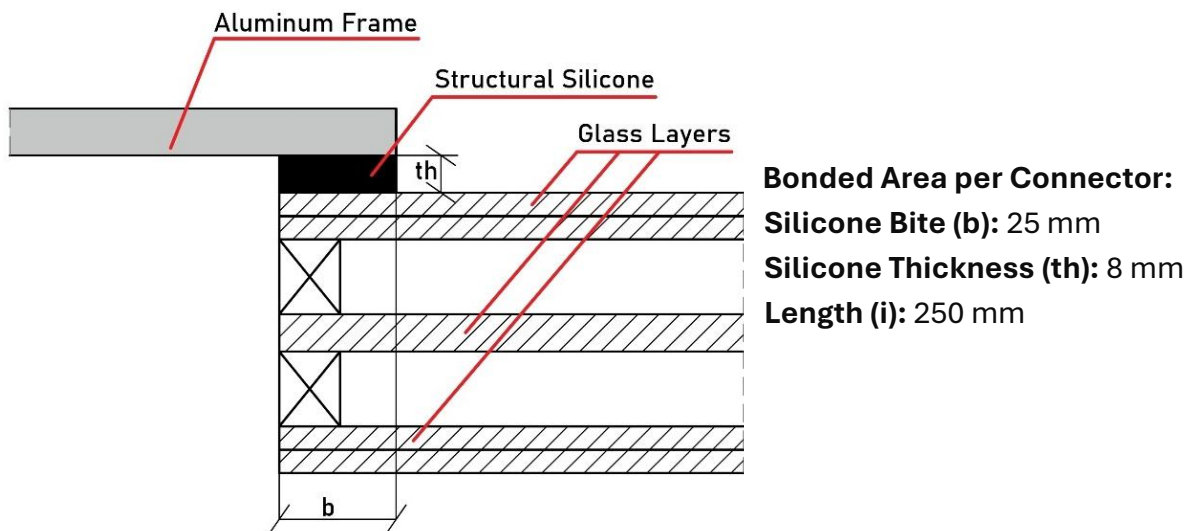


Figure 5- 5. Glass-frame silicone connector cross-section.

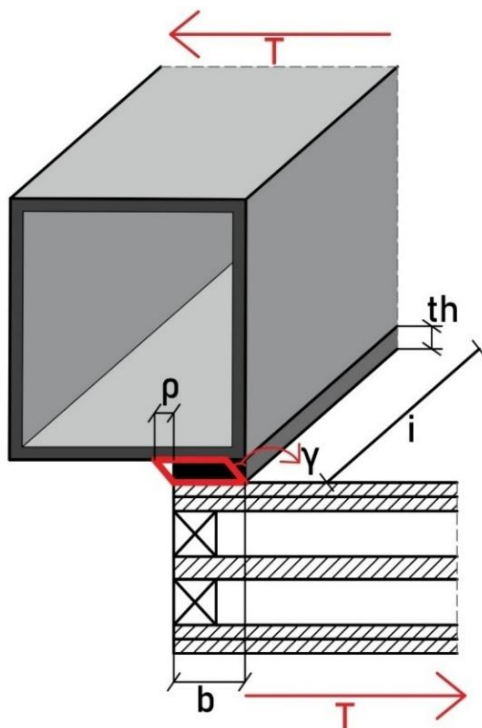
After confirming the individual spring constants, the next goal is to map how each spring channels sideways load into the surrounding aluminum frame.

When a 24-mm story drift is applied, shear forces travel through all 48-silicone links straight into the mullions and transoms. Since that load enters at the corners of each panel, it creates a couple that in turn generates a base-bending moment and a corresponding lateral deflection shape. Whether the EN AW-6063-T6 extrusions stay within their elastic limit therefore rests on knowing link stiffness exactly.

Table 5-4. illustrates how the stiffness of the silicone rubber connector was calculated step by step. It indicates the process of the formulas step by step, starting with the basic shear force and strain relationships and leading to a final simplified formula.

Table 5- 4. Stiffness Calculation Steps of Silicone Rubber Connector.

Steps-Description	Formulas
1-Shear Force	$T = \tau.A = \tau.b.i$
2-Shear Stress Relation	$\tau = G.\gamma$
3-Combine to get T	$T = G.\gamma.b.i$
4-Shear Strain Definition	$\gamma = \frac{\rho}{th}$
5-Stiffness Formula from T and ρ	$K = \frac{T}{\rho} = \frac{G.\gamma.b.i}{\gamma.th}$
6-Stiffness Formula	$K = \frac{G.b.i}{th}$



The key parameters shown in the figure:

- **i**: bonded length
- **b**: silicone bite
- **th**: silicone thickness
- **T**: shear force
- **ρ** : displacement
- **γ** : resulting strain

Figure 5- 6. Silicone joint shear schematic with dimensions and forces.

Table 5- 5. Parameters for calculating Shear Stiffness (K).

Parameters	Unit	DOWSIL™ 993 Silicone
Elastic modulus (E)	MPa	2
Shear modulus (G)	MPa	0,7
Silicone Bite (b)	mm	25
Silicone Thickness (th)	mm	8
Bonded Length (i)	mm	250

$$K\tau = 0,7 \times 25 \times 250 / 8$$

Shear Stiffness ($K\tau$): 547 N/mm

$$K\sigma = 2 \times 25 \times 250 / 8$$

Axial Stiffness ($K\sigma$): 1562 N/mm

The calculated stiffness values (Table 5-5.) reflect the mechanical response of the silicone connector under deformation. The shear stiffness ($K\tau=547$ N/mm) indicates the silicone joint's resistance to in-plane displacement, which is the primary loading condition during seismic drift. The axial stiffness ($K\sigma=1562$ N/mm) although not directly engaged under lateral displacement, characterizes the material's response under vertical or out-of-plane tension and is included here for completeness.

The results indicate that the silicone acts as a moderately flexible connection that allows movement while effectively transferring force between the glass and the frame. This force derived from the stiffness under the imposed drift condition will be the calculation base of the internal bending moment of the aluminum frame, as described in the following section.

5.4. Boundary Conditions and Loading

The boundary conditions and loading approach incorporated into the model were designed to reflect the experimental setup from the reference experimental study. In the research, unitized curtain wall system seismic performance was evaluated through a set of displacement-driven tests, including cyclic, crescendo, earthquake record and monotonic loading protocols. These tests were performed in various directions and combinations.

This research narrows down the focus to the cyclic test condition applied in the Type 3 configuration, specifically in the horizontal in-plane direction (X-axis). In this analysis, a façade panel under horizontal cyclic loading is studied to identify its in-plane shear response; thus, the choice of cyclic loading scenario allows capturing its fundamental behavior without the additional complexities of vertical displacement cases. The displacement that was set for the simulation is 24 mm, which is one of the fundamental shear values that were tested during the experimental matrix. In addition to that, all of the corners of the aluminum frame were fully fixed to eliminate any enabled movement in any direction.

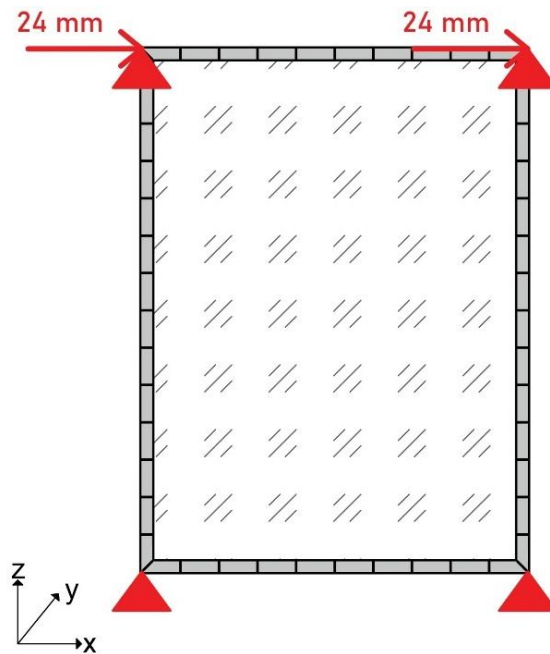


Figure 5- 7. Boundary conditions, 24 mm top-corner displacement.

A lateral displacement of 24 mm on the X-axis was applied at the top corners of the glass panel. The glass panel was not directly loaded; rather, it was constrained to move with the frame through silicone spring connectors. This displacement was created due to a 10 mm offset in the Y-direction, which in turn caused shear and rotational effects on the glass due to eccentric loading. This configuration is schematically illustrated in Figure 5-7.

Chapter 6

Structural Response of the Glazing Unit

The current chapter focuses on the outcomes obtained from the FEA performed on the glass-aluminum façade panel through horizontal displacement. The emphasis is placed on the mechanistic understanding of the systemic deformation, as well as the response of each part individually considered: the frame, the glass and the structural silicone links. The results are given in form of displacement value, rotational effect, internal force build-up and stress distribution.

6.1. Displacement Response of the Frame

The structural boundary of the façade unit is captured by the aluminum frame. The unit experiences significant geometric change along the Z-axis drift is placed. The imposed 24 mm in-plane displacement induces a racking effect, altering the orthogonal geometry of the originally rectangular frame into a parallelogram-like configuration. This deformation mechanism is typical in slender façade systems subjected to horizontal loading and is particularly critical for evaluating the drift compatibility of curtain wall panels in seismic scenarios.

For the purpose of measuring the level and type of deformation, analysis proposes the following criteria:

- **Elongation (ϵ)** of the diagonal,
- **Rotation (α)** of the frame,
- **Distortion (θ)** of the corner angles.

The regional and global displacement behavior of the frame is evaluated through these parameters which derived from the deformed finite element model. Unlike simple displacement readings at individual nodes, these geometric metrics capture integrated deformation effects, offering a more holistic understanding of how the frame adapts to lateral actions.

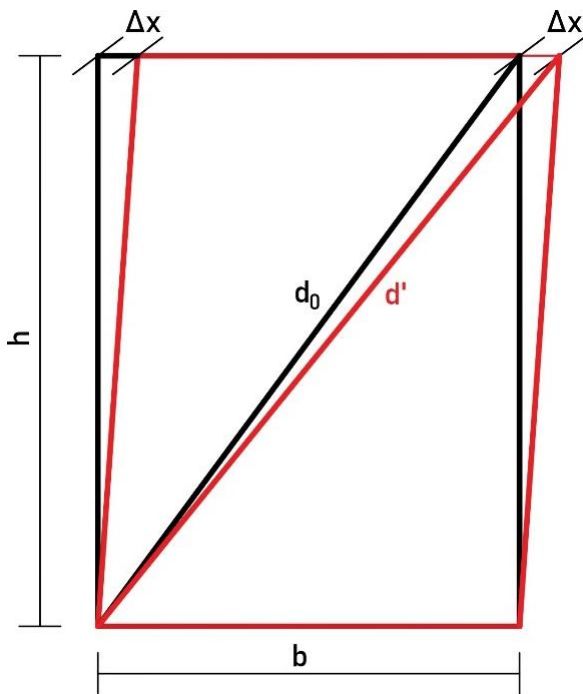
The quantitative evaluation of these indicators helps assess the structural integrity along with other factors such as the structural condition of the frame under drift, keeping its alignment with the glass panel, and considering the unit performance of the entire façade. Each of those parameters is explored in depth in the next subsections.

6.1.1. Frame Elongation (ε)

Frame elongation (ε) measures the increase of a diagonal length due to in-plane shear deformation, and therefore, provides a quantifiable assessment of rotational frame deformation resulting from lateral drifting and yielding of parts of the frame.

Using the Pythagorean theorem with a horizontal displacement of 24 mm at the top corners, the original and deformed diagonals are derived from the initial frame width and height.

$$\varepsilon = \left(\frac{d' - d_0}{d_0} \right) \quad \begin{aligned} (d_0)^2 &= b^2 + h^2 \\ (d')^2 &= (b + \Delta x)^2 + h^2 \end{aligned}$$



In the equation, $b = 2535$ mm, $h = 3430$ mm and $\Delta x = 24$ mm is the horizontal shift at top corners.

$$d_0 = \sqrt{2535^2 + 3430^2} = 4265,105 \text{ mm}$$

$$d' = \sqrt{2559^2 + 3430^2} = 4279,413 \text{ mm}$$

$$\varepsilon = \left(\frac{4279,413 - 4265,105}{4265,105} \right)$$

$$\varepsilon = 0,0033$$

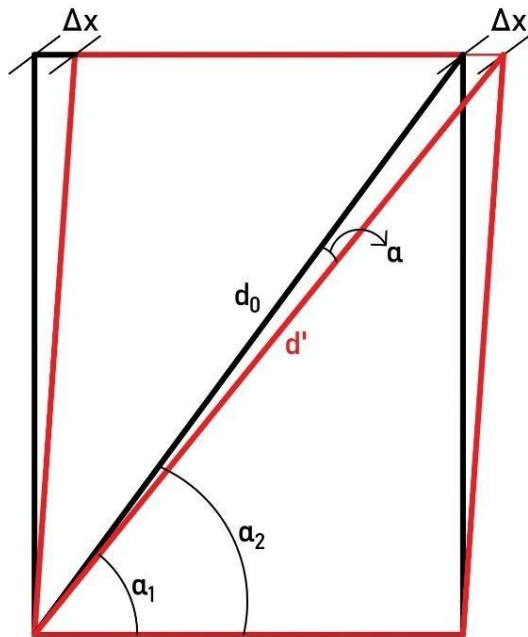
Figure 6- 1. Elongation (ε) of the diagonal caused by in-plane shear.

Figure 6-1. shows the relation between the undeformed and elongated diagonals and marks the change in geometry because of shear.

6.1.2. Frame Rotation (α)

Frame rotation (α) denotes the angular shift of the frame's diagonals with respect to each other and to the vertical axis as a result of the imposed drift. In contrast to the idea of rotation at a single joint, this parameter is meant to capture the global inclination of the frame and its deviation from the original vertical orientation.

The rotation is calculated from the difference between the vertical edge and the diagonal in both undeformed and deformed positions:



In the equation, $\Delta x = 24$ mm is the imposed lateral displacement and $h=3430$ is the panel height.

$$\alpha = |\alpha_1 - \alpha_2|$$

$$\alpha_1 = \arcsin\left(\frac{h}{d_0}\right)$$

$$\alpha_2 = \arcsin\left(\frac{h}{d'}\right)$$

$$\alpha = 0,26^\circ$$

Figure 6- 2. Rotation (α) of the vertical member due to lateral drift.

The concept of rotational displacement with its geometric interpretation is presented in Figure 6-2., which substantially focuses on the angular displacement of the vertical member.

6.1.3. Frame Distortion (θ)

Frame distortion (θ) quantifies the change to the internal right angles of the frame due to shear. It specifically reflects how much the 90° corner angles are reduced under lateral deformation, which is fundamental to the position of the curtain wall components, their alignment and the function of the connectors.

The shear angle (γ) is determined as:

$$\gamma = \arctan\left(\frac{\Delta x}{h}\right)$$

$$\theta = 90^\circ - \gamma$$

$$\gamma = 0,4^\circ$$

$$\theta = 89,6^\circ$$

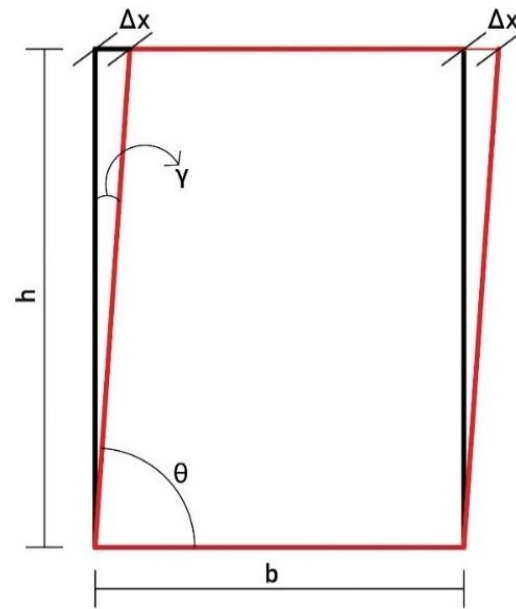


Figure 6- 3. Distortion (θ) of the internal angle reflecting racking deformation.

This verifies a small deviation from the original geometry within the elastic range for aluminum frames of this configuration, typical of racking behavior. The slight deviation also confirms the greater need for flexibility in the joints and connections to such distortions in order to avoid stress concentrations. As illustrated in Figure 6-3., this issue relates to façade design where alignment visually and connection tolerances need to be maintained when movements occur.

6.2. Bending Moment Distribution in the Aluminum Frame

The force transferred through the silicone rubber connection contributes directly to the internal bending moment experienced by the aluminum frame. In the case of lateral displacement, the silicone modeled as a linear spring, thus resisting the movement generating a shear force. The shear force is calculated with the shear stiffness and imposed displacement, acts at the panel height, thereby creating a bending moment at the base of the frame.

In this structural configuration, the aluminum frame acts as a closed rectangular ring. The top and bottom horizontal members are subjected to shear forces or shear coupling moments due to the connector forces, and these forces act in opposite directions. The side vertical mullions serve as moment-resisting links, forming a quasi-rigid frame under racking deformation. Therefore, it creates bending moments that do not follow a uniform

distribution but have maximum values at positions where boundary conditions (fixed base) and segment interactions (spring nodes) are present and most critical.

In SAP2000, this bending response is captured using the Moment 3-3 output, which is typically the axis vertical to the frame's wide flange, and includes the bending response. The analysis suggests that the concentration of the moment intensity is at the top and bottom corners, those two extremities are where the combination of lateral displacement and restraints leads to the highest curvature of the structure.

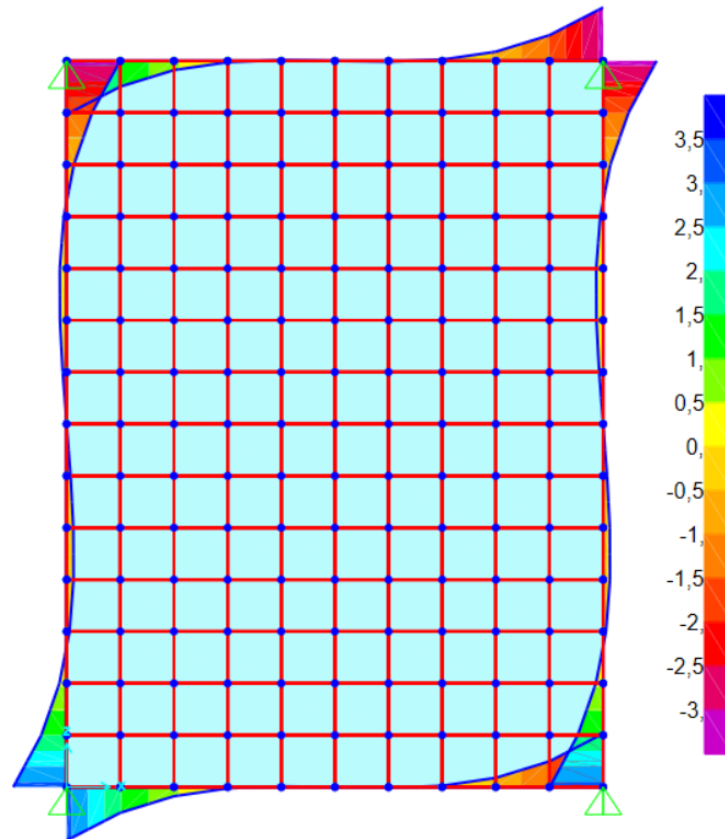


Figure 6- 4. Moment distribution (M3-3) in the aluminum frame.

Max. Bending Moment = $\pm 3,5$ kN.m

Figure 6-4. shows color scaling within the diagram indicating the applied bending moment directions and values.

- **Purple to orange tones** represent negative moments, indicating compression on the inner face
- **Blue to green tones** represent positive moments, indicating tension on the inner face of the aluminum section.

As shown in the figure, the highest moment intensity occurs at the top and bottom corners of the frame, reaching approximately $\pm 3,5$ kN.m, indicating significant bending due to the 24 mm impose drift while the corners are fully restrained. The resulting distribution forms a symmetric pattern, which aligns well with the boundary conditions and lateral loading configuration, confirming the expected structural behavior under in-plane seismic action.

6.3. Von Mises Stress Distribution in the Aluminum Frame

The stress response of the aluminum frame under lateral drift is governed by the combined effects of bending, axial load transfer, and localized shear near the spring connector zones. To evaluate this cumulative stress state, von Mises stress (σ_{VM}) was used as the primary performance indicator, offering a scalar value that represents the equivalent uniaxial stress under multiaxial loading conditions.

SAP2000 provides von Mises stress output based on internal force and moment results along each frame element. This output considers both normal (bending/axial) and shear components, calculated using the following formulation:

$$\sigma_{VM} = \sqrt{\sigma^2 + 3\tau^2}$$

Where:

- σ = Normal (bending or axial) Stress
- τ = Shear Stress

The color contour in Figure 6-5. represents the magnitude of combined stress intensity in MPa. The analysis shows that the highest von Mises stresses are located at all four corners of the frame, zones where lateral drift forces intersect with joint restraints and where structural members meet.

These areas exhibit stress concentrations due to:

- Localized bending moments,
- Spring connection resistance,
- Frame fixity and edge restraint.

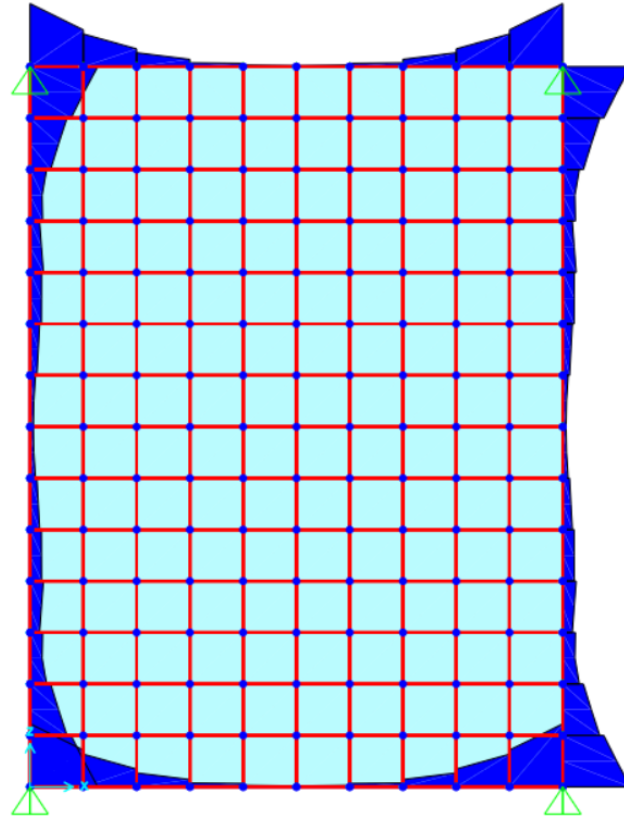


Figure 6- 5. Von Mises stress distribution in the aluminum frame.
Peak Stress = 59,1 MPa.

According to the SAP2000 results:

- The top corners reach stress values up to 59,1 MPa, driven by torsional effects and lateral drift resisted by the silicone springs.
- The bottom corners display slightly lower stress levels around 58 MPa, attributed to the combined action of imposed displacement and full fixity at supports.

These data suggest that the most intense mechanical demand is concentrated at the top corners near the region where lateral loads were applied and where deformation was both active and resistive, controllable to a certain extent. The stress pattern validates the observation that the top frame components are subjected to the maximum level of moment and equilibrium spring force interaction.

For the purpose of estimating structural safety, the calculated Von Mises stress is benchmarked against the yield strength of the alloy utilized for the frame structure, 6063-T6, which typically ranges between 250 and 300 MPa. It is noted that the peak value of stress calculated falls within these limits.

$$\sigma_{VM} = 59,1 \text{ MPa} < f_{yi} = 260 \text{ MPa}$$

This confirms that the aluminum frame is fully contained within the elastic range during the design-level lateral displacement of 24 mm. Consequently, potential risk for plastic deformation or local yielding in the case of the imposed load scenario is negligible for the imposed load case.

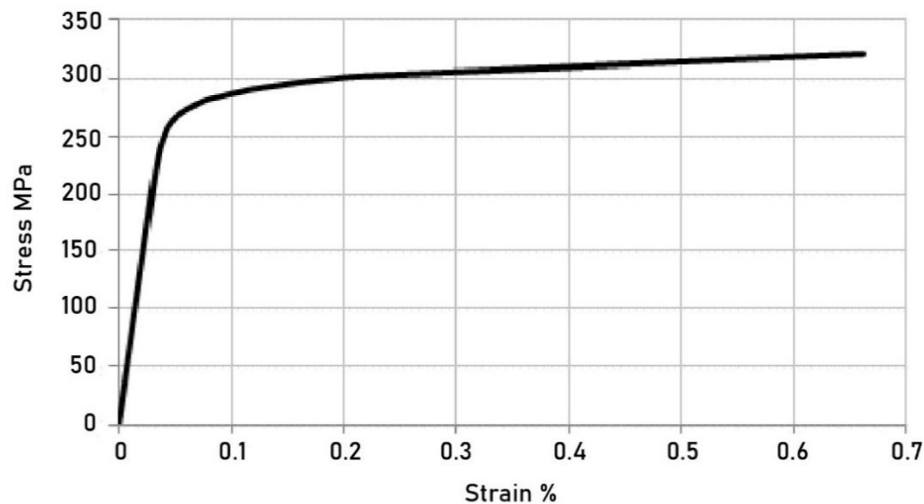


Figure 6- 6. Stress-strain curve of 6063-T6 aluminum alloy.

Moreover, the outcomes provided both the validation of the structural integrity of the current design and confirming the estimation of SAP2000 modeling assumptions. While the simulated drift aligns with a performance-level seismic event, actual building codes such as Eurocode 8 and ASCE 7 do impose safety limits on top of material capacity as well as load actions. Therefore, even under these considerations, the design is exceptional in terms of structural integrity [8] [9].

In conclusion, while the global performance is adequate, the existence of locally high stress concentrators at the frame corners highlights the need for attention in the detail design in these areas. In particular bolted stiffeners for corners, corner stiffeners and other forms of long-term fatigue mitigating design that enhance system durability and robustness in actual earthquake engineering in real-world.

6.4. Displacement Response of the Glass

Structural response of the glass panel was evaluated based on the imposed in-plane displacement of 24 mm, excluding other load combinations such as dead load. In the SAP2000 model, the glass was represented as a single shell element with a total thickness of 28 mm, connected to the aluminum frame through link (spring) elements and positioned with a 10 mm offset in the Y-direction, causing load transfer. With this configuration, the panel exhibited not only translation but also a distinct rotation around its centroid.

The displacement output of the top and bottom glass corners was extracted from SAP2000 under the displacement-only load case. The key parameters analyzed were:

- **Ux**: Translation in the X-direction (horizontal movement).
- **Uz**: Translation in the Z-direction (vertical shift).
- **R2**: Rotation about the Y-axis (torsional behavior).

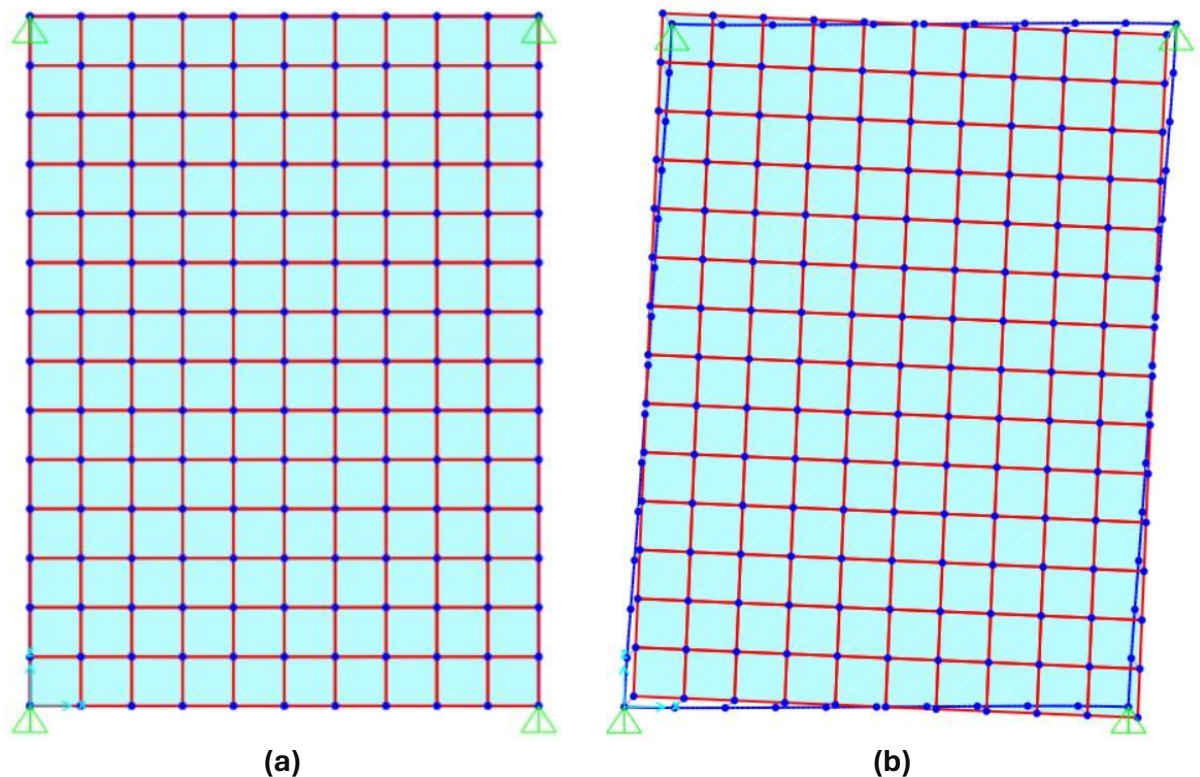


Figure 6- 7. a) SAP2000 model; b) Deformation under 24 mm in-plane displacement.

The displacement output from SAP2000 is shown in Figure 6-7. a) marks the initial undeformed shape of the façade unit shows full alignment between the glass shell element and the aluminum frame. The panel appears flat, and no deformation is visible.

After the application of the 24 mm displacement load at the top corners of the frame, the resulting deformed shape is shown in Figure 6-7. b). In this figure, the red outline (glass) is visibly rotated compared to the blue outline (frame), indicating torsional behavior caused by the spring connection layout.



Joint	Object	1	2	3
Trans		0,0047	0,	0,00537
Rotn		0,	0,00424	0,

Figure 6- 8. Joint 1-displacement output from SAP2000 (left-bottom corner).



Joint	Object	1	2	3
Trans		0,0193	0,	0,00537
Rotn		0,	0,00424	0,

Figure 6- 9. Joint 4-displacement output from SAP2000 (left-top corner).

Table 6- 1. Glass corner-joint displacements by SAP2000.

Joint Number	Position of the Corner	Ux [m]	Uz [m]	R2 [rad]
Joint 1	Left- Bottom	0,0047	0,00537	0,00424
Joint 2	Right-Bottom	0,0193	-0,00537	0,00424
Joint 3	Right-Top	0,0193	-0,00537	0,00424
Joint 4	Left-Top	0,0047	0,00537	0,00424

The results presented in Table 6-1. indicate:

- **U_x** values varied across the panel width, with the right-side joints (Joints 2 and 3) displacing more than the left-side joints (Joints 1 and 4), confirming differential lateral motion.
- **U_z** values remain constant at all four corners, showing uniform vertical deformation.
- **R₂** values were also identical across all corners, confirming that the glass rotated as a rigid body around its vertical axis.

The above findings show that the glass did not undergo rigid body motion. Rather, it exhibited bending and torsional deformation mostly seen in façade elements attached by flexible connectors.

Centroidal Rotation and Translation Check:

The panel was further examined around its centroid in terms of displacement and rotation to verify the behavior. In the mechanics of a façade, analyzing the corners and centroid is necessary to differentiate between true rotational deformation and rigid translation. In instances where a panel acts as a rigid body, the movement at the centroid would be the result of rotation at the corners and not any additional rotational component of the panel.

To verify these results geometrically, a simplified physical boundary relationship was applied to compute centroidal behavior using boundary displacement inputs. In this case, the reference point chosen was the left-top corner of the panel with the applied relationships aimed to validate the observed displacement and rotation patterns.

Table 6- 2. Parameters for displacement and rotation calculations.

Parameters	Descriptions
δx	Centroidal displacement in the X-direction
ϕ	Rotation about the Y-axis
b	Width of the panel (2,535 m)
h	Height of the panel (3,430 m)

Horizontal Displacement (U_x):

This equation represents how the rotation ϕ contributes to horizontal displacement at the top edge of the panel. Since the centroid is vertically centered, any rotation ϕ will result in arc-shaped motion at the edges proportional to $\frac{h}{2}$.

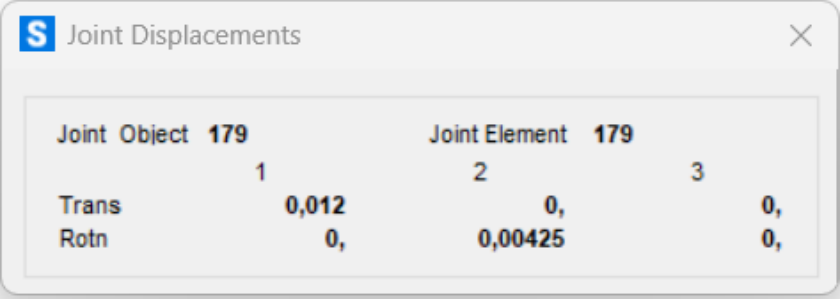
$$U_{X_4} = \delta x + \phi \cdot \frac{h}{2}$$

Vertical Displacement (U_z):

This equation describes the vertical displacement at the corner due to the rotation about the centroid. The rotation causes the left and right corners to move vertically in opposite directions, proportional to half the panel width.

$$U_{Z_4} = \phi \cdot \frac{b}{2}$$

As a result of these equations, the left-top corner displacements can be used to verify the centroidal displacement (δx) and rotation (ϕ) obtained from the SAP2000 simulation.



	Joint Object 179	Joint Element 179		
	1	2	3	
Trans	0,012	0,	0,	
Rotn	0,	0,00425	0,	

Figure 6- 10. Joint 179-displacement output from SAP2000 (centroidal joint).

These calculated displacements match exactly with the SAP2000 output for Joint 4 (top-left corner), confirming the consistency and accuracy of the model. It also verifies that the glass behaves as a rigid body rotating about its centroid under in-plane drift, with symmetric vertical displacement at corners and predictable horizontal offset due to torsion (Figure 6-11.).

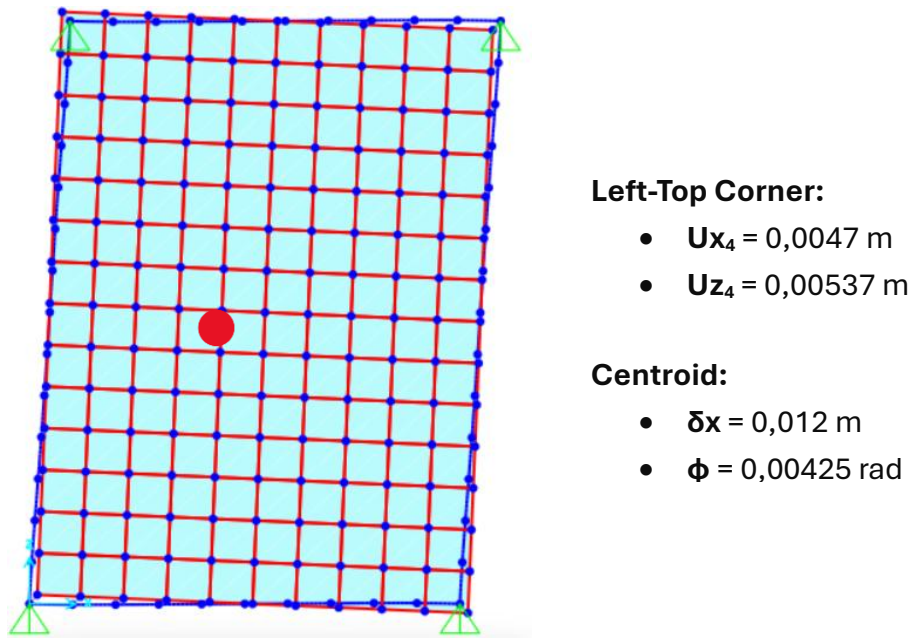


Figure 6- 11. The centroid (Joint 179) displacements, the SAP2000 results.

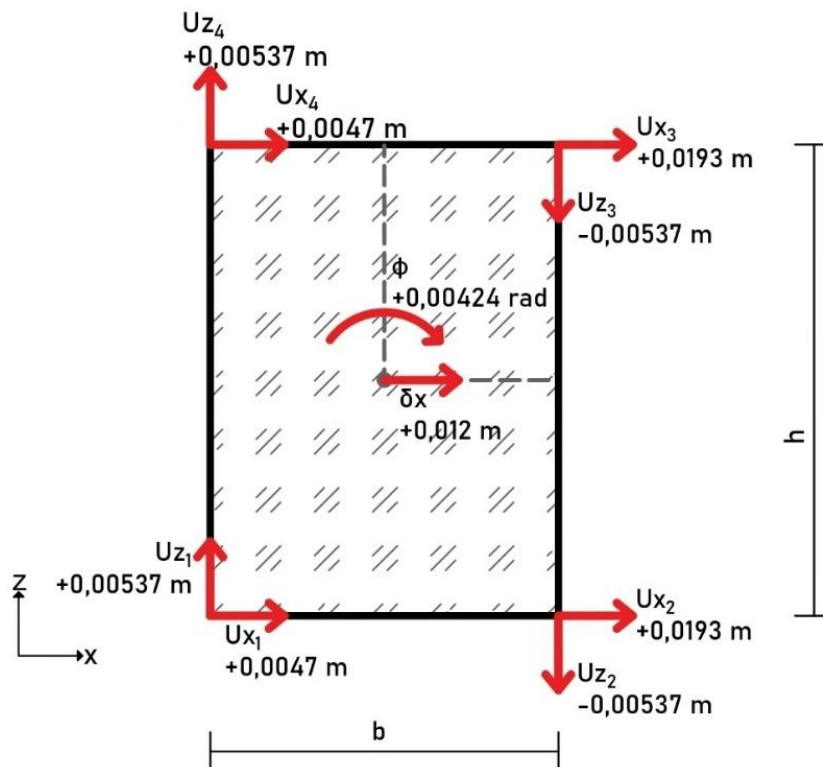


Figure 6- 12. Glass-panel kinematics under lateral drift.

A schematic representation highlighting this rotational behavior about the centroid is presented in Figure 6-12., illustrating how the panel twists around its geometric center as a response to the applied displacement.

6.5. Principal Stress in the Glass Panel

The structural response of the glass panel to an in-plane displacement of 24 mm was assessed further by estimating the stress distribution using SAP2000. To evaluate the critical stress areas, the Smax (maximum principal stress) component from the SAP2000 shell element outputs was selected. This parameter is particularly important in the context of glass design, since glass fails under tensile stress and the maximum principal stress helps to highlight areas which are most prone to failure. Unlike ductile materials, glass does not yield significantly before failure. However, it is more appropriate to monitor the peak tensile stress rather than the Von Mises stress for this material.

Under lateral seismic loading, the panel is subjected to a complex combination of translational displacements, rotational effects and frame flexibility. These global displacement boundary conditions lead to non-uniform stress distributions developing over time which has the potential of being magnified at the edges or corners of the panel depending on the panel's geometry and the specific restraint configuration.

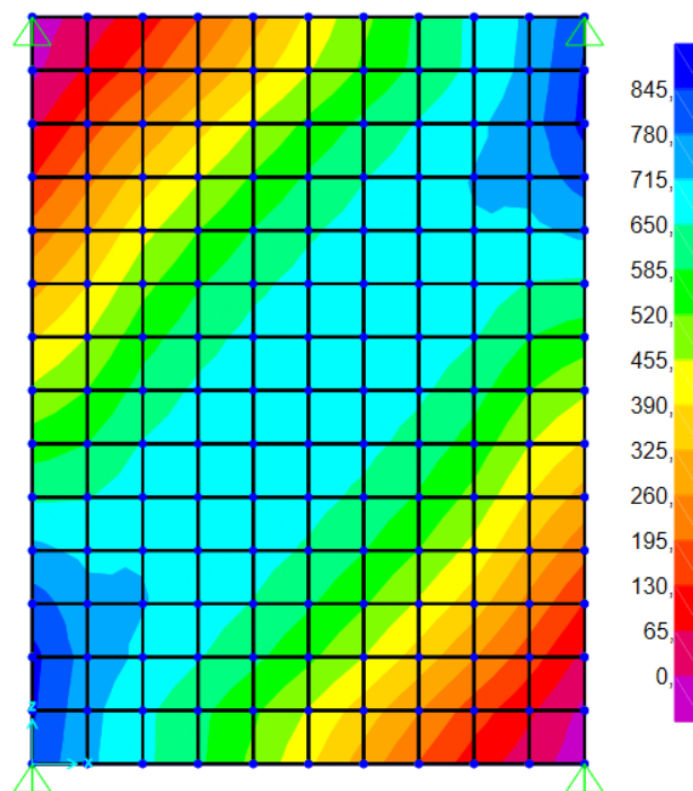


Figure 6- 13. Maximum principal stress distribution in the glass.
Peak Smax = 845 kPa (0,845 MPa).

Figure 6-13. shows that the greatest peak in tensile stress occurs along the diagonal of the panel, most notably at the extreme right-top and left-bottom corners. These areas experience maximum tension due to the frame coupled racking and torsional deformation. The stress pattern is responsive to the 10 mm vertical Y-offset of the glass and therefore asymmetric deformation rotation leads to vertical deformation asymmetry. Although, being geometrically centered, the centroid of the panel does not behave as a stress-neutral zone due to the combined influence of lateral displacement and spring configuration layout along the sides.

The level of maximum stress does not exceed 0,845 MPa and remains significantly below the tensile strength of standard float glass, which depends on edge condition and treatment ranges between 30-90 MPa for laminated glass. Even when applying safety factors, observed stress is comfortably above the failure threshold, which confirms the hypothesis that the glass panel remains functional elastically and safely withstands applied drift.

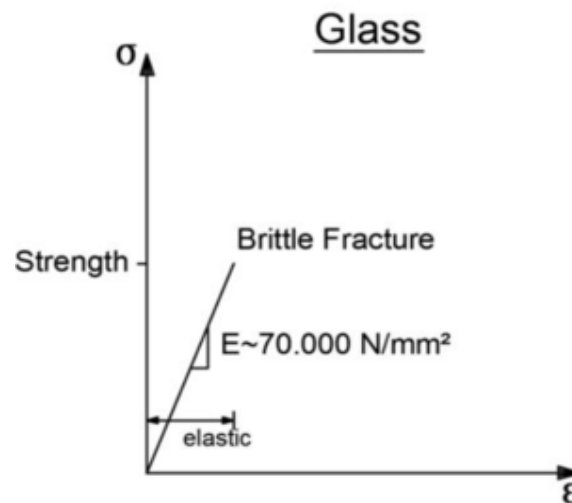


Figure 6- 14. Stress-strain curve of laminated glass.

Glass, as shown in Figure 6-14., behaves with a linear-elastic characteristic and does not display any considerable post-yield behavior. It undergoes sudden and catastrophic failure when the tensile strength is exceeded. This characteristic emphasizes the necessity of strict stress control in design and analysis. With regard to S_{max} from SAP2000, it is clear that the glass in this system remains within the allowable limits, thus confirming the assumptions made by both the design and assessing the structural performance of the panel during seismic racking.

Figure 6-14. adapted from: https://www.researchgate.net/figure/Stress-strain-curves-of-steel-and-glass-for-an-uni-axial-tensile-loading-scenario-redrawn_fig50_313662114

6.6. Principal Stress in the Silicone Connectors

For the Type 3 façade configuration, the silicone connectors are characterized by a 25 mm silicone bite, 250 mm bonded length and 8 mm silicone thickness. The link-element formulation described in ‘5.3.4. *Silicone Connector Definition*’ was assigned an elastic shear stiffness of $K = 547 \text{ kN/m}$.

A displacement-controlled drift of 24 mm (global X-direction) was applied in SAP2000, and the resulting shear forces at the I-end of Link 2 (the representative spring along the vertical mullion mid-height) were exported for post-processing.

Table 6- 3. Shear Reactions for Silicone Connectors.

Parameters	Symbols	Values
Shear Stiffnes	K	547 kN/m
Shear Force (in-plane 2-direction)	V2	-2,77 kN
Shear Force (in-plane 3-direction)	V3	-2,57 kN

Extracted shear forces from SAP2000, as illustrated in Table 6-3., were applied to the representative spring location to compute the in-plane shear reactions. These values were calculated into shear stresses following the methodology presented in Table 6-4. with regard to the bonded area of the connector.

Table 6- 4. Shear-Stress Parameters for Silicone Connector Evaluation.

Parameters	Descriptions
V2 and V3	Shear forces (in kN)
b	Silicone Bite (in mm)
i	Bonded length (in mm)
T2 and T3	Shear stress components (in MPa or N/mm^2)

Using the in-plane shear reactions extracted from SAP2000, the corresponding shear stresses acting on the adhesive layer are obtained directly from formulas:

$$\tau_2 = \frac{V_2}{A} = \frac{V_2}{b.i} \quad \tau_3 = \frac{V_3}{A} = \frac{V_3}{b.i}$$

The resultant shear stress (τ_R) was then calculated using the vector sum of the two orthogonal shear stress components:

$$\tau_R = \sqrt{\tau_2^2 + \tau_3^2}$$

However, to more accurately evaluate the stress state within the silicone connectors under multiaxial loading, the maximum principal stress (σ_1) was adopted as the primary assessment criterion. In such a case the best estimate will be provided assuming multiaxial stress loading condition. Principal stresses are the normal stresses which act on a given plane when shear stress is zero. Among them, when drawing Mohr's circle for stress, σ_1 corresponds to the maximum tensile stress found at that point and is vital to some extent for materials such as silicone structural which is much more prone to tensile failure than shear yielding.

In the design of adhesive joints, considering only shear-based metrics like resultant shear stress (τ_R) evaluation is likely to underestimate failure risk, as it does not take into consideration how the shear components will create tensile zones within the adhesive layer. The maximum principal stress (σ_1), on the other hand, gives a scalar value to the peak tensile stress resulting from the combination of shearing components; thus, capturing more accurately conditions that drive failure.

The maximum principal stress value for the Pure Shear case is calculated using Mohr's circle transformation. If normal stresses are assumed to be zero and there are only two shear stresses acting in orthogonal directions (such as τ_{xz} and τ_{yz} in this case), the value of maximum principal stress is given by the following equation:

$$\sigma_1 = \sqrt{\tau_2^2 + \tau_3^2}$$

This transformation effectively converts the biaxial shear state into a single equivalent tensile stress. These results were obtained using Granit Engineering's Mohr 3D calculator [69] and these results corroborated the theoretical values of σ_1 based on shear values obtained from SAP2000 simulation outputs.

Shifting from τ_R to σ_1 gives a better approximation with the actual failure mechanisms of structural silicones, such as DOWSIL™ 993, which typically fail under tensile stress and rather than shear. As stated in the official DOWSIL™ 993 technical datasheet [70], its tensile strength is approximately 0,95 MPa, which is now a more appropriate estimate of safety limit threshold under varied deformation circumstance.

Obtained value of σ_1 computed in this study is noticeably less than this limit value which means that the silicone spring connectors perform well under the elastic region. As a result, there is no damage nor failure inflicted by the actuator because the imposed 24 mm in-plane drift is within design limits.

Table 6- 5. Stress Results and Tensile Capacity.

Parameters	Unit	Values
τ_2	MPa	-0,443
τ_3	MPa	-0,411
σ_1	MPa	0,605
Tensile Strength	MPa	0,95

Table 6-5. shows that the peak principal tensile stress in the structural-silicone joint ($\sigma_1 = 0,605$ MPa) reaches only about 64 % of the manufacturer-reported tensile capacity of DOWSIL™ 993 (0,95 MPa). Since both orthogonal shear components (τ_2 , τ_3) are well within the elastic envelope and the combined stress state never approaches the material limit.

The Type 3 connector measuring 25 mm × 250 mm × 8 mm is designated as safe for a design drift of up to 24 mm. It can be deduced with certainty that no bond tearing, edge debonding or stiffness decay will occur, confirming that this joint geometry is sufficient to ensure adequate seismic resilience for the unitized curtain-wall module.

Chapter 7

Parametric Numerical Study

This chapter presents an integrated comparative study of the effect of key design parameters on the structural behavior of a glass-aluminum façade unit under lateral in-plane drift loading. The analysis focuses on three primary categories of variation: silicone connector geometry, overall panel/frame sizes and boundary restraint conditions. Each structural parameter listed affects the deformation, force transmission, stress concentration and accumulation in a seismic-type loading system.

Regarding the model's comparability, a uniform in-plane displacement of 24 mm is applied to all configurations. The base configuration aligns with the Type 3 used in the TU Delft-Permasteelisa Group experimental study and serves as the control configuration for the performance baseline set.

The three comparative parameter groups investigated are:

- **Silicone Connector Geometry Variants:**
Explores the effect of bonded area and aspect ratio of the spring connectors (Types A, B and C) on shear force transfer while keeping the material properties constant. The purpose is to explain the deformation induced stress concentrations on the frame and the glass resulted from a changing shape of the connector.
- **Frame and Panel Dimension Variants:**
Analyzes the structural response for three configurations (Type 1, Type 3 and Type 6) based on the reference experimental study. These changes also affect height, width and aspect ratio which in turn influences the bending moment development, frame stiffness, glass rotation about the axis perpendicular to lateral displacement and lateral displacement.
- **Boundary Restraint Condition Variants:**
Evaluates the role of support flexibility and vertical loading to the displaced boundaries of the base model (restrained configurations), such as fully fixed corners as opposed to flexible restraints. Also analyze the effect of self-weight application.

All variants are simultaneously computed and analyzed with SAP2000. Among the metrics of interest are connector elongation, frame and glass displacements, moment distribution, von Mises stress in the aluminum, and principal stress in the glass and in the silicone connectors. This structured approach supports capturing the analytical level complexity where façade performance offers geometric and boundary dependence which optimized stress, stiffness, flexibility and enhanced seismic endurance by system.

7.1. Influence of Silicone Geometry

This part describes an analytical study concerning the overall response of the façade unit with regard to its silicone connector geometry. The reference configuration, named as Type A (Type 3 in the experimental study), follows the default geometry as silicone bite of 25 mm and bonded length of 250 mm with constant silicone thickness of 8 mm. Two additional configurations, Type B and Type C, were developed to reduce the silicone bite but keep the length and thickness the same, hence reducing the shear stiffness of the spring elements.

All three configurations are assigned the same silicone material properties as those listed in *Table 5-3. (Section 5.3.4.)* in order to ensure that the comparison is made only in terms of geometry without changing materials.

Table 7- 1. Matrix of bonded area configurations for silicone connectors.

Variations	Bite (b)	Length (i)	Thickness (th)	Shear Stiffness (K)
Type A (Base)	25 mm	250 mm	8 mm	547 N/mm
Type B	20 mm	250 mm	8 mm	437,5 N/mm
Type C	10 mm	250 mm	8 mm	218,75 N/mm

These stiffness values were calculated using the shear stiffness formula:

$$K = \frac{G.b.i}{th}$$

As it can be seen in the Table 7-1., a reduction in width of the silicone bite results in reduced joint stiffness for the silicone joint. The resultant stiffness values were in turn assigned to the spring (link) elements in three separate SAP2000 models, where all other geometric and boundary conditions were held constant.

Previously (*In Chapter 6*), stresses within the connectors were evaluated, here in this case the stress is with regard to the aluminum frame, the glass panel and the silicone connector in three configurations with varying silicone stiffness.

The comparative analysis includes:

- Bending moment and Von Mises stress distribution in the aluminum frame
- Displacement response of the glass panel
- Principal stress distribution in the glass panel
- Principal stress distribution in the silicone connectors

7.1.1. Bending Moment Distribution in the Aluminum Frame

This chapter analyzes how changes in silicone connector geometry impacts internal bending moment of the frame for the case of 24 mm in-plane displacement. Moment component Moment 3-3, corresponding to bending about the local strong axis of the section of the frame, was noted from SAP2000 for all three connectors and their configurations.

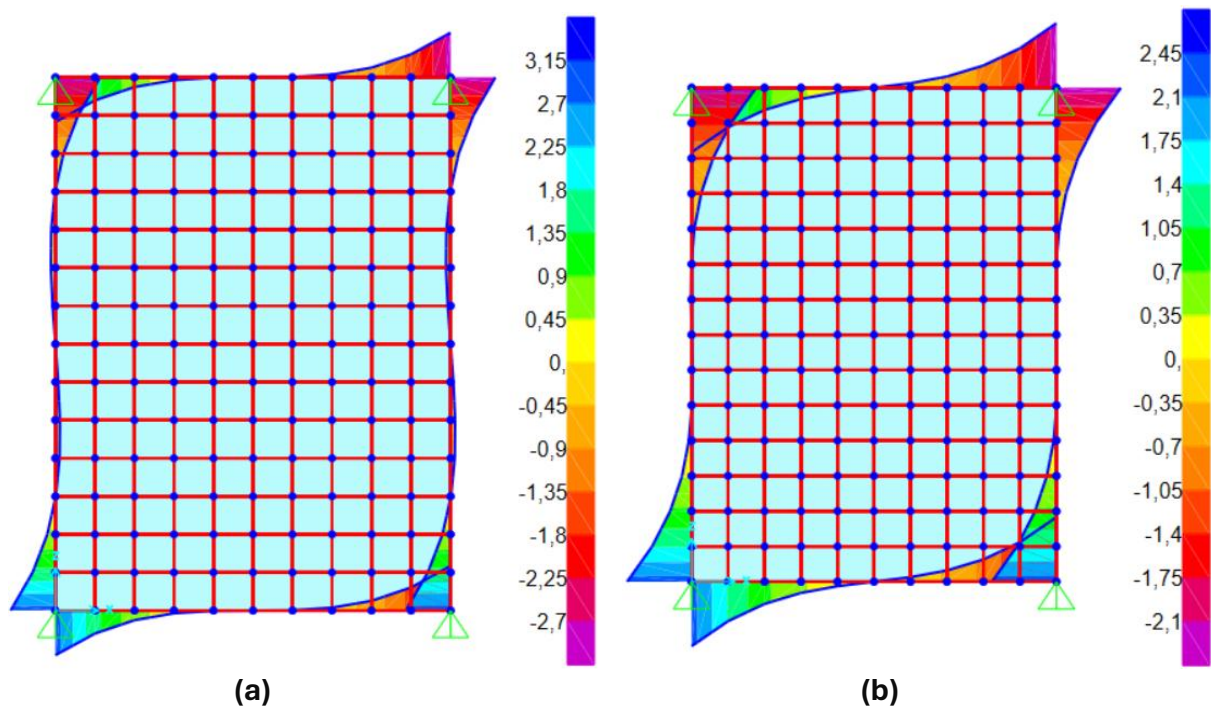


Figure 7- 1. Moment distribution (M3-3) in the aluminum frame.

a) Type B-Max. Bending Moment = $\pm 3,15$ kN.m

b) Type C-Max. Bending Moment = $\pm 2,45$ kN.m

With all configurations, moment concentration is strongest at the four corners of the frame, being the edges where the glass panel is integrated with the frame and is connected using springs and where support restraints provided (Figure 7-1.). The vertical mullions alongside the frame undergo the most severe moment accumulation due to the lateral shear transfer from the glass shell.

Table 7- 2. Peak M3-3 Bending Moment in the aluminum frame by connector type.

Variations	Shear Stiffness (K)	Max. Moment 3-3	Relative Frame Demand
Type A (Base)	547 kN/m	±3,50 kN.m	High - stiff connectors transmit more force into the frame.
Type B	437,5 kN/m	±3,15 kN.m	Medium – moderately reduced moment response.
Type C	218,75 kN/m	±2,45 kN.m	Low – flexible connectors dissipate more deformation internally

Table 7-2. demonstrates that the stiffness of the connector influences the moment demand on the aluminum frame. In Type A, the stiffest configuration, more lateral force is transferred directly from the glass panel to the frame, resulting in more internal bending. On the other hand, Type C permits relatively large deformations in the connector and consequently reduces the bending stress on the aluminum members.

This result supports the interpretation of flexible silicone joints as passive dampers that help relieve excessive structural demand under seismic drift conditions. While this might increase the deformation of the glass panel or connectors, it does ensure a more favorable force profile within the framing system.

7.1.2. Von Mises Stress Distribution in the Aluminum Frame

This subsection focuses on the effect that the stiffness of the silicone spring connectors has on stress development in the façade unit's aluminum frame. Von Mises stresses were obtained from SAP2000 simulations for all three types of simulation frames under identical conditions of 24 mm in-plane lateral drift. Identifying as close as possible the most stressing zones to verify the safety and efficiency of stress transfer in the frame critical configurations was the main objective during these analyses considering operational capacity limits.

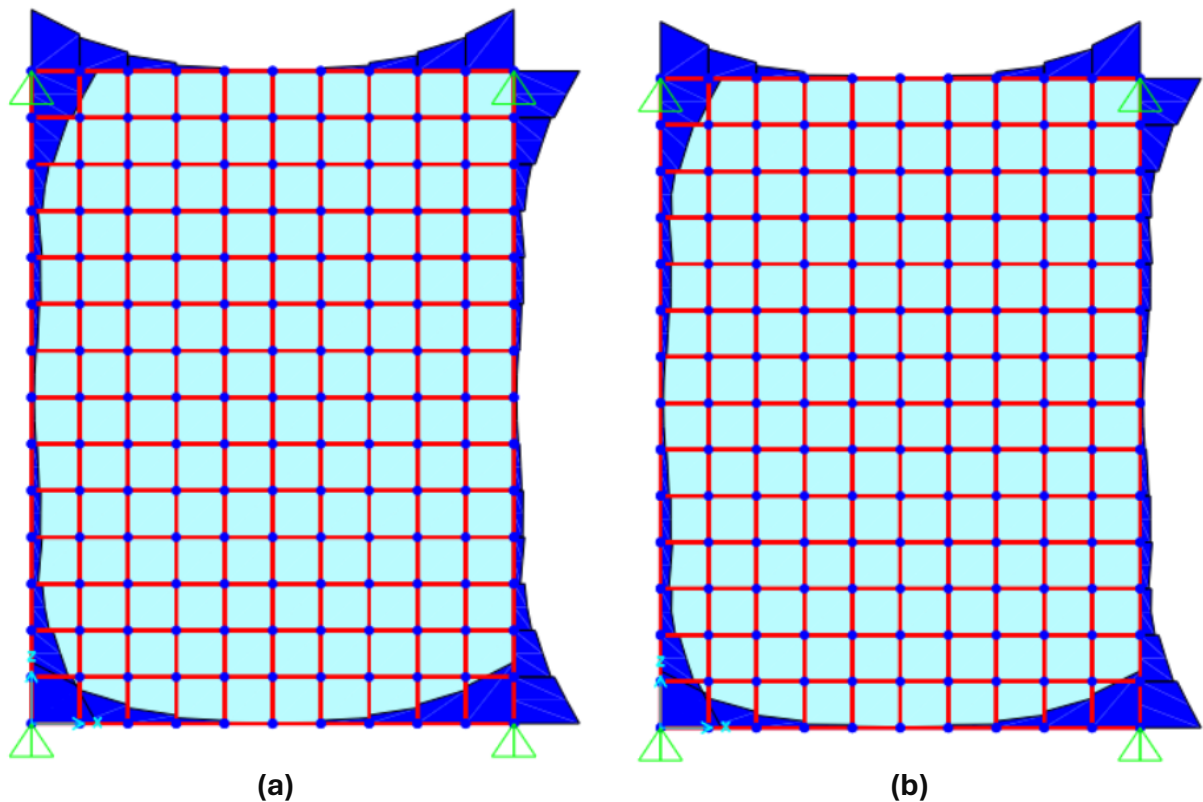


Figure 7- 2. Von Mises stress distribution in the aluminum frame.
a) Type B-Peak stress = 53,4 MPa. **b)** Type C-Peak stress = 40,3 MPa.

The von Mises stress diagrams demonstrate that in every case examined the peak stress areas are at the four corner regions of the frame which are also the points of maximum deflection (Figure 7-2.). These regions correlate with the joints of the vertical and horizontal members, as well as the connection points with the spring elements.

Table 7- 3. Peak Von Mises stress in the aluminum frame by connector type.

Variations	Shear Stiffness (K)	Peak Von Mises Stress (σ_{VM})	Yielding Strength (f_{yi})
Type A (Base)	547 kN/m	59,1 MPa	260 MPa
Type B	437,5 kN/m	53,4 MPa	260 MPa
Type C	218,75 kN/m	40,3 MPa	260 MPa

With a decrease in the stiffness of the connectors, the stress becomes more evenly distributed along the frame members (Table 7-3.). This occurs due to the greater flexibility results in higher deformation accommodation at the connectors themselves, which leads to a reduction in the abrupt transmission of forces and the formation of maximum stresses.

As a result, the compliant configuration promotes a more gradual load path between the glass and the frame, limiting the buildup of critical stress zones. This phenomenon is useful in the case of seismic design, as the reduction of concentration areas serves to enhance the façade systems ductility and energy dissipating capacity. All configurations remain within the elastic range of the aluminum material, ensuring structural safety under the modeled displacement conditions.

7.1.3. Displacement Response of the Glass

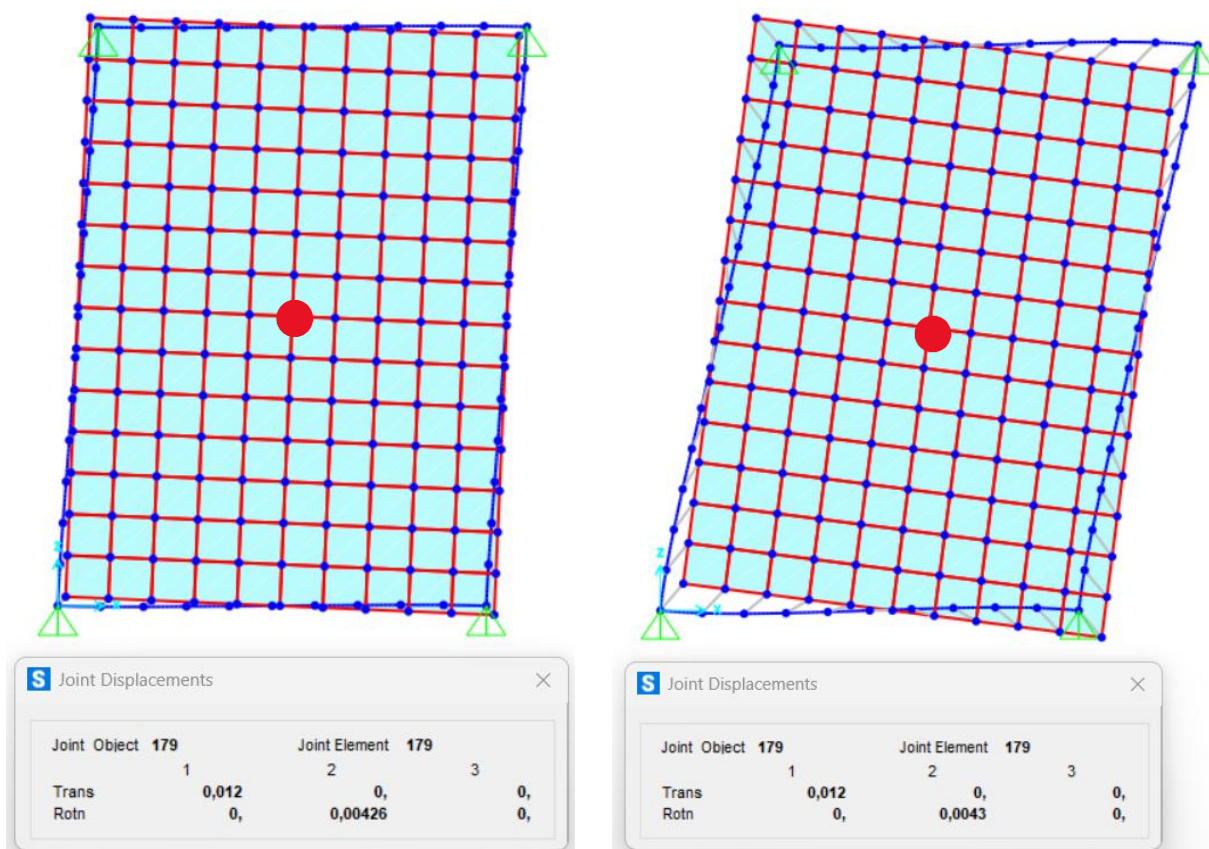
The rotational response of the glass panel under lateral drift is a key parameter for assessing the integrity and stability of unitized curtain wall systems. In this case, the focus is set on rotational behavior of three distinct configurations: Type A, Type B and Type C which differ by degree of silicone connector stiffness.

With SAP2000, all configurations with a focus on Joint 179 as the centroidal joint were monitored for two key outputs: centroidal Displacement (δx) and centroidal Rotation (ϕ).

Table 7- 4. Glass centroidal translation and rotation outputs by connector type.

Variations	Shear Stiffness (K)	Centroidal Displacement (δx)	Centroidal Rotation (ϕ)
Type A (Base)	547 kN/m	0,012 m	0,00425 rad
Type B	437,5 kN/m	0,012 m	0,00426 rad
Type C	218,75 kN/m	0,012 m	0,00430 rad

Despite the variation in connector stiffness, all configurations show identical horizontal displacement due to the controlled boundary condition. However, centroidal rotation shows a subtle increase from Type A to Type C, reflecting the growing flexibility of the silicone joints.

**Figure 7- 3.** Type B-Deformed shape. Showing R2 = 0,00426 rad.**Figure 7- 4.** Type C-Deformed shape. Showing R2 = 0,00430 rad.

This near-uniformity in rotation across all types supports the conclusion that the global glass behavior remains stable and torsional consistent regardless of minor reductions in connector stiffness (Figure 7-3. And 7-4.). From these assumptions, it is inferred that connector dimensions may be optimized for stress management without compromising system kinematics.

7.1.4. Principal Stress in the Glass Panel

This section presents the maximum principal stress (S_{max}) distribution in the glass panel under 24 mm imposed in-plane displacement, comparing the response across the three silicone connector configurations. Data was obtained using SAP2000 and was extracted utilizing shell element stress output.

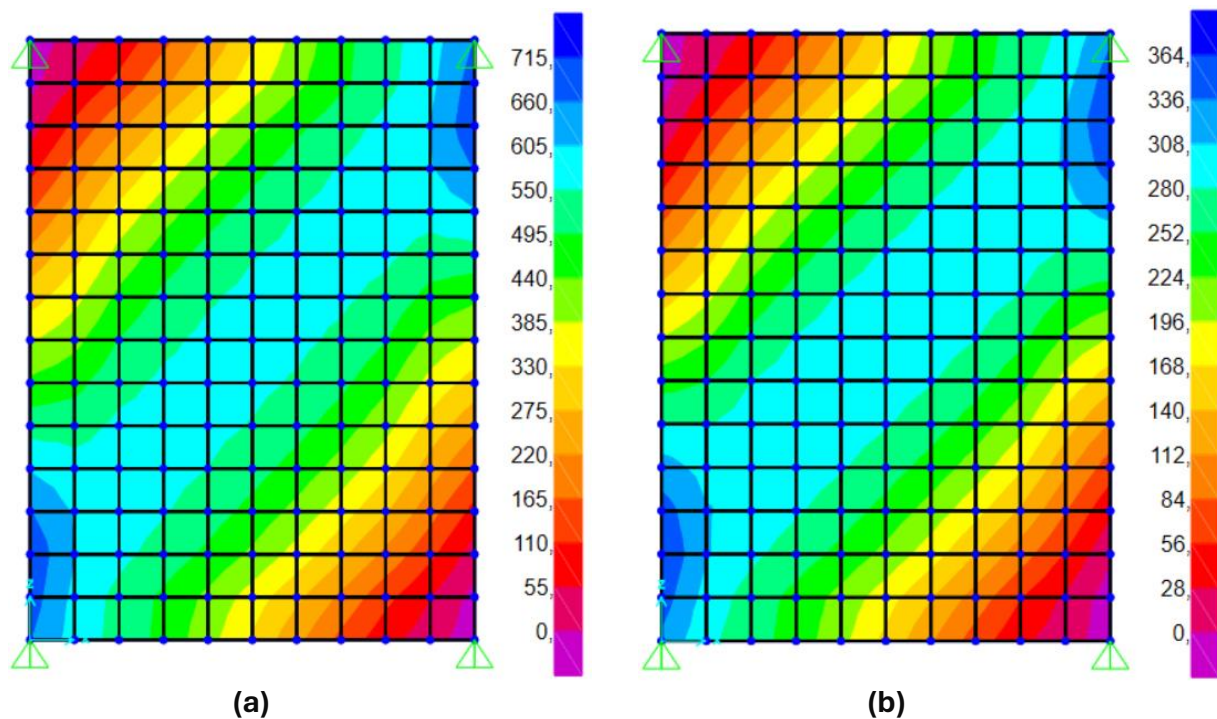


Figure 7- 5. Maximum principal stress distribution in the glass panel.

a) Type B-Peak S_{max} = 715 kPa (0,715 MPa). **b)** Type C-Peak S_{max} = 364 kPa (0,364 MPa).

The S_{max} contour plot reveals a distinct diagonal pattern of tensile stress at the left-bottom and right-top sides of the panel (Figure 7-5.). This distribution represents the superposition of translational, rotational deformations resulting from the configuration of the aluminum frame and spring connectors. While all three types display similar stress orientation, the intensity and concentration of stress zones vary with connector stiffness.

As the degree of stiffness in silicone connectors of Type A to Type C decreases, the stress concentrations in the glass panel significantly reduce. This can be explained by the increased deformability of the more flexible connectors, which better accommodate interfacial movement and reduce rigid body force transmission to the glass. On the other hand, stiffer connectors do not allow panel movement and therefore increase stress transfer and rigid body force concentration at the corners and edges of the panel.

Table 7- 5. Maximum principal tensile stress in the glass panel by connector type.

Variations	Shear Stiffness (K)	Max Principal Stress (Smax)	Yielding Strength (fyi)
Type A (Base)	547 kN/m	0,845 MPa	45 MPa
Type B	437,5 kN/m	0,715 MPa	45 MPa
Type C	218,75 kN/m	0,364 MPa	45 MPa

All values remain well below the typical tensile strength of laminated glass (Table 7-5.), ensuring structural safety. In addition, the reduction in peak stress with more flexible connectors underlines their effectiveness in limiting stress concentrations and enhancing the resilience of façade systems during seismic events.

7.1.5. Principal Stress in the Silicone Connectors

The corresponding force data for each model was obtained from the Excel files generated by SAP2000. The primary focus of the analysis is Link 2, which is a connector element included in all three models to facilitate comparison. The shear forces in the V2 and V3 directions were captured at the I-End of Link 2 for the 24 mm imposed lateral displacement. This loading condition was selected as the reference case for assessing and comparing the structural response of different connector geometries under the identical deformation demands.

Table 7- 6. Link 2 – In-Plane Shear Forces (24 mm drift).

Variations	Shear Stiffness (K)	V2	V3
Type A (Base)	547 kN/m	-2,77 kN	-2,57 kN
Type B	437,5 kN/m	-2,195 kN	-2,047 kN
Type C	218,75 kN/m	-1,04 kN	-1,011 kN

For the purpose of this comparison, three distinct SAP2000 models were developed, each corresponding to a different type of silicone connector geometry, Type A, B and C. These models differed only in the spring stiffness associated with the silicone link elements.

Once the elastic shear stiffness of each configuration (Type A, B and C) was established, the same post-processing route used for the single-panel study (*6.6. Principal Stress in the Silicone Connectors*) was applied to the façade-level results. The in-plane reactions extracted at Link 2 (V2 and V3 in Table 7-6.) were first normalized by the bonded contact area (bite × length) to obtain the orthogonal shear stresses τ_2 and τ_3 for every connector geometry. These two components were then combined vectorially to yield the resultant shear stress τ_R , and, since silicone failure is governed by tension rather than pure shear, the Mohr-circle transformation was invoked to compute the maximum principal (tensile) stress σ_1 . Finally, each σ_1 value was benchmarked against the manufacturer-reported tensile capacity of DOWSIL™ 993 (0,95 MPa) to quantify the utilization ratio. The complete stress comparison for all three bite widths is summarized in Table 7-7.

Table 7- 7. Silicone Connector Stress-to-Strength Check.

Variations	τ_2 (MPa)	τ_3 (MPa)	σ_1 (MPa)	Tensile Strength (MPa)	Status
Type A (Base)	-0,443	-0,411	0,605	0,95	Safe
Type B	-0,439	-0,409	0,600	0,95	Safe
Type C	-0,416	-0,404	0,580	0,95	Safe

The data suggests that all configurations of silicone connectors withstand the imposed 24 mm lateral displacement without failure. Both the resultant shear stress (τ_R) and the maximum principal stress (σ_1) clearly stayed under the capacity limit of the structural silicone. Even the force transmitting configuration Type A, which is most stiff and has the highest shear force, does not exceed the material's tensile strength limit, indicating that unitized curtain wall systems are highly resilient structures.

The evaluation of stress outcomes across the three configurations displays the direct relationship between connector geometry and mechanical performance. Type A delivered the highest shear forces and highest stress magnitudes including a resultant shear stress (τ_R) of 0,605 MPa. This is linked to the shears bite width in silicone of 25 mm and shear stiffness of 547 N/mm. On the contrary, with a silicone bite of 10 mm leading to the smallest bonded area and lowest stiffness of 218,75 N/mm, Type C exhibited the lowest shear forces and stress, and therefore the most compliant behavior, with a τ_R of 0,580 MPa.

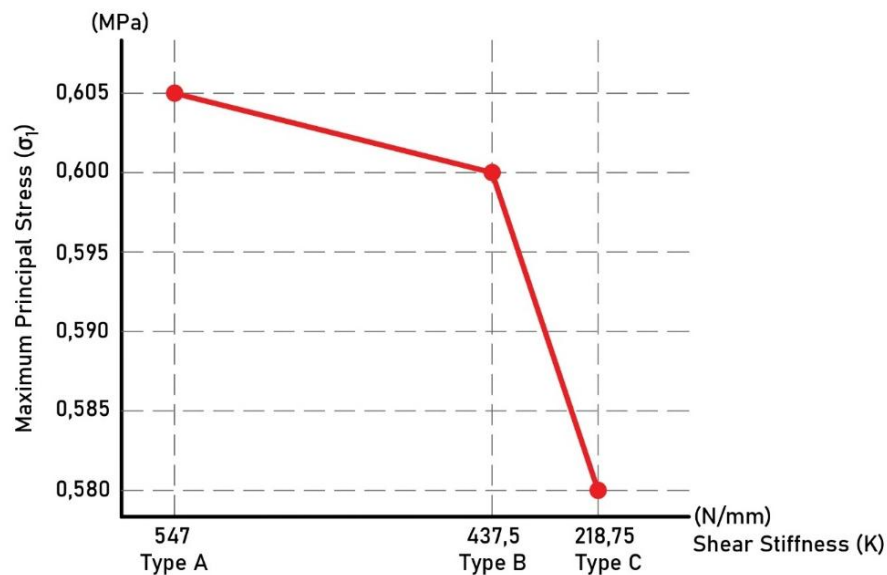


Figure 7- 6. Comparison of principal tensile stress by connector stiffness.

When benchmarked against the tensile strength of DOWSIL™ 993 structural silicone, taken as 0,95 MPa, the maximum principal stress (σ_1) values indicate the following utilization ratios:

- **Type A:** $\sigma_1 = 0,605$ MPa → 63,6% of tensile capacity
- **Type B:** $\sigma_1 = 0,600$ MPa → 63,2% of tensile capacity
- **Type C:** $\sigma_1 = 0,580$ MPa → 61,1% of tensile capacity

The analysis illustrates how critical balance suspension is using appropriate connector dimensions and stiffness to enable bending while maintaining overall structural integrity. It also emphasizes the need to use maximum principal stress (σ_1) as the main criteria for evaluating silicone joint failure risk, as it captures more precisely a mode of failure that is tensile driven in ductile adhesives such as DOWSIL™ 993.

7.1.6. Parametric Evaluation of Silicone Geometry

This section focuses on consolidating the primary performance outputs from the prior analyses to investigate how changes in the geometry of silicone connectors affect the structural behavior of the façade panel system with regard to the silicone connector's mechanical properties.

Table 7- 8. Structural response by silicone connector geometry.

Parameters	Unit	Type A (Base)	Type B	Type C
Silicone Bite (b)	mm	25	20	10
Silicone Length (i)	mm	250	250	250
Thickness (th)	mm	8	8	8
Shear Stiffness (K)	kN/m	547	437,5	218,75
Max. Moment in Frame (M3-3)	kN.m	±3,50	±3,15	±2,45
Max. Frame Stress (σ_{VM})	MPa	59,1	53,4	40,3
Max. Glass Stress (Smax)	MPa	0,845	0,715	0,364
Glass Rotation (ϕ)	rad	0,00425	0,00426	0,00430
Max. Silicone Stress (σ_1)	MPa	0,605	0,600	0,580

The recorded results (shown in Table 7-8.) indicate that decreasing the stiffness of the silicone connectors leads to a moderate increase in the glass panel's rotational deformation. Accompanying this added rotation, however, is marked by a significant reduction in internal forces and stress concentrations in both the aluminum frame and the glass panel.

Achieving the lowest stress levels in both frame and glass while slightly inhibiting rotation, Type A, with the stiffest connectors, has the highest stress levels. This configuration may be the most suited for high-performance envelopes where minimal deformation is prioritized, provided the stress levels remain within material limits.

Considering the context, Type B appears the most stress-friendly, reducing stress magnitudes while still managing deformation control. These findings lead to the conclusion that optimal connector performance may be achieved with moderate stiffness due to system benefits from both strength and flexibility.

Type C, with the most flexible connectors, records the lowest peak bending moment and stress in both frame and glass components. This observation supports the contribution of flexible connectors to the reduction of stress and deformation during seismic loading. On the other hand, over-flexibility alters the system's ability to restrict displacement or maintain serviceability performance under certain conditions.

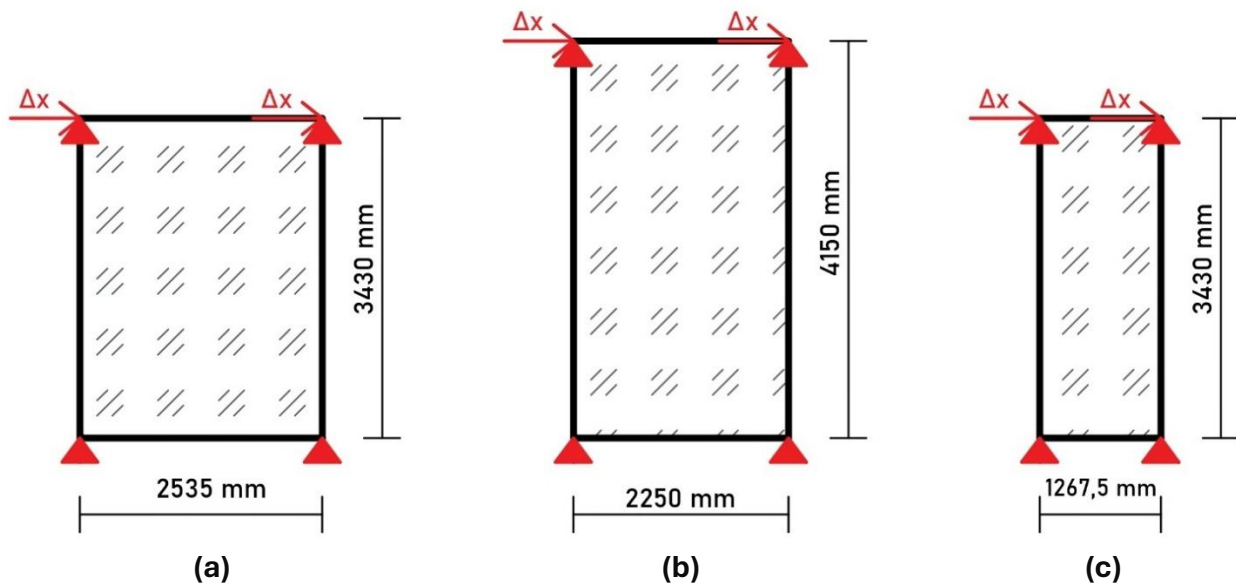
7.2. Influence of Panel Dimension

This part analyzes how the overall dimensions of a façade panel impact structural response of a glass-aluminum unitized system when subjected to horizontal in-plane displacement. This section seeks to understand how the height and width, as well as aspect ratio, of the panel influences the stress distribution pattern and deformation across the façade unit. To achieve this, the geometry of the aluminum frame and the bonded glass panel was altered while controlling the material properties, connector characteristics and boundary conditions.

Type 3, Type 6 and Type 1 panels were developed and studied based on real-world curtain wall geometries utilized in the experimental study conducted at TU Delft in collaboration with the Permasteelisa Group, thus ensuring practical value but also facilitate relevance and comparison. This enables an assessment of the impact of change in panel dimensions and aspect ratio on such deformation mechanisms: frame elongation, rotational drift, racking distortion and glass panel response.

Table 7- 9. Matrix of panel geometry variations.

Variations	Panel Height (h)	Panel Width (b)	Unit Aspect Ratio (h/b)
Type 3 (Base)	3430 mm	2535 mm	1,35
Type 6	4150 mm	2250 mm	1,84
Type 1	3430 mm	1267,5 mm	2,71


Figure 7- 7. Frame Dimension Variants.

a) Type 3 (Base). **b)** Type 6. **c)** Type 1.

The following results are included in the next subsections:

- A summarization of frame deformation patterns relative to lateral drift,
- Stress concentration in the aluminum frame,
- Stress concentration in the aluminum frame,
- Displacement and torsion of the glass panel,
- Distribution of tensile stresses in the glass panel,

This study is designed to demonstrate the impact that unit proportions have on the structural efficiency, stress concentration and durability of curtain walls subjected to racking deformation caused by wind or seismic forces.

7.2.1. Displacement Response of the Frame

This section aims to evaluate the structural deformation corresponding with the façade unit by considering the aluminum frame of this unit and applying a lateral displacement of 24 mm. In this analysis, the frame is evaluated with the aid of geometric-based output parameters in three primary indicators of deformation:

- **Elongation (ϵ)** – the increase in the length of a diagonal line joining two corners of the frame, due to in-plane stretching.
- **Rotation (α)** – measures the angular drift of the frame due to horizontal displacement.
- **Distortion (θ)** – defines the internal angular distortion which results from the right angles rotating asymmetrically.

These parameters are defined for every frame configuration from purely analytical calculations using existing geometry of original and deformed (diagonal) lengths, vertical height and imposed lateral shift (Table 7-10.).

Table 7- 10. Frame kinematics by panel variant (24 mm drift).

Variations	Panel Height (h) [mm]	Panel Width (b) [mm]	Aspect Ratio (h/b)	Elongation (ϵ) [%]	Frame Rotation (α) [°]	Frame Distortion (θ) [°]
Type 3	3430	2535	1,35	0,0033	0,26	89,60
Type 6	4150	2250	1,84	0,0024	0,30	89,67
Type 1	3430	1267,5	2,71	0,0022	0,37	89,60

Type 3, which was used as the base case and has a more balanced aspect ratio of 1,35, exhibits the highest elongation and moderate rotational drift. This proportioned frame cross section allows for more uniform distribution of shear and stretching deformations, suggesting the optimized geometry to withstand lateral load while maintaining flexibility and stress concentration.

Type 6 bears intermediate elongation with rotation and is the tallest and the broadest panel in the study with an aspect ratio of 1,84. Its larger height contributes to increase the stiffness in the vertical direction and the span is wider providing stable lateral resistance. This combination has low distortion angles and a controlled rotational pattern which, in this case, means there is efficient deformation absorption with minimal localized stress concentration that leads to injury.

Type 1, characterized by the tallest and the narrowest configuration with an aspect ratio of 2,71, shows the highest rotational response and the lowest elongation out of the three types. This is because of its small horizontal width cross-section, which leads to lower lateral stiffness of the frame, causing greater angular drift for in-plane displacement.

7.2.2. Bending Moment Distribution in the Aluminum Frame

This subsection calculates the internal bending moment distribution (regarding local 3-3 axis) of the aluminum frame for the three panel dimension types subjected to a constant 24 mm in-plane displacement. The moment outputs were obtained from SAP2000 with frame element stress outputs enabled.

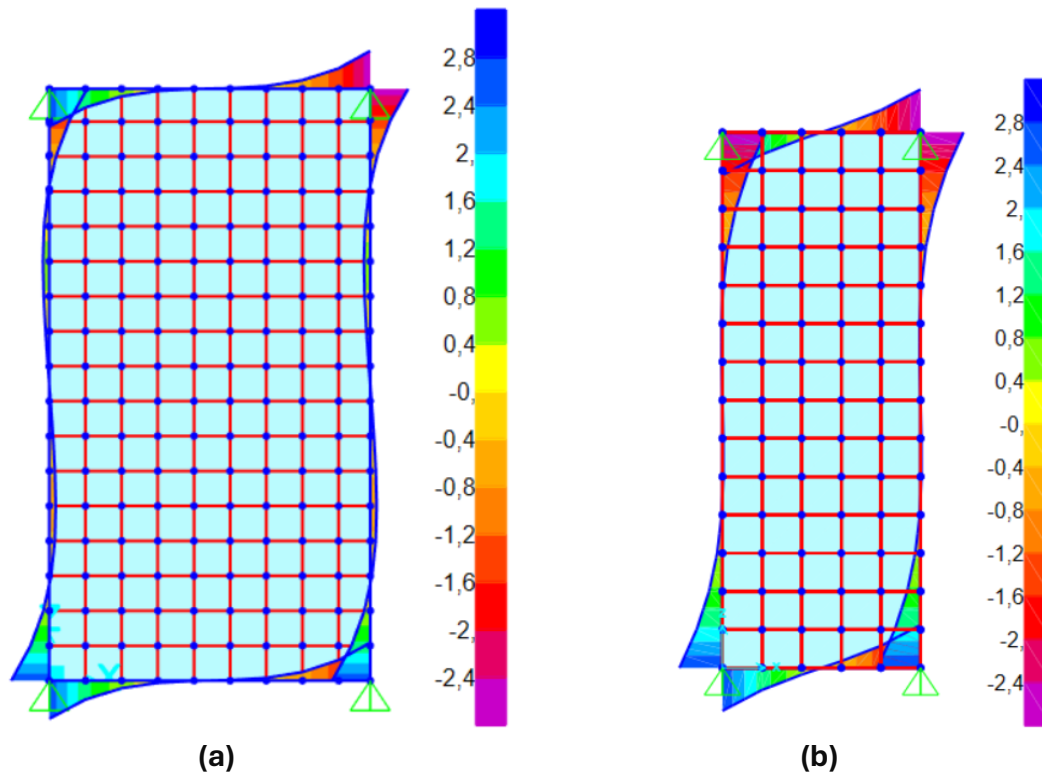


Figure 7- 8. Moment distribution (M3-3) in the aluminum frame.

a. Type 6-Max. Bending Moment = $\pm 2,8$ kN.m

b. Type 1-Max. Bending Moment = $\pm 2,8$ kN.m

These results shown in Figure 7-8. validate that the overall panel geometry has a considerable effect on the flexural demand of the aluminum frame. The most balanced proportions, Type 3 configuration, exhibit the most considerable moment around support regions resulting in the highest observed values. The Type 6 panel exhibits intermediate behavior due to increased width that aids force distribution. The Type 1 panel exhibits reduced moment transfer because its geometry promotes rotational drift instead of flexural engagement.

This information will help designers to navigate both spatial and architectural needs while constraining structural demand. Balanced panel geometry improves the efficiency of curtain wall systems and resilience to seismic forces.

Table 7- 11. Peak M3-3 Bending Moment in the aluminum frame by panel variant.

Variations	Panel Dimensions (hxb)	Aspect Ratio (h/b)	Max. Moment 3-3	Relative Frame Demand
Type 3	3,43 m × 2,535 m	1,35	±3,5 kN.m	Higher – balanced layout amplifies flexural response.
Type 6	4,15 m × 2,25 m	1,84	±2,8 kN.m	Moderate – height increases leverage, but width distributes load.
Type 1	3,43 m × 1,2675 m	2,71	±2,8 kN.m	Lower – narrow geometry reduces moment transfer.

7.2.3. Von Mises Stress Distribution in the Aluminum Frame

The goal in this section is analyzing how the different parameters of the overall panel dimensions affect the von mises stress of the aluminum frame which is under in-plane displacement of 24 mm. The maximum stress from the most critical corner joints were considered for the SAP2000 simulation since they are the most mechanically stressed because of the lateral drift, fixity of the supports and force transfer from the connectors.

The results of the simulation show that the geometry of the panel has a major effect on the stress response of the frame. The von Mises stress is maximum on Type 3, primarily due to its dimensions are proportionate to the moments caused by bending at the corners. With greater height, the Type 6 configuration has lower stress, it distributes stress more efficiently due to increased vertical flexibility, leading to slightly reduced stress. The Type 1 panel, on the other hand, has the highest aspect ratio with narrow width and generates the lowest stress values. Since its geometry favors rotation over flexural engagement, thus minimizing internal frame demand.

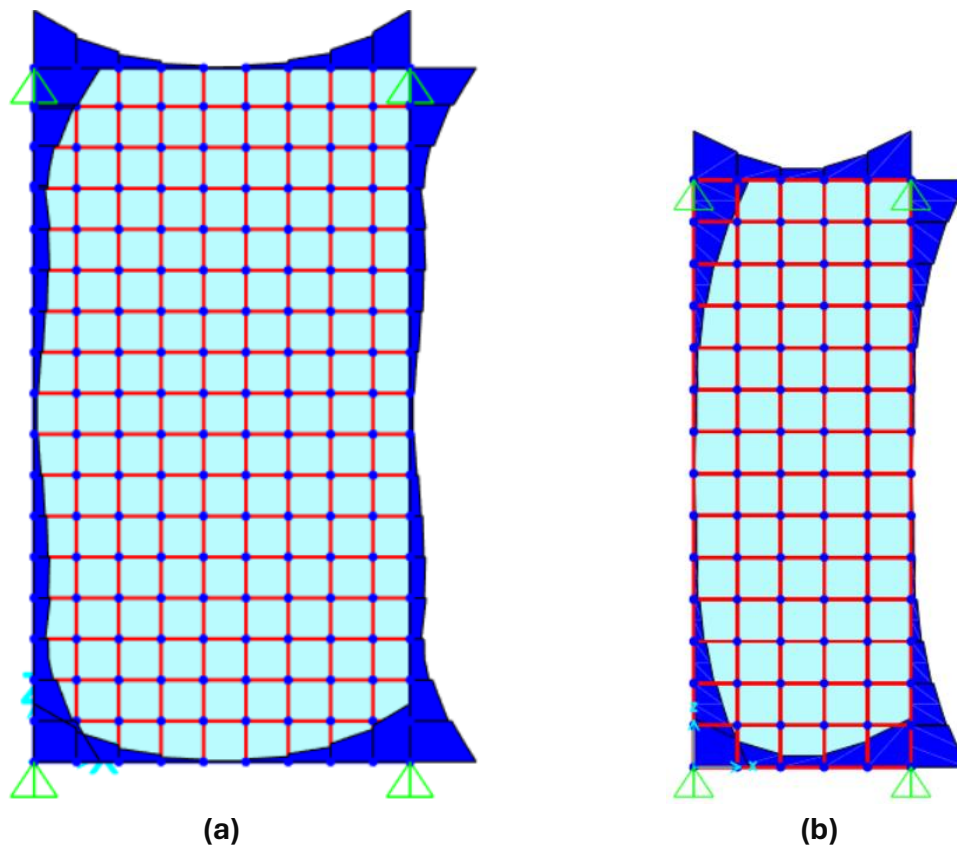


Figure 7- 9. Von Mises stress distribution in the aluminum frame.
a) Type 6-Peak stress = 56,3 MPa. **b)** Type 1-Peak stress = 48,2 MPa.

These results strongly suggest why ratios of geometry are equally as critical as controlling the stress energy in the frame, offering important insights for optimizing panel layout in façade systems subject to seismic or shear loading.

Table 7- 12. Peak Von Mises stress in the aluminum frame by panel variant.

Variations	Panel Height (h)	Panel Width (b)	Aspect Ratio (h/b)	Peak Von Mises Stress (σ_{VM})	Yielding Strength (f_{yi})
Type 3	3,43 m	2,535 m	1,35	59,1 MPa	260 MPa
Type 6	4,15 m	2,25 m	1,84	56,3 MPa	260 MPa
Type 1	3,43 m	1,2675 m	2,71	48,2 MPa	260 MPa

7.2.4. Displacement Response of the Glass

This segment examines the behavior of the glass panel subjected to a constant 24-mm in-plane shift, testing three curtain-wall layouts that differ in frame sizing. The analysis centers on the manner in which each frame's geometry governs the resultant glass displacements, paying particular attention to corner rotation and twisting induced by the yielding silicone seals. By contrasting Type 1 and Type 6 with the reference Type 3, the analysis illustrates how alterations to the height-width ratio systematically modify panel response under side drift (Figure 7-10.).

Table 7- 13. SAP2000 output parameters for glass-panel movement.

Output Parameters from SAP2000:	
Ux	Horizontal Displacement (X-axis)
Uz	Vertical Displacement (Z-axis)
R2	Rotation about Y-axis (torsional rotation)

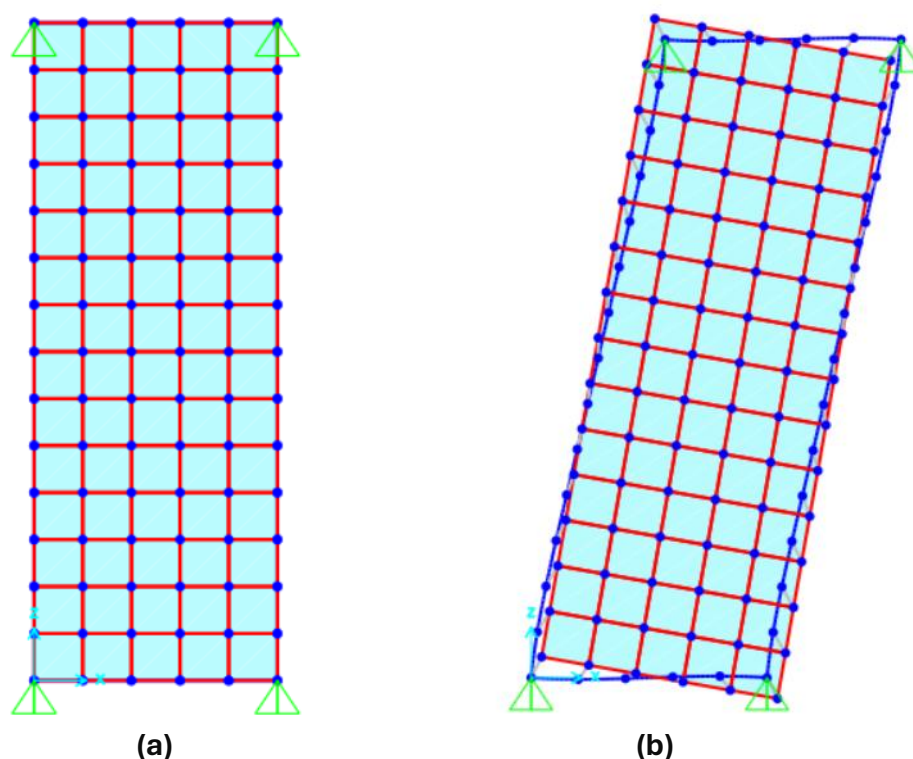
Type 1:

Figure 7- 10. Type 1 façade unit under 24 mm in-plane displacement.
a) Undeformed SAP2000 model. **b)** Deformed model.

S Joint Displacements			
Joint Object 4		Joint Element 4	
	1	2	3
Trans	0,02214	0,	0,00373
Rotn	0,	0,00589	0,

Figure 7- 11. Joint 4-displacement output from SAP2000 (left-top corner).

The displacement output of Joint 4 from SAP2000 (Figure 7-11.) confirms nearly full lateral drift transmission and vertical displacement consistent with rotation.

- **Horizontal displacement (U_x):** 0,02214 m
 Which is roughly equal to the imposed lateral drift displacement of 24 mm indicating full volume transmission which explains the value.
- **Vertical displacement (U_z):** 0,00373 m
 Upward movement due to torsional rotation, consistent with the corner's location relative to the rotation center.

- **Rotation about Y-axis (R2):** 0,00589 rad

This proves the glass panel undergoes rigid body rotational motion while in plane shear is applied.

S Joint Displacements					
Joint Object 176			Joint Element 176		
	1		2	3	
Trans	0,012		0,	7,484E-04	
Rotn	0,		0,00591	0,	

Figure 7- 12. Joint 176-displacement output from SAP2000 (centroidal joint).

The verification using the centroid (Joint 176) shown in Figure 7-12. confirms the calculated torsional rotation of $\phi = 0,00591$ rad and centroidal translation of $\delta x = 0,012$ m aligning within the simulations executed.

Type 6:

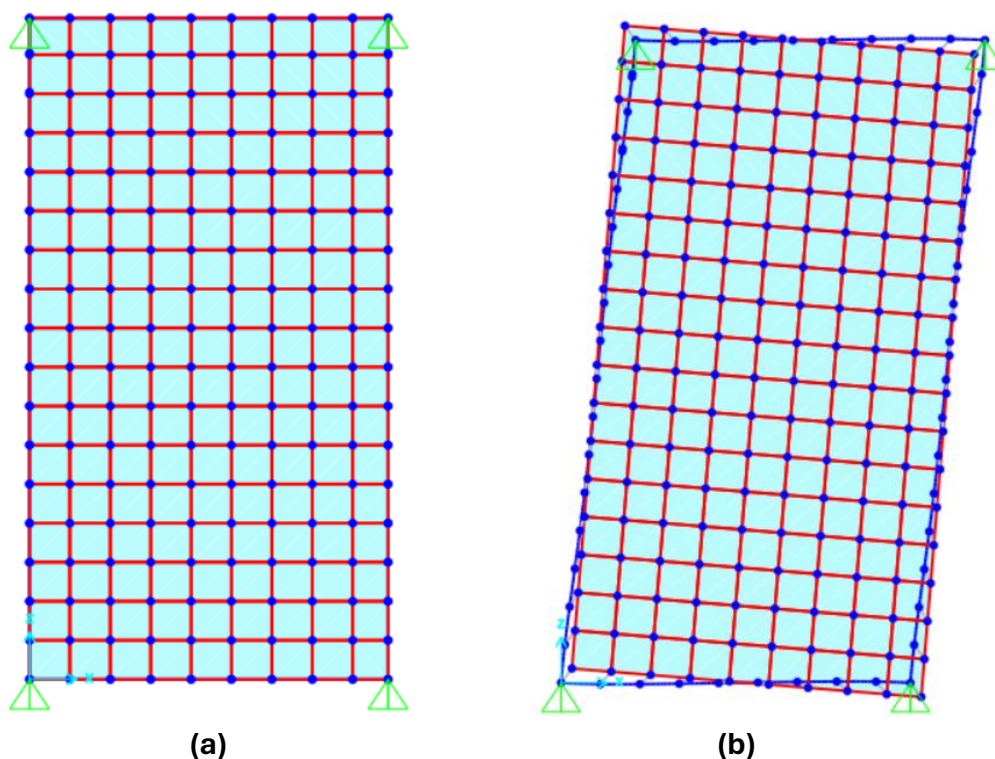


Figure 7- 13. Type 6 façade unit under 24 mm in-plane displacement.
a) Undeformed SAP2000 model. **b)** Deformed model.

S

Joint Displacements

Joint Object	104	Joint Element	104	
	1	2	3	
Trans	0,02055	0,	0,00463	
Rotn	0,	0,00409	0,	

Figure 7- 14. Joint 104-displacement output from SAP2000 (left-top corner).

- **Horizontal displacement (Ux):** 0,02055 m
Suggests lateral drift restriction compared to Type 1 due to the panel's larger width and altered stiffness distribution.
- **Vertical displacement (Uz):** 0,00463 m
Aligns with glass edge's motion above the centroid and confirms upward movement due to torsional rotation.
- **Rotation about Y-axis (R2):** 0,00409 rad
Confirms displacement in rotation for the glass under in-plane loading, though to a lesser extent than narrower panels.

S

Joint Displacements

✕

Joint Object	200	Joint Element	200
	1	2	3
Trans	0,01255	0,	4,780E-04
Rotn	0,	0,00411	0,

Figure 7- 15. Joint 200-displacement output from SAP2000 (centroidal joint).

Both displacement outputs from joint 104 (Figure 7-14.) and joint 200 (Figure 7-15.) show a systematic response. The calculated torsional rotation of $\phi = 0,00411$ rad and centroidal translation of $\delta x = 0,01255$ m are in agreement with the results from SAP2000, confirming that the deflection is mainly due to frame rotation and translation rather than bending of the glass.

Table 7- 14. Glass centroidal translation and rotation outputs by panel variant.

Variations	Panel Height (h) [m]	Panel Width (b) [m]	Aspect Ratio (h/b)	Centroidal Displacement (δx) [m]	Centroidal Rotation (ϕ) [rad]
Type 3	3,43	2,535	1,35	0,00424	0,012
Type 6	4,15	2,25	1,84	0,00411	0,01255
Type 1	3,43	1,2675	2,71	0,00591	0,012

Type 3 has the lowest ratio of width to height, which leads to moderate rotation and intermediate displacement. This configuration allows for the most even response to deformation. Type 6 is the tallest and also the widest panel, but sustains the least amount of rotation of any panel. It has slightly greater centroidal translation because it has a higher frame which increases the amount of torque that can be efficiently distributed across the glass. Type 1, which has the narrowest width and largest ratio between width and height, shows the most torsional rotation, indicating that the panel is prone to rotation due to low lateral stiffness.

These results (Table 7-14.) prove that as the ratio of height to width increases, the degree of twisting increases. Wider or more balanced panels reduce the degree of twisting under lateral loads.

7.2.5. Principal Stress in the Glass Panel

This subsection focuses on calculating the value of maximum principal tensile stress (S_{max}) in the glass panels for three configurations of the façade with different dimensions. The value used in this case is obtained from the results of SAP2000 shell element modeling, where S_{max} indicates critical areas of tensile failure, significant in evaluating the remaining structural integrity of brittle glass during in-plane seismic drift.

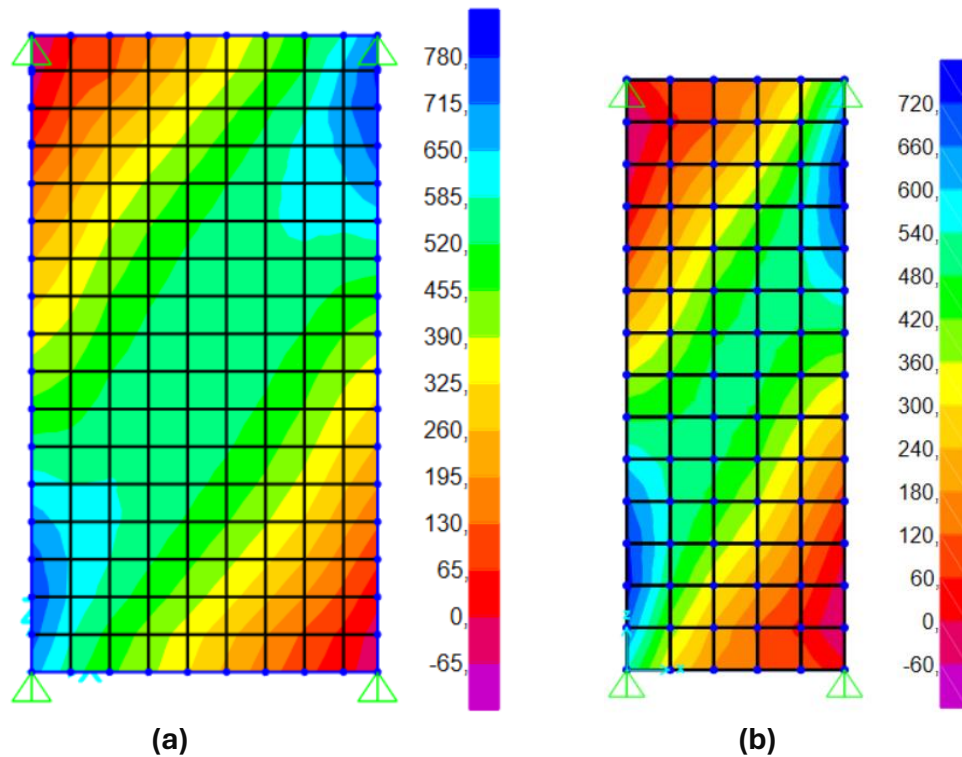


Figure 7- 16. Maximum principal stress distribution in the glass panel.
a) Type 1- Peak S_{max} = 720 kPa (0,72 MPa). **b)** Type 6- Peak S_{max} = 780 kPa (0,78 MPa).

As shown in Table 7-15. and Figure 7-16., the distribution and magnitude of maximum principal tensile stress (S_{max}) within the glass panel are closely tied to the panel's aspect ratio and overall geometry.

Across the configurations, the results demonstrate distinct differences. The Type 3 panel shows the highest principal stress (0,845 MPa) due to sensitivity to frame deformation and increased concentration of tensile zones, which is more pronounced in the balanced geometry model. The Type 6 configuration, which is taller, distributes the deformation more uniformly across the glass surface and achieves moderately high but more even stress (0,780 MPa). In the case of Type 1 panel, which is narrower in width, it has the lowest S_{max} value amongst all panels (0,720 MPa), most likely due to reduced lateral engagement and a more localized response.

Table 7- 15. Maximum principal tensile stress in the glass panel by panel variant.

Variations	Panel Height (h)	Panel Width (b)	Aspect Ratio (h/b)	Max Principal Stress (S _{max})	Yielding Strength (f _{yi})
Type 3	3,43 m	2,535 m	1,35	0,845 MPa	45 MPa
Type 6	4,15 m	2,25 m	1,84	0,780 MPa	45 MPa
Type 1	3,43 m	1,2675 m	2,71	0,720 MPa	45 MPa

The analysis in the previous paragraph confirms that the stress behavior in the glass panel is very sensitive to geometry configuration of the panel, where wider configuration is more prone to experience high tensile zones due to racking, whereas narrow panels are likely to experience less stress build-up from constrained deformation paths.

7.2.6. Parametric Evaluation of Panel Dimension

Among the types of geometries, Type 3 with the most balanced aspect ratio appears to be the most mechanically engaged. This geometry encourages all structural elements to participate more equally; the frame bends more, the glass panel is under greater tensile stress and the connectors are able to carry larger forces. The consequence is, a more complex deformation pattern with elevated internal force demands.

Type 6 with more moderate value of aspect ratio results in more distributed load response. Increased height of the panel results in higher rotation, while added width helps to spread the stresses more effectively. This causes moderate demand on the frame as well as on the glass panel. The behavior of the configuration indicates that mid-range aspects may offer a favorable compromise between stiffness and flexibility, reducing peak stresses without overly limiting energy dissipation mechanisms.

Type 1 has the greatest aspect ratio, showing rigid-body behavioral displacement. Its tall and narrow geometry reduces the extent of bending and shear interactions, resulting in lower stress accumulation to the frame and the glass panel. This indicates that higher aspect ratio panels are more likely to accommodate drift through rotation instead of internally deforming, which minimizes materials used, but could increase sensitivity to flex in the connectors and edge effects.

Table 7- 16. Structural response by panel dimension variants.

Parameters	Unit	Type 3 (Base)	Type 6	Type 1
Panel Height (h)	m	3,43	4,15	3,43
Panel Width (b)	m	2,535	2,25	1,2675
Aspect Ratio (h/b)	-	1,35	1,84	2,71
Elongation (ϵ)	%	0,0033	0,0024	0,0022
Frame Rotation (α)	°	0,26	0,30	0,37
Frame Distortion (θ)	°	89,60	89,67	89,60
Max. Bending Moment in Frame (M3-3)	kN.m	±3,5	±2,8	±2,8
Max. Frame Stress (σ_{VM})	MPa	59,1	56,3	48,2
Max. Glass Stress (Smax)	MPa	0,845	0,780	0,720
Glass Rotation (ϕ)	rad	0,00424	0,00411	0,00591
Glass Centroid Displacement (δx)	m	0,012	0,01255	0,012

These observations suggest the importance of aligning panel geometry with expected levels of drift and performance targets, particularly in seismic-prone contexts where both flexibility and structural reliability must be blended. Overall, the comparative study of the panel dimension variants indicates that aspect ratio is critical in determining the structural behavior of glass-aluminum façade systems undergoing lateral drift. Panels with higher aspect ratio, such as Type 1, tend to favor accommodation of rotation with less internal stress. While lower aspect ratio designs, Type 3, apply and withstand lateral loads more evenly but increase bending and tensile stresses. Intermediate geometries like Type 6 display moderate deformation and stress response, which gives it a balanced behavior.

7.3. Influence of Restraint Condition

This subsection focuses on the impact of varying restraint conditions on the structural behavior of the glass-aluminum façade system with respect to lateral drift. Both models considered in this comparison share the same overall geometry (Type 3), including panel measurements of 3430 mm in height and 2535 mm in width, but differ in support configuration within the frame.

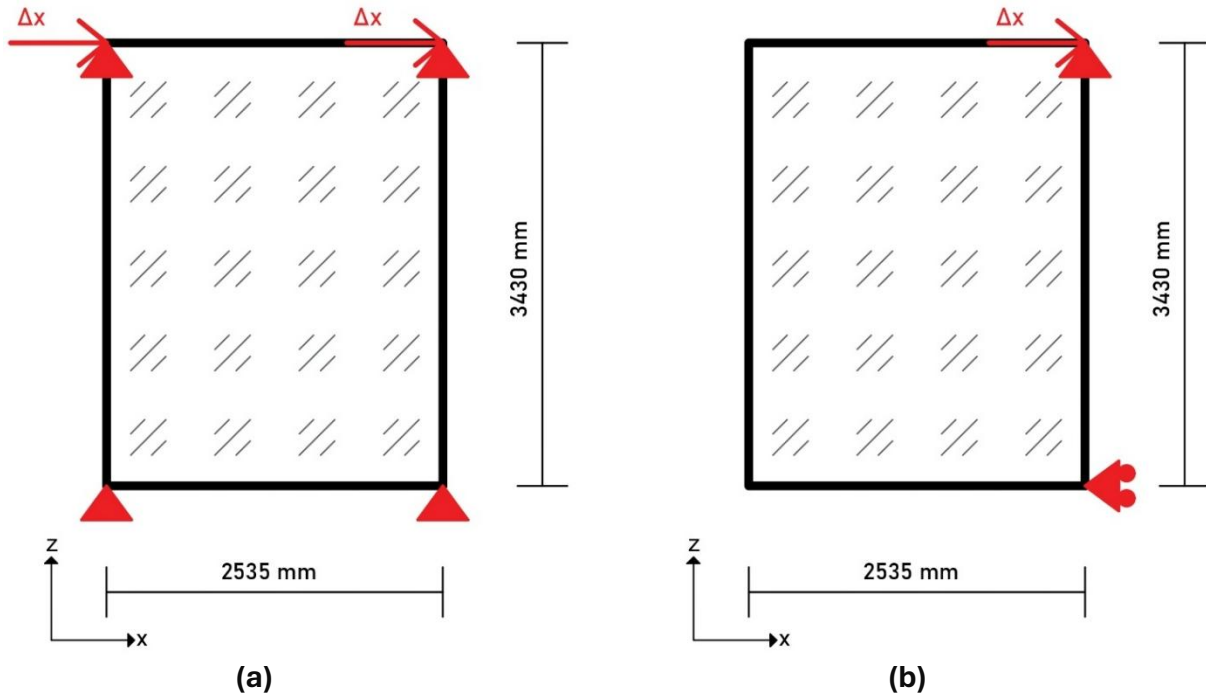


Figure 7- 17. Matrix of support configurations.
a) Type 3. b) Type R.

Type 3, as illustrated in Figure 7-17. a), is the base model with symmetric hinged supports at the four corners of the aluminum frame which are placed with hinges. These supports provide restraint to some translational degrees of freedom but make rotation unconstrained.

The asymmetrical restraint layout of the Type R configuration is illustrated on Figure 7-17. b). In this configuration, the left-side corners (top and bottom) are completely unrestrained and unsupported, while the top right corner has hinged support and the bottom right corner contains roller support that restricts horizontal (X-axis) translation while allowing vertical (Z-axis) movement.

Furthermore, this model has one of the critical internal modifications to the frame's configuration, which is moment releases (M3) applied to all four corners of the aluminum frame. These internal releases allow for bending moment continuity between frame members, which means all joints are able to rotate freely, simulating pin-connected corners. This results in a more flexible system and accurately represents the actual frame behavior in unitized curtain wall systems.

As opposed to the previous sections where only lateral displacement was accounted for, in this analysis both configurations (Type 3 and Type R) are subjected to combination loading: the same 24 mm in-plane displacement at the top corners, along with the inclusion of self-weight. This change enables the introduction of the gravitational effects into the system, which facilitates the assessment of vertical load interaction with lateral deformation under asymmetric restraint conditions.

(COMB1: 24-mm imposed horizontal in-plane displacement + self-weight)

This analysis aims to describe how varying parameters in external support locations and internal rotational degree of freedom change global deformation behavior, stress distribution in the aluminum frame and glass panel, and the activity of silicone connectors. More attention is directed towards understanding if asymmetric restraint results in deformation that causes the structure to fail at lower load levels, higher stress concentrations, larger permanent displacement, or more complex strain patterns. By answering these questions, façade systems can be better designed to meet realistic boundary conditions.

7.3.1. Displacement Response of the Frame

In assessing the effect of boundary conditions on the structural response of an aluminum frame, the degree of deformation for panel configurations, Type 3 (symmetrically supported) and Type R (asymmetrically supported with internal moment releases), is determined through joint displacement data processing in SAP2000. The analysis is performed based on the load combination stated in COMB1.

The displacement data was obtained using the Joint Displacements table interface and stored in Excel format. The table below summarizes the horizontal (Ux) and vertical (Uz) displacements of the four corner joints of the aluminum frame: left-bottom (Joint 1), right-bottom (Joint 2), right-top (Joint 3) and left-top (Joint 4). Excel files were generated through the Show Tables function under *Output Tables > Joint Output > Joint Displacements*.

The original frame geometry was a rectangle measuring 3430 mm in height and 2535 mm in width, with its four joints representing the corners.

Table 7- 17. Corner joint displacements (U_x , U_z) for Type 3 and Type R under COMB1.

Joint Number	Position of the Corner	Type 3		Type R	
		U_x [m]	U_z [m]	U_x [m]	U_z [m]
Joint 1	Left-Bottom	0,0	0,0	0,00003	0,016
Joint 2	Right-Bottom	0,0	0,0	0,0	-0,00009
Joint 3	Right-Top	0,024	0,0	0,024	0,0
Joint 4	Left-Top	0,024	0,0	0,0239	0,016

The data (Table 7-17.) indicates that there is a notable difference between the two configurations. In Type 3, all four corners are equipped with symmetrical hinge supports, and this leads to uniform and balanced displacement profile across the structure. The frame is able to maintain a stable, elastic structure when both vertical and lateral loads are applied. The displacement values are identical on both sides confirming that the drift is balanced with no major vertical or horizontal distortion.

On the other side the Type R model displays pronounced asymmetry. The unsupported left-side corners are in contrast with the right side which has a hinge on the top right and a roller on the bottom right. Furthermore, M3 moment releases have been applied to all four frame corners leading to unrestrained rotation at the member intersections.

These conditions give rise to behavior of a mechanism where the frame does not deform as a rigid body but instead, it experiences segmental motion. This can be seen from the larger vertical key displacements at the left side (16 mm vertical lift at both top-left and bottom-left corners), relative to almost zero values on the right side. In the horizontal direction, top corners have nearly the same value of U_x displacement. However, the free vertical shift on the left side causes a diagonal skewing of the frame.

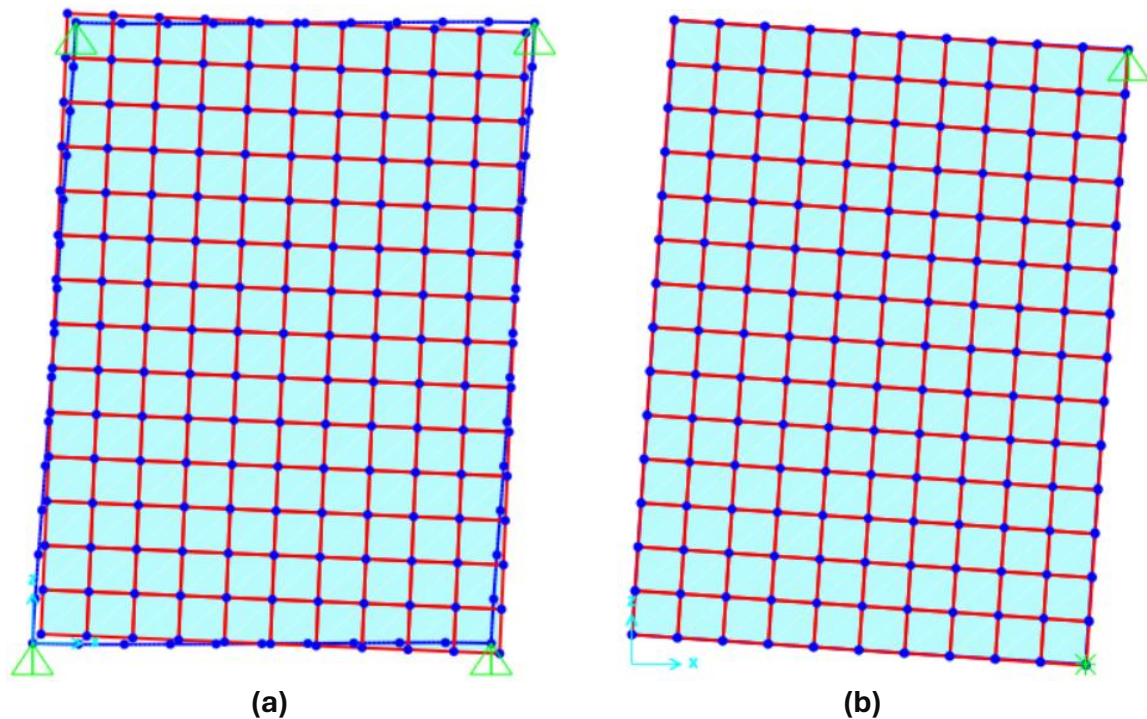


Figure 7- 18. Deformed SAP2000 model under COMB1.
a) Type 3. **b)** Type R.

In support of these interpretations visually, Figure 7-18. a) and b) show the deformed shape of the models as rendered in SAP2000 under COMB1. Type 3 shows a frame that is rectangular and slightly leaning but not vertically deformed, while Type R is shown to illustrate a tilted and warped frame geometry due to asymmetric boundary and internal release configuration driving the frame.

7.3.2. Bending Moment Distribution in the Aluminum Frame

This section analyzes the internal bending moment distribution within the aluminum frame (Moment 3-3 concerning the local axis) for the two restraint condition variants, Type 3 and Type R, under the COMB1 loading scenario. Moment outputs were obtained using frame element output in SAP2000, focusing on how the support layout affects overall frame demand in bending.

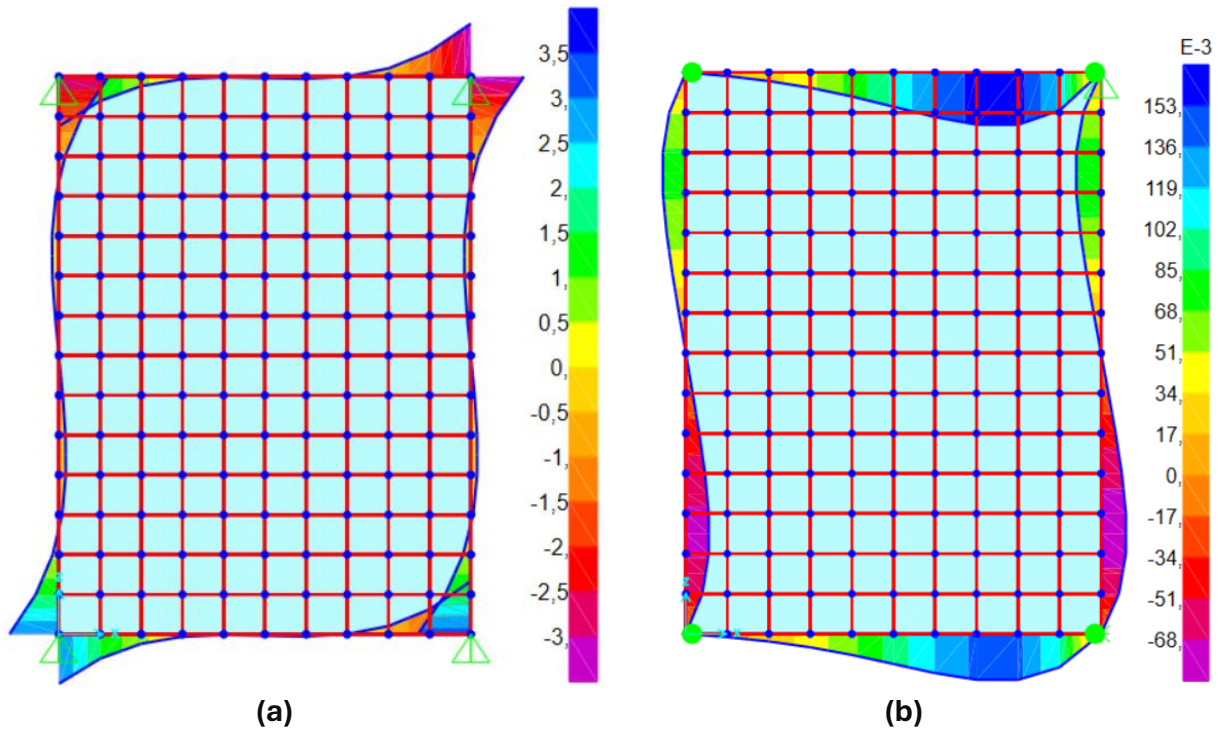


Figure 7- 19. Moment distribution (M3-3) in the aluminum frame.

a) Type 3-Max. Bending Moment = $\pm 3,5$ kN.m

b) Type R-Max. Bending Moment = $\pm 0,153$ kN.m

As follows from Figure 7-19. a), in Type 3 configuration, vertical mullions and corner supports experience peak bending moments of approximately $\pm 3,5$ kN.m. This indicates a considerable amount of rotational restraint and stiffness as the frame is assumed to undergo flexural deformations. The structure accommodates the applied drift by enabling bending of the frame segments, especially around the support locations where the moments are highest.

On the contrary, Figure 7-19. b) shows that, for Type R, the updated results are far more flexible. The maximum moment registered is $+0,153$ kN.m, while the minimum registered moment is $-0,068$ kN.m, and both nearly an order of magnitude lower than in Type 3. These low values result from the combination of corner moment releases and asymmetric support layout, which allow joints to rotate freely and prevent significant moment buildup.

Table 7- 18. Peak M3-3 Bending Moment in the aluminum frame by restraint variant.

Variations	Max. Moment 3-3	Relative Frame Demand
Type 3	±3,5 kN.m	High
Type R	±0,153 kN.m	Low

These results (Table 7-18.) highlight the need for consideration of restraint detailing in applications subjected to seismic activity. A stiffer frame such as Type 3 may provide better resistance to lateral loads; however, it also concentrates bending moments at the connectors and corners, which might add stress to silicone joints and the glass edges, thereby increasing potential failure mechanisms.

On the other hand, a more flexible frame, Type R, allows for increased drift through articulation which reduces peak moment value but could increase deformation, serviceability issues and overall concerns. Therefore, a balanced approach to strength and flexibility for curtain wall systems with detailing sensitivity should drive the choice of restraint strategy.

7.3.3. Von Mises Stress Distribution in the Aluminum Frame

The analysis focuses on how the restraint conditions affect the distribution of Von Mises stress (σ_{VM}) in the aluminum frame under combined loading. The stress data was obtained from SAP2000 using frame element output for each combination of restraints, taking into account where the maximum stress value occurred due to force redistribution and the support layout as well as the rotational flexibility that was caused by moment releases.

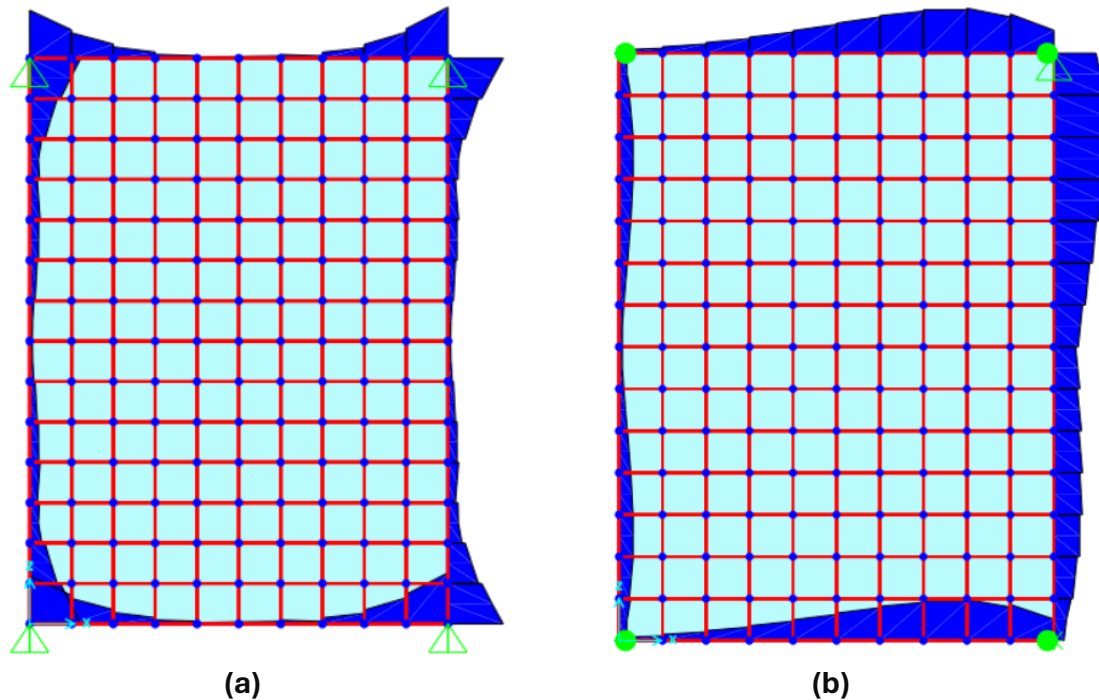


Figure 7- 20. Von Mises stress distribution in the aluminum frame.
a) Type 3-Peak stress = 59,4 MPa. **b)** Type R-Peak stress = 4,39 MPa.

In the Type 3 configuration, shown in Figure 7-20. a), with all four corners of the frame simultaneously and symmetrically supported with hinges, the maximum stress occurs at the corners due to accumulation of lateral and vertical forces and thereby high shear strain. The highest recorded von Mises stress is 59,4 MPa, primarily at the upper and lower connection zones. This stress pattern is representative of the rigid joint behavior where the rotation is limited which leads to these boundary points being forced and thereby subjected to increasing bending and shear response by the frame members.

In regard to the Type R configuration, illustrated in Figure 7-20. b), featuring an asymmetrical support configuration with full moment releases at each of the four frame corners, it exhibits a far more flexible response. The SAP2000 output indicates that corner stresses are significantly reduced in this case (1,04 MPa at the left-bottom corner, 0,291 MPa at the left-top corner and 2,265 MPa at the right-top corner). However, the maximum stress of 4,39 MPa is located along the right vertical frame element, just below the right-top corner. A secondary concentration of stress of 3,63 MPa is also observed on the top horizontal member, slightly offset from the right corner. These changes in stress concentration are representative of how releasing rotational restraints shift the force flow from the joints towards mid-span elements or into the remaining constrained regions of the frame, resulting in a change in stress concentration pattern.

These observations suggest flexible boundary configurations effectively lower peak local stress levels at conventional high-demand locations (corners) while increasing the overall ductile nature of stress distribution throughout the structure. Such redistribution is beneficial in limiting localized stress concentrations and improving the long-term performance of connector zones in curtain wall applications.

Table 7- 19. Peak Von Mises stress in the aluminum frame by restraint variants.

Variations	Peak Von Mises Stress (σ_{VM})	Stress Concentration Zones	Yielding Strength (fyi)
Type 3	59,4 MPa	Corner regions (top and bottom connections)	260 MPa
Type R	4,39 MPa	Right vertical frame & top horizontal frame (near end)	260 MPa

These results (Table 7-19.) highlight the fact that restraint configuration not only impacts deformation, but also governs the stress flow and accumulation within a façade system. While corner releases aid in the reduction of joint overloading, they may also transfer critical stress regions to different problem locations, such as those highly near unbalanced supports (over detailing in those areas may be necessary). That is fundamental for structural optimization, in particular with regards to fatigue on connectors and durability when considering factors such as seismic and wind effects.

7.3.4. Glass Panel Displacement and Rotation

This section analyzes the in-plane response of the glass panel under case of combined horizontal displacement and self-weight (COMB1) for Type 3 and Type R configurations. The main focus is to evaluate how the layout of restraints affects the translation of glass, torsional rotation and the overall deformation pattern, with particular emphasis to flexible silicone connectors placed between the frame and glass.

The boundary conditions greatly influence the response of the glass panel, as the silicone joints not only transfer the motion to the frame, but to the glazing. During seismic or lateral drift, a glass panel does not remain independent, but follows the deformation path dictated by the surrounding aluminum frame.

Therefore, even the slightest asymmetry in support conditions tends to yield marked differences in how the glass panel deforms, particularly the edge lift, rotation and local torsional effects. This justifies why the comparison between symmetrically supported Type 3 and asymmetrically supported Type R is critical in understanding the performance in real façade designs.

Type 3:

Type 3 configuration has an aluminum frame symmetrically restrained, which provides stable boundary conditions for the glass panel. The panel is subjected to uniform lateral displacement and a small amount of torsional twist, as shown in Figures 7-21. a) and b).

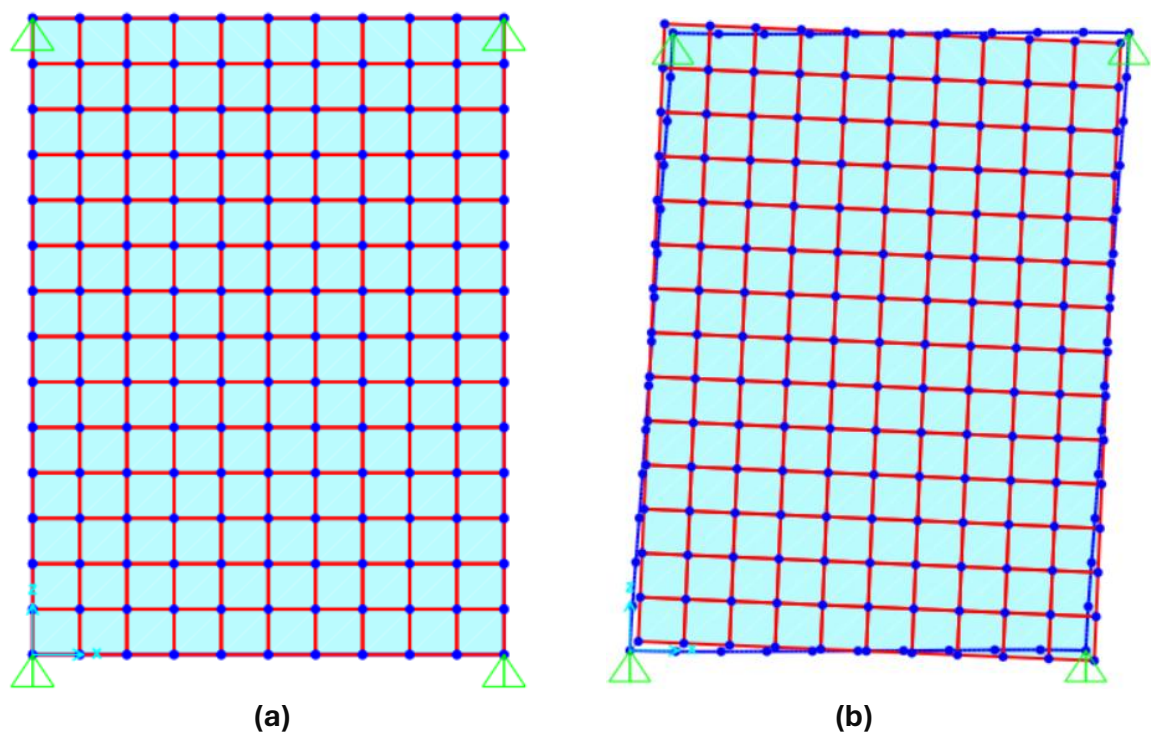


Figure 7- 21. Type 3-Façade unit under COMB1.
a) Undeformed SAP2000 model. **b)** Deformed model.

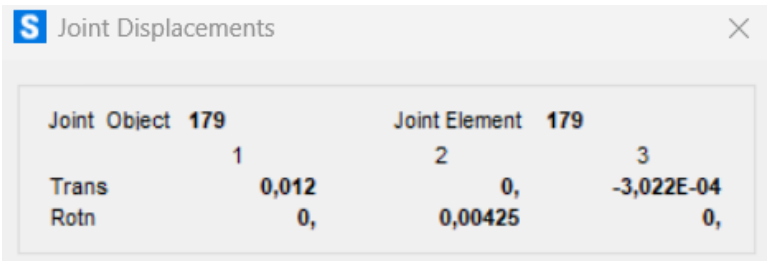
The image shows a screenshot of the 'Joint Displacements' window in SAP2000. The window has a title bar with an 'S' icon and a close button. It contains a table with displacement data for Joint 4. The table has three columns for displacement components (1, 2, 3) and two rows for translation (Trans) and rotation (Rotn). The data values are: Trans 1 = 0,0193, Trans 2 = 0, Trans 3 = 0,00506; Rotn 1 = 0, Rotn 2 = 0,00424, Rotn 3 = 0,.

Joint	Object	4	Joint Element	4	
		1	2	3	
Trans		0,0193	0,	0,00506	
Rotn		0,	0,00424	0,	

Figure 7- 22. Type 3-Joint 4-displacement output from SAP2000 (left-top corner).

Vertical displacement due to rotation together with transmitted lateral drift is confirmed in the top-left corner (Joint 4) by the SAP2000 output, shown in Figure 7-22.

- **Horizontal displacement (Ux):** 0,0193 m
This value is almost equal to the set value of 24 mm in-plane displacement, thus confirming that there is perfect control on the amount of lateral drift transmission to the glass.
- **Vertical displacement (Uz):** 0,00506 m
Slight vertical displacement, suggesting minor torsional lift at the top-left corner.
- **Rotation about Y-axis (R2):** 0,00424 rad
Small rotation about the Y-axis, pointing to mild torsional behavior of the panel edge.



The image shows a screenshot of the 'Joint Displacements' window in SAP2000. The window title is 'Joint Displacements' with a close button (X) in the top right corner. The window contains a table with the following data:

Joint	Object	179	Joint Element	179
		1	2	3
Trans		0,012	0,	-3,022E-04
Rotn		0,	0,00425	0,

Figure 7- 23. Type 3-Joint 179-displacement output from SAP2000 (centroidal joint).

Displacement results with respect to the centroid of the glass (Joint 179) are displayed in Figure 7-23. Displacement of centroid ($\delta x = +0,012$ m) reflects the average in-plane response of the panel. In addition, rotation around the Y-axis ($\phi = +0,00425$ rad) indicates that the rotation due to torsional motion, though limited in magnitude.

These outcomes suggest that the glass operates like a rigid body, undergoing uniform lateral translation with minor angular rotation. The close alignment of centroidal and edge displacements also supports the balanced and stable deformation pattern that minimizes motion and stress concentrations on silicone connectors during seismic or lateral loading.

Type R:

For Type R, the behavior of the glass panel is characterized by asymmetrical support conditions to the glass and internal moment releases at the corners of the frame. In the COMB1 loading case, the glass panel exhibits a more flexible deformation pattern, particularly characterized by increased vertical displacement at the top-left corner and greater torsional rotation.

These behaviors are explainable by the absence of restraint on the left side of the frame, which allows larger movements of the edge and redistributes the imposed drift through both translation and rotation. The layout of the supports allows for the rotation and lifting of the glass, warping it in torsion. While the warping is not extreme, it is greater than with symmetrically supported configurations.

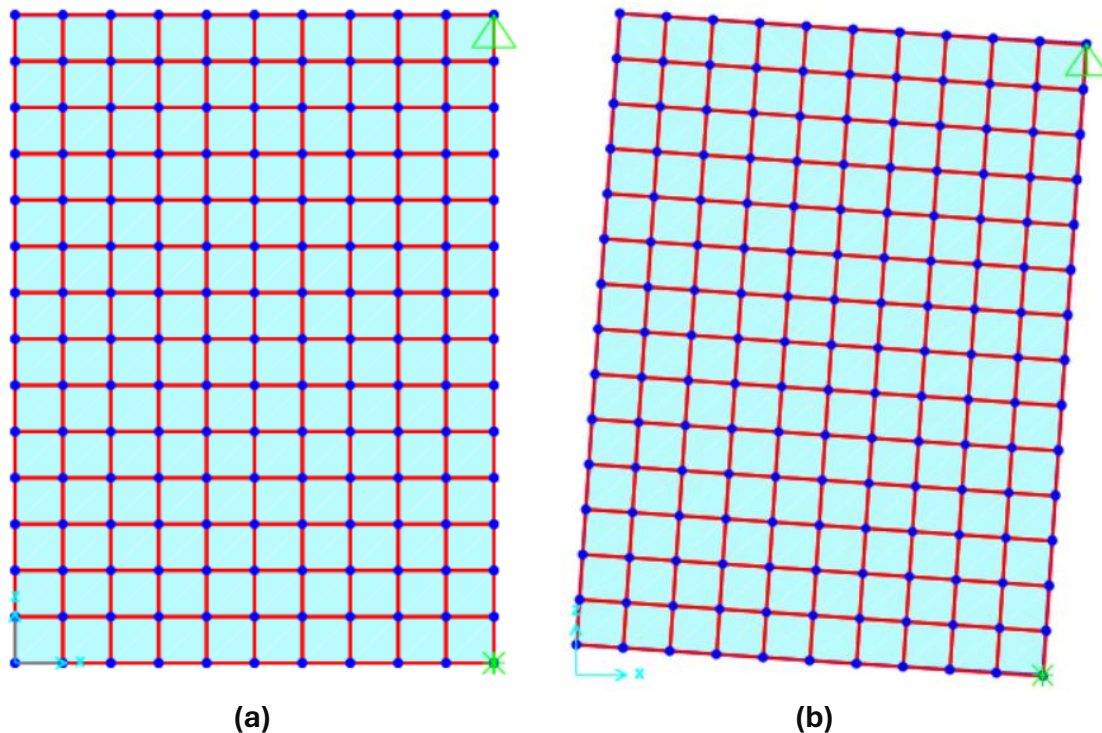
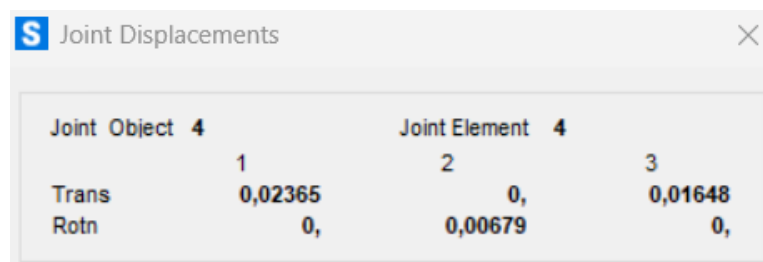


Figure 7- 24. Type R-Façade unit under COMB1.
a) Undeformed SAP2000 model. **b)** Deformed model.



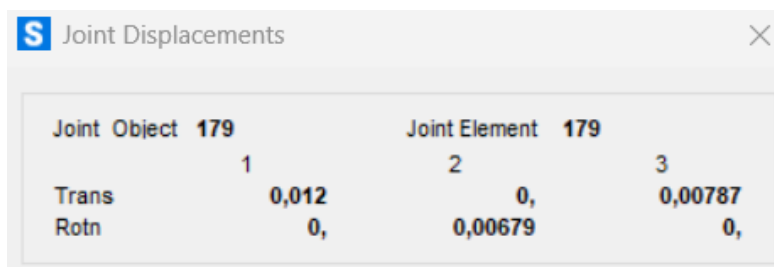
The screenshot shows the 'Joint Displacements' window for Joint 4. It displays the displacement values for three degrees of freedom: Translation (Trans), Rotation (Rotn), and Joint Element 4. The values are as follows:

Joint	Object	4	Joint Element	4	3
Trans	1	0,02365	2	0,	0,01648
Rotn		0,	0,00679		0,

Figure 7- 25. Type R-Joint 4-displacement output from SAP2000 (left-top corner).

The data from SAP2000 with respect to the left-top corner (Joint 4) of the glass panel shows this deformation behavior (Figure 7-15.):

- **Horizontal displacement (U_x):** 0,2365 m
Closely aligned with the 24-mm imposed drift, showing that lateral displacement is fully transmitted to the glass edge.
- **Vertical displacement (U_z):** 0,01648 m
Indicates an upward shift at the unrestrained top-left edge, reflecting the torsional response induced by asymmetrical support.
- **Rotation about Y-axis (R_2):** 0,00679 rad
Demonstrates torsional rotation concentrated near the panel edge due to flexible frame conditions.



The screenshot shows the 'Joint Displacements' window for Joint 179. It displays the displacement values for three degrees of freedom: Translation (Trans), Rotation (Rotn), and Joint Element 179. The values are as follows:

Joint	Object	179	Joint Element	179	3
Trans	1	0,012	2	0,	0,00787
Rotn		0,	0,00679		0,

Figure 7- 26. Type R-Joint 179-displacement output from SAP2000 (centroidal joint).

The results of displacement at the glass centroid (Joint 179) are displayed in Figure 7-26. The value of centroidal translation which is $\delta x = 0,012$ m confirms the in-plane shifting of the glass panel. The rotation about the Y-axis for this configuration is highlighted by $\phi = 0,00679$ rad which quantifies the increase in torsional deformation as compared to Type 3 configuration.

This clearly shows that glass undergoes a stable lateral displacement, while the asymmetrical restraining structure enables more vertical displacement and additional twisting at the panel level.

Table 7- 20. Glass centroidal translation and rotation outputs by restraint variant.

Variations	Joint 4 (Top-Left Corner)			Joint 179 (Centroidal)	
	Ux [m]	Uz [m]	R2 [rad]	Displacement (δx) [m]	Rotation (ϕ) [rad]
Type 3	0,0193	0,00506	0,00425	0,012	0,00425
Type R	0,02365	0,01648	0,00679	0,012	0,00679

The effects of restraint conditions on the displacement and rotational behavior for the glass panel are presented in Table 7-20., focusing on comparative results. Both Type 3 and Type R in the plane rotational centroidal translation exhibit equality ($\delta x = 0,012$ m), however, this similarity does not persist. Type R sustains comparatively larger vertical shift displacement on the left-top corner while sustaining greater torsional rotation about the Y-axis. These values imply that, relative to symmetric support conditions, the panel sustains greater geometric distortion especially at the unsupported edges.

The configuration of Type 3 with symmetric restraints allows the glass panel to be stabilized, thus also allowing vertical and rotational motion, resulting in-plane uniform deformation which lowers the excess forces forwarded to silicone connectors. In turn, Type R configuration applies flexible boundary conditions, inducing uplift at the edges with torsional warping, which may compromise long-term serviceability and stress distribution under seismic or lateral loading scenarios. This type also experiences stress redistribution. These findings reinforce the importance of support layout in curtain wall design, particularly for controlling torsional effects and maintaining panel integrity.

7.3.5. Principal Stress in the Glass Panel

This section focuses on analyzing the principal tensile stress concentration (S_{max}) within the glass panels concerning two restraint configurations, Type 3 and Type R, for the in-plane displacement and self-weight loading combination. The data used in this work was obtained from SAP2000 using shell element output files, where principal stress values on the glass surface were utilized.

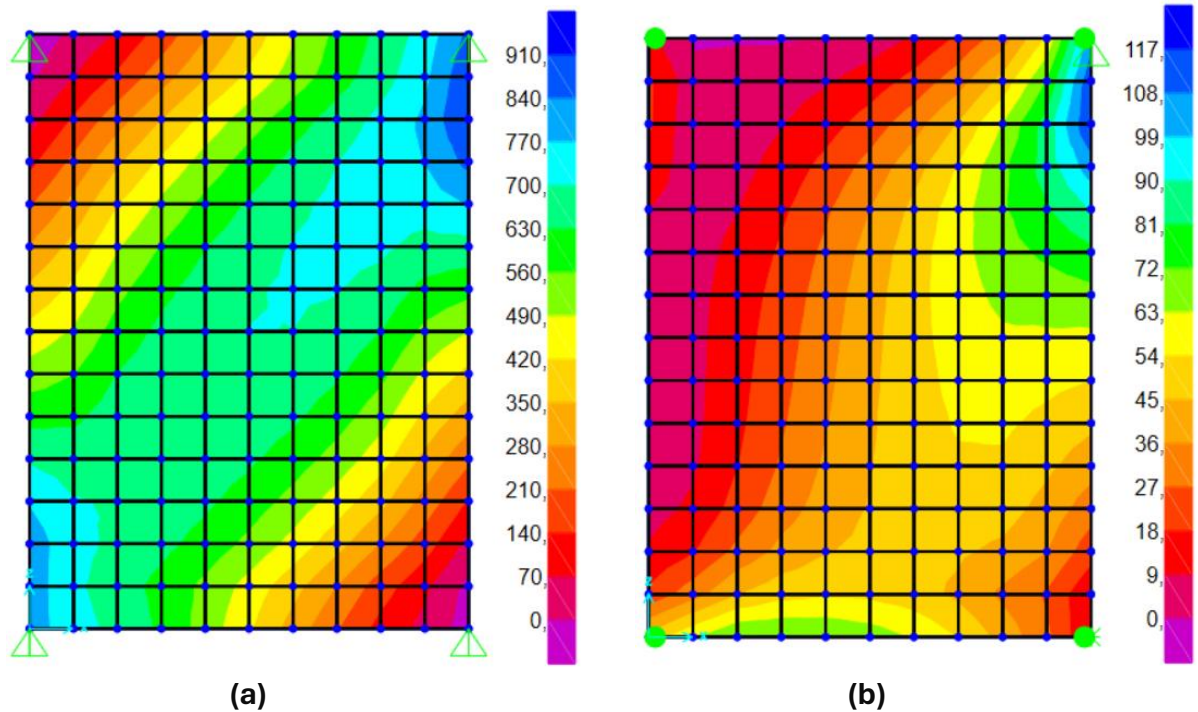


Figure 7- 27. Maximum principal stress distribution in the glass panel.
a) Type 3-Peak Smax = 910 kPa (0,91 MPa). **b)** Type R- Peak Smax = 117 kPa (0,117 MPa).

In the Type 3 configuration (Figure 7-27. a)), where the support is symmetrically placed to the aluminum frame, the glass panel experiences the maximum peak principal tensile stress of 0,910 MPa. This stress is distributed diagonally across the panel, from the left-top corner to the right-bottom corner, forming a distinct tension band. This specific diagonal stress path is a result of the yielding lateral drift and self-weight of the structure as it is transferred through the rigid frame supports and strongly confined silicone connectors. This feature results in higher stress concentrations near the diagonal axis of the deformation and tends to result in the most pronounced concentrated stresses.

As seen in the Type R configuration (Figure 7-27. b)), which includes asymmetric support with complete moment releases at the corners, there is an apparent reduction in stress pattern that is still observable. The peak principal tensile stress is 0,117 MPa which is almost eight times lower than in the Type 3 configuration and still quantifiable. Unlike Type 3, this stress value is distributed over a much larger area and lacks sharply defined boundaries, which suggests that the glass is deformed more gently, or softened. This is because more allowed rotational freedom will lead the frame to limit the excessive tensile stress concentration regions to be redistributed rather than being directly applied.

Table 7- 21. Maximum principal tensile stress in the glass panel by restraint variant.

Variations	Max Principal Stress (Smax)	Yielding Strength (fyi)
Type 3	0,91 MPa	45 MPa
Type R	0,117 MPa	45 MPa

The obtained results clearly illustrate the advantage for stress distribution of incorporating corner releases and flexible support conditions with respect to peak tensile stress in the glass (Table 7-21.). While Type 3 configuration transmits drift with satisfactory efficiency, it suffered from excessive stress concentration. On the other hand, Type R configuration was more favorable in terms of stress modulation due to its greater deformation adaptability. These findings are important in the context of designing glass façades, especially regarding their performance under seismic or lateral drift loads which is critical for minimizing brittle material failure.

7.3.6. Parametric Evaluation of Restraint Condition

In this final section of the restraint case analysis, a summary metric is integrated that combines all performance metrics noticed in all previous subsections to evaluate how the restraint configuration affects the façade performance. Comparison of structural responses for Type 3 with symmetrical corner hinges and Type R with asymmetrical bracing and full moment releases is performed to understand what level of limit flexibility is structurally effective given real seismic loading conditions.

These are performance parameters that capture both the kinematic motion of the glass and the internal force motion of the structural components (Table 7-22.):

- **Glass kinematics**, which include centroidal translation (δx) and rigid-body rotation (ϕ), representing the global movement and torsional deformation of the panel.
- **Structure performance** indicators, which include the maximum bending moment (M3-3) of the frame to the cross section with most influence, von Mises stress (σ_{VM}) in the frame and the maximum principal tensile stress (Smax) in the glass panel, along with degree of imposed lateral drift and self-weight (dead load) (COMB1).

Table 7- 22. Structural response by restraint condition variants.

Parameters	Unit	Type 3	Type R
Support Configuration	-	Symmetric (4 Hinged Corners)	Asymmetric (Hinge + Roller + Free)
Corner Moment Releases	-	None	M3 at all corners
Glass Rotation (ϕ)	rad	0,00425	0,00679
Glass Centroid Displacement (δx)	m	0,012	0,012
Max. Bending Moment in Frame (M3-3)	kN.m	$\pm 3,5$	$\pm 0,153$
Max. Frame Stress (σ_{VM})	MPa	59,4	4,39
Max. Glass Stress (Smax)	MPa	0,91	0,117

The Type 3 configuration has the highest internal forces of a mechanical demand, with large bending moments, concentrated von Mises stress at corner joints and high tensile forces on the glass. The symmetric and fully restrained corner arrangement results in uniform and stable deformation, yet, this stiff behavior also increases local concentration stress, particularly at structural connections, leading to increase the vulnerability of silicone joints or glazing under cyclic drift conditions.

On the other hand, Type R shows a more flexible structural response, characterized by more uniform force path redistribution and lower stress levels. The lack of rotating moment continuity at the corners allows the system to adaptively deform, despite having larger global glass rotation ($\phi = 0,00679$ rad).

The reduction of bending moments and frame stresses is evident through the mechanical response provided by the free corners and the good distribution of the tensile stress in the glass throughout the element. This redistribution strategy increases the resilience of the building's façade, especially in seismic areas, as control over relative movement and stress significantly enhances durability and safety.

In summary, these outcomes verify that the restraint conditions are a determining consideration in the performance of a façade unit, as they influence the deformation mechanisms, the internal stress progression and the seismic safety margins. Permitting some degree of freedom at the boundaries through moment releases, asymmetric supports or controlled articulation improves the displacement absorbing capability of the system while protecting the critical stress concentration areas and vital stress support zones from damage.

Chapter 8

Conclusion

This thesis has focused on the seismic performance of non-structural glass curtain walls, particularly through the case study of unitized curtain wall system consisting of glass panels, aluminum framing, and silicone joints. As these systems are more frequently used in modern skyscraper design, their potential seismic performance has become significantly challenging. The study in question sought to define how these façade units undergo deformation as loads are transferred through them due to inter-story drifting, which occurs during moderate to severe earthquakes. For this purpose, a finite element model was created in SAP2000 with varying connector geometries, panel sizes and restrain condition boundaries. The simulations were informed by recent experimental results and placed against the background of relevant international seismic design codes.

Glass façades have become striking features of contemporary urban skylines as architecture continues to adopt a fixation on transparency, lightness and energy efficiency. Glass is also expected to serve aesthetic purposes while being reliable to environmental and mechanical stressors such as temperature changes and earthquakes. Unlike traditional load-bearing construction materials, glass operates differently under lateral deformation due to its lack of ductility and post-failure capacity; this behavior is important both from an architectural design point view and structurally. The unitized curtain wall systems that are the focus of this thesis exemplify advanced prefabrication approaches that integrate performance testing, modularity and prefabrication; however conventional design approaches have inadequately examined their application in seismic regions.

The first parametric analysis looked into the geometry and shear stiffness of the silicone connectors. Results showed that increasing either the stiffness or bonded area of a silicone connection improved system rigidity. However, this resulted in greater stress concentration marks in both the aluminum frame and glass panel. On the other hand, using lower stiffness connectors produced favorable deformation compatibility, which reduced local peak stresses, but increased global displacement. These results document optimal balancing of stiffness and flexibility to prevent damage from stress rupture on interfaces where material property differences are sharp.

The second variation focused on outline dimensions of the panels, paying attention particularly to their aspect ratios (height/width). Panels with greater width exhibited lesser deformation susceptibility at lower ratio values, but significantly higher internal forces in the frame. Taller and narrower panels responded more flexibly, displaying lower internal stresses but glass rotation and overall displacement response was greatly increased. These trade-offs show that façade panel geometry fundamentally influences seismic resilience while affecting mechanically how units respond, as well as aesthetically how they visually perform through glazing.

The latest set of analyses looked into the impact of restraint boundary conditions by contrasting a fully symmetric configuration with four hinged corners against one that incorporates moment releases and asymmetric supports. The findings showed that rigid boundary conditions enhance stability and contain global motion, but tend to exacerbate significant stress accumulation at joints and corners. On the other hand, asymmetric or partially released configurations enable better force redistribution within the system, resulting in decreased local stresses as well as greater capacity to undergo deformation without structural failure. This provides further evidence in support of the notion that flexibility under control at anchorage points enhances performance during seismic activities for glazed façades.

In order to frame the numerical results within the context of seismic engineering as a whole, an assessment of some international regulatory documents was conducted. While both Eurocode 8 (Europe) and ASCE 7-16 (US) operate on force-based and hybrid approach, JASS 14 (Japan) and NZS 1170.5 (New Zealand) lean toward deformation control through displacement-based design. The diversity among these regulations illustrates an emerging shift concerning façade design paradigm.

In conclusion, the seismic performance of unitized curtain walls is determined by an intricate combination of materials and their mechanical properties, geometry and boundary conditions. This work enhances understanding relevant to façades designed with regard to performance metrics by providing an extensive parametric numerical analysis grounded in experiments and prevailing regulations. The results highlight critical considerations concerning deformation compatibility, detailing in connectors used, adaptive restraints appropriate for various loading scenarios and overall architectural envelope performance in seismically active regions which improve safety and resilience. Ultimately, these findings are intended to guide high-performance glazing systems and advance integrated design approaches where architectural expression does not compromise structural integrity.

REFERENCES

- [1] Arifin, A. (2018). *Seismic design and loss assessment of curtain wall systems*. PEER Report. Doi: https://www.researchgate.net/publication/352414726_Performance_comparison_of_standard_and_seismic_glazing_systems
- [2] Arifin, A., Pampanin, S., & Palermo, A. (2020a). *Seismic performance comparison between standard and flexible curtain wall glazing systems*. Journal of Façade Design and Engineering.
- [3] Passoni, C. (2022). *The Role of Life Cycle Structural Engineering in the Transition towards a Sustainable Building Renovation: Available Tools and Research Needs*. Doi: <https://www.mdpi.com/2075-5309/12/8/1107>
- [4] Dhakal, R. P. (2010). *First step towards loss optimisation seismic design (LOSD)*. Doi: https://www.researchgate.net/publication/299008152_First_step_towards_loss_optimisation_seismic_design_LOSD
- [5] Sucuoglu, H., & Vallabhan, C.V.G. (1997). *Behavior of window glass panels during earthquake*. Doi: https://www.researchgate.net/publication/222626013_Behaviour_of_window_glass_panels_during_earthquakes
- [6] Aiello, M., & Caterino, N. (2019). *The Role of Details for Seismic Performance of a Full-Scale Glass Façade*. Doi: https://www.researchgate.net/publication/333396140_The_Role_of_Details_for_Seismic_Performance_of_a_Full_Scale_Glass_Facade
- [7] Permasteelisa Group & TU Delft (2024). *Influence of design variables on seismic performance of unitized curtain walls: A parametric experimental study*. Doi: https://www.researchgate.net/publication/381613695_Influence_of_design_variables_on_seismic_performance_of_unitized_curtain_walls_a_parametric_experimental_study
- [8] EN 1998 (Eurocode 8) (2004). *Design of Structures for Earthquake Resistance – Part 1: General Rules*. Doi: <https://www.phd.eng.br/wp-content/uploads/2015/02/en.1998.1.2004.pdf>
- [9] ASCE/SEI 7-22 (2022). *Minimum Design Loads and Associated Criteria for Buildings and Other Structures*. Doi: <https://www.asce.org/publications-and-news/asce-7>

- [10] CEN/TS 19100 (2022). *Design of Glass Structures – Technical Specification*.
Doi: <https://link.springer.com/article/10.1007/s40940-023-00219-y>
- [11] Tait, H. (1991). *Five Thousand Years of Glass*. British Museum Press. Doi:
<https://archive.org/details/fivethousandyear0000unse/page/n259/mode/2up>
- [12] Brill, R. H. (1999). *Chemical Analyses of Early Glasses*. Corning Museum of Glass.
Doi: <https://info.cmog.org/sites/info.cmog.org/files/pdf/5052FA17-E769-478E-A9B4-0F89C6458478.pdf>
- [13] Marks, R. (1993). *Stained Glass in England during the Middle Ages*. Routledge.
- [14] Bill Addis. (2006). *The Crystal Palace and its Place in Structural History*.
Doi: https://www.researchgate.net/publication/245526024_The_Crystal_Palace_and_its_Place_in_Structural_History
- [15] Curtis, W. J. R. (1996). *Modern Architecture Since 1900*. Phaidon Press.
Doi: <https://archive.org/details/modernarchitectu0000curt>
- [16] Baillie, C. (2013). *Structural Glass Facades and Enclosures*. Doi: https://www.academia.edu/75459578/Structural_Glass_Facades_and_Enclosures
- [17] Permasteelisa Group. (2021). *Projects and Innovations*.
Doi: <https://www.permasteelisagroup.com>
- [18] Feldmann, M., Kasper, R., et al. (2014). *Guideline for European Structural Design of Glass Components*. RWTH Aachen / European Union. Doi:
<https://publications.jrc.ec.europa.eu › JRC86637>
- [19] Louter, C., Nussbaumer, A., et al. (2020). *Glass performance*. TU Delft.
Doi: https://www.researchgate.net/publication/339312818_Glass_performance
- [20] EN 572-1 (2012). *Glass in Building – Basic Soda Lime Silicate Glass Products – Definitions and General Physical and Mechanical Properties*. Doi:
<https://cdn.standards.iteh.ai/samples/64297/f5a90d1ca54641b2aa8cd1ed2da4f5dc/SIST-EN-16612-2020.pdf>
- [21] ASTM E1300-16. *Standard Practice for Determining Load Resistance of Glass in Buildings*. Doi: <https://store.astm.org/e1300-16.html>
- [22] F, A, Veer. (2007). *The strength of glass, a nontransparent value*. Heron Journal.
Doi: <https://heronjournal.nl/52-12/4.pdf>

- [23] Anna Jóźwik. (2023). *Introduction to structural design of glass according to current European standards*. Warsaw University of Technology. Doi: https://www.researchgate.net/publication/368544008_Introduction_to_structural_design_of_glass_according_to_current_European_standards
- [24] Guardian Glass, 2020. *Heat-Strengthened Glass Specification Sheet*. Doi: <https://www.guardianglass.com>
- [25] K, C, Datsiou. M, Overend. (2017). *The strength of aged glass*. Doi: https://www.researchgate.net/publication/318291365_The_strength_of_aged_glass
- [26] Bianchi, S. (2022). *Seismic testing and multi-performance evaluation of full-scale unitized curtain walls: research overview and preliminary results*. SPONSE Conference Proceedings. Doi: <https://www.researchgate.net/publication/367476969>
- [27] Bianchi, S. (2023). *Seismic assessment and finite element modeling of traditional vs innovative point fixed glass facade systems (PFGFS)*. Doi: <https://doi.org/10.1007/s10518-023-01622-0>
- [28] Bonati, A. *Experimental assessment of the seismic performance of full-scale curtain wall systems*. Doi: <https://www.researchgate.net/publication/351102087>
- [29] FEMA E-74 (2012). *Reducing the Risks of Nonstructural Earthquake Damage – A Practical Guide*. Doi: https://www.fema.gov/sites/default/files/2020-07/fema_earthquakes_reducing-the-risks-of-nonstructural-earthquake-damage%E2%80%94a-practical-guide-fema-e-74.pdf
- [30] Galli, U. (2011). *SEISMIC BEHAVIOUR OF CURTAIN WALL FACADES*. Doi: https://www.politesi.polimi.it/retrieve/a81cb059-f9bf-616b-e053-1605fe0a889a/2012_04_Galli.pdf
- [31] ETAG 002 (2012). *Guideline for European Technical Approval of Structural Sealant Glazing Systems*. Doi: http://www.sgpstandard.cz/editor/files/stav_vyr/dok_es/eta/etag/002_1_en.pdf
- [32] Bianchi, S. (2024). *Damage States of Structural Silicone Glazed Facades*. Doi: https://www.researchgate.net/publication/382062398_DAMAGE_STATES_OF_STRUCTURAL_SILICONE_GLAZED_FACADES

- [33] Sivaprakasam, T. (2020). *Full-scale tests of aluminum mullion couples in unitized facades under wind actions*. Doi: <https://www.sciencedirect.com/science/article/abs/pii/S0141029620301759>
- [34] DOWSIL. (2020). *Structural Sealant Glazing Technical Manual*. Doi: <https://www.dow.com/documents/63/63-6132-01-structural-sealant-glazing-manual-asia.pdf?iframe=true>
- [35] Lugaresi, F. (2023). *Thermal response of a curtain wall framing system under fire conditions*. Fire Safety Journal. Doi: <https://doi.org/10.1016/j.firesaf.2023.103850>
- [36] Micheli, L. Laflamme, S. (2019). *Data-Driven Risk-Based Assessment of Wind-Excited Tall Buildings*. Doi: <https://www.researchgate.net/publication/333204358>
- [37] Murray, S. (2009). *Contemporary Curtain Wall Architecture*. Princeton Architectural Press. Doi: <https://www.scribd.com/document/364498115/Contemporary-Curtain-Wall-Architecture>
- [38] Gargallo Sanz de Vicuña, M. (2021). *A systematic approach for unitized curtain wall design based on project requirements and industry limitations*. Doi: <https://www.scribd.com/document/658652695/Mercedes-Gargallo-Sanz-de-Vicuna>
- [39] K-Zan. (2023). *Curtain Wall Systems: Types, Benefits, Design and Trends*. Doi: <https://qstuts.com/curtain-wall-systems-types-benefits-design-and-trends/>
- [40] Mannlee. (2025). *Stick vs Unitized Curtain Wall: Comparison & Best Uses*. Doi: <https://www.mannleecw.com/stick-vs-unitized-curtain-wall/>
- [41] Jaspers Eysers Architects. Reynaers Campus – Duffel, Belgium. CW 86-EF/SG. *Unitised Element Façades*. Doi: https://www.reynaers.es/sites/default/files/public/2022-08/element_facades_lr.pdf
- [42] Caterino, N. (2021). *A simplified analytical approach for assessing non-linear in plane seismic response of stick-built glass curtain walls*. Doi: <https://www.sciencedirect.com/science/article/pii/S2352012423001133?via%3Dihub>
- [43] Permasteelisa Group. The Shard. Doi: <https://www.permasteelisagroup.com/project-detail?project=791>

- [44] Benson Group. One World Trade Center. Doi: <https://www.bensonglobal.com/portfolio-item/one-world-trade-center/>
- [45] Yuanda. Shangai Tower. Doi: <https://www.yuandacn.com/index.php/en/projects-cn-2/103-domestic/shanghai/216-shanghai-center-building-2.html>
- [46] Foster + Partners. Apple Park. Doi: <https://architizer.com/blog/inspiration/stories/architectural-details-apple-park-windows/>
- [47] Gehry Partners. Fondation Louis Vuitton. Doi: <https://www.fondationlouisvuitton.fr/en/fondation/the-building>
- [48] Zaha Hadid Architects. Guangzhou Opera House. Doi: <https://www.zaha-hadid.com/architecture/guangzhou-opera-house/>
- [49] Schlaich Bergermann Partner. Time Warner Center Atrium. Doi: <https://enclos.com/project/time-warner-center/>
- [50] Foster + Partners. Gartner–Permasteelisa. Hearst Tower Lobby. Doi: <https://www.permasteelisagroup.com/project-detail?project=8&>
- [51] Foster + Partners. 30 St Mary Axe. Doi: <https://www.fosterandpartners.com/projects/30-st-mary-axe>
- [52] Permasteelisa Group. Intesa Sanpaolo Office Building. Doi: <https://www.permasteelisagroup.com/project-detail?project=1936&>
- [53] I. M. Pei & Partners. RFR. Louvre Pyramid. Doi: <https://www.francisdesign.com/project/le-louvre/>
- [54] OMA + LMN. Seattle Central Library. Doi: <https://www.oma.com/projects/seattle-central-library>
- [55] Naeim, F. (2015). *Performance Based Seismic Design Guidelines for Tall Buildings and their Applications*. Doi: https://northridge20.peer.berkeley.edu/wp-content/uploads/2010/10/Tall_Building_Guidelines_Naeim1.pdf
- [56] Pampanin, S. Palermo, A. *Facade damage assessment of multi-story buildings in the 2011 Christchurch earthquake*. Doi: <https://www.researchgate.net/publication/265077229>

- [57] Swanson, D. Aveyard, D. (2019). *2017 Central Mexico Earthquake Reconnaissance Report*. Reid Middleton. Doi: <https://www.reidmiddleton.com/wp-content/uploads/2020/04/MexicoCityEQ-Report-eidMiddleton0119.pdf>
- [58] Britannica. Article History. *Ring of fire-Seismic Belt*. Doi: <https://www.britannica.com/place/Ring-of-Fire>
- [59] Special Earthquakes, Earthquake Sequences, and Fault Zones. Doi: <https://www.usgs.gov/programs/earthquake-hazards/special-earthquakes-earthquake-sequences-and-fault-zones>
- [60] Ishibe, T. Shimazaki, K. (2009). *Seismicity in source regions of large inter-plate earthquakes around Japan and the characteristic earthquake model*. Doi: <https://earth-planets-space.springeropen.com/articles/10.1186/BF03352955>
- [61] Wu, F. Taymaz, T. Irmak, T. S. (2023). *Pulse-like ground motion observed during the 6 February 2023 M 7.8 Pazarcık Earthquake (Kahramanmaraş, SE Türkiye)*. Doi: <https://www.sciencedirect.com/science/article/pii/S1674451923000290>
- [62] Qu, Z. Wang, F. (2023). *Rapid report of seismic damage to hospitals in the 2023 Turkey earthquake sequences*. Doi: <https://doi.org/10.1016/j.eqrea.2023.100234>
- [63] Taghavi, S. Miranda, E. (2003). *Response Assessment of Nonstructural Building Elements*. Doi: https://peer.berkeley.edu/sites/default/files/0305_s._taghavi_e._miranda_.pdf
- [64] Nardini, V. Doebl, F. (2016). *Performance-Based Concept for Design of Structural Silicone Joints in Façades Exposed to Earthquake*. Doi: <https://doi.org/10.7480/cgc.5.2253>
- [65] Mayoral, J. Frane, W. K. (2017). *Mexico City Earthquake: Important Findings from the Field*. Doi: <https://www.sciencedirect.com/science/article/abs/pii/S0267726118310479>
- [66] FEMA 460. (2005). *Seismic Considerations for Steel Storage Racks Located in Areas Accessible to the Public*. Doi: <https://www.wbdg.org/FFC/DHS/fema460.pdf>
- [67] FEMA 461. (2007). *Interim Testing Protocols for Determining the Seismic Performance Characteristics of Structural and Nonstructural Components*. Doi: <http://atcouncil.org/pdfs/FEMA461.pdf>

- [68] Standards New Zealand. NZS 1170.5:2004. *Structural Design Actions Part 5 Earthquake Actions*. Doi: <https://www.standards.govt.nz/shop/nzs-1170-52004-excludes-amdt-1>
- [69] Granit Engineering. Mohr 3D. Doi: <https://www.graniteng.com/mohr-3d>
- [70] DOW. DOWSIL™ 993 Structural Glazing Sealant. Doi: <https://casteleinsealants.be/wp-content/uploads/2020/05/ENG-06-DOWSIL-993-2020-04-01.pdf>